INFORMATION TO USERS

University of Alberta

Adhesion Measurement and Stability of Bulk Polymer Phases and Thin Polymer Films

by

Manav R. Lahoti ©

A thesis submitted to the Faculty of Graduate Studies and Research
in partial fulfillment of the requirements for the degree of
MASTER OF SCIENCE

Department of Chemical and Materials Engineering

Edmonton, Alberta
Spring, 1997

National Library
of Canada

Bibliothèque nationale
du Canada

Acquisitions and
Bibliographic Services

Acquisitions et
services bibliographiques

395 Wellington Street
Ottawa ON K1A 0N4
Canada

395, rue Wellington
Ottawa ON K1A 0N4
Canada

The author has granted a non-exclusive licence allowing the National Library of Canada to reproduce, loan, distribute or sell copies of his/her thesis by any means and in any form or format, making this thesis available to interested persons.

The author retains ownership of the copyright in his/her thesis. Neither the thesis nor substantial extracts from it may be printed or otherwise reproduced with the author's permission.

L'auteur a accordé une licence non exclusive permettant à la Bibliothèque nationale du Canada de reproduire, prêter, distribuer ou vendre des copies de sa thèse de quelque manière et sous quelque forme que ce soit pour mettre des exemplaires de cette thèse à la disposition des personnes intéressées.

L'auteur conserve la propriété du droit d'auteur qui protège sa thèse. Ni la thèse ni des extraits substantiels de celle-ci ne doivent être imprimés ou autrement reproduits sans son autorisation.

0-612-21183-5

Canada

University of Alberta

Library Release Form

Name of Author	:	Manav R. Lahoti
Title of Thesis	:	Adhesion Measurement and Stability of Bulk Polymer Phases and Thin Polymer Films
Degree	:	Master of Science
Year This Degree Granted	:	1997

Permission is hereby granted to the University of Alberta Library to reproduce single copies of this thesis and to lend or sell such copies for private, scholarly, or scientific research purposes only.

The author reserves all other publications and other rights in association with the copyright in the thesis, and except as hereinbefore provided, neither the thesis nor any substantial thereof may be printed or otherwise reproduced in any material form whatever without the author's written permission.

3A - 8904, 112 St.

Edmonton, Alberta

T6G 2C5

January 28, 1997
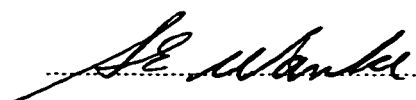
UNIVERSITY OF ALBERTA

FACULTY OF GRADUATE STUDIES AND RESEARCH

The undersigned certify that they have read, and recommended to the Faculty of Graduate Studies and Research for acceptance, a thesis entitled **Adhesion Measurement and Stability of Bulk Polymer Phases and Thin Polymer Films** submitted by **Manav R. Lahoti** in partial fulfillment of the requirements for the degree of **MASTER OF SCIENCE**.
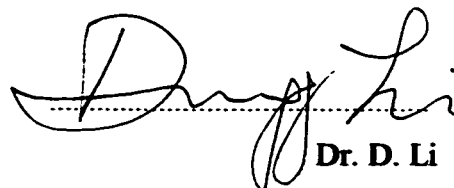
Dr. Uttandaraman Sundararaj (Supervisor)

Dr. S. E. Wanke

Dr. M. C. Williams

Dr. D. Li

Date : December 3, 1996

ABSTRACT

Adhesion of ethylene-vinylacetate (EVA) copolymers to polycarbonate (PC), polystyrene (PS) and poly(ethylene-terephthalate) (PET) was characterized using three tests. A Peel test was used to measure adhesion for PC sheet (~3mm)/EVA and PET film (~50μm)/EVA systems. The effect of annealing time, annealing temperature, vinylacetate (VA) content and molecular weight of EVA on adhesion was investigated. For the PET/EVA system, a maximum in adhesion was found as the thickness of EVA changed. An automated Double Cantilever Beam (DCB) test was used to obtain bulk adhesion values for PS/EVA and PC/EVA systems. The effect of annealing time, sample surface roughness, VA content, elastic modulus and contaminants on adhesion was studied. A Microscratch test was used to measure the adhesion for a thin PS film (~0.5μm)/EVA system. The adhesion was calculated using a linear elastic fracture mechanics (LEFM) model incorporating viscoelastic behavior.

The stability of polymer films (0.2-3μm) embedded within a polymer substrate was studied. Holes formed in these films, grew at a constant velocity into polygonal structures and finally broke into drops. Hole velocity was not affected by film viscosity, but increased with decreasing matrix viscosity. The breakup process was reasonably predicted using an energy balance.

Acknowledgment

I would like to express my heartfelt gratitude and appreciation to Dr. U. Sundararaj for his support, encouragement and personal and academic guidance through the course of my program. I have learned from Dr. Sundararaj's example to always be open to new ideas and new opportunities, and to make the most of available resources.

I would like to acknowledge Dr. W. W. Gerberich at the University of Minnesota for allowing me to work on the Microscratch Test (Chapter 4) at their laboratory. I would also like to thank Dr. John Nelson at the University of Minnesota for teaching me the working of the equipment and for helping me understand and explain some of the results. Special thanks are due to the Polymer Group at the University of Minnesota and particularly Yoav Dori for allowing me the use of their facilities and equipment.

I have been helped tremendously by various undergraduate students who have helped in collecting data for the projects in this thesis. I would like to acknowledge Peter Poruks for helping in the design and setup of the Double Cantilever Beam Test (Chapter 3) and Rathini Pillai for obtaining data using this test. I would like to thank Ryan Chu for performing sheet breakup experiments (Chapter 5) and some image analysis. In addition, I wish to acknowledge the help provided by Walter Boddez and Richard Cooper of the Chemical Engineering Instrument Shop, and the assistance by the Chemical Engineering Machine Shop for the design and construction of various experimental equipment.

Table of Contents

List of Tables

List of Figures

CHAPTER 1

Adhesion in Polymer Systems

1.1. Introduction

In today's polymer industry, pure polymers have only limited use in high performance applications. In practice, a variety of products are made by combining or joining two or more different polymers. Each component is added to improve one or more properties for use in different applications. Most polymers are inherently incompatible with each other and each component in a multicomponent system exists in its own phase and there is an interface between the phases. The properties of these products depends to a large extent on the interactions between the polymers at the interface. These interactions might be mechanical, chemical or electrostatic in nature and the strength of the interaction between these polymers is termed "adhesion".

Although any definition of "adhesion" must account for both the thermodynamic and the mechanical aspects of adhesion, in this work, we define adhesion as "the state in which two dissimilar bodies are held together by intimate interfacial contact such that mechanical force or work can be transferred across the interface" (Wu, 1982). The mechanical strength of a system depends not only on the interfacial forces but also the mechanical properties of the interfacial zone and the two bulk phases. In blends of polymers, optimum properties can be achieved by increasing the adhesion between the polymer phases comprising the blend. In applications like laminations, the mechanical integrity of the product depends upon the adhesion between the laminate layers.

Despite a considerable number of studies on adhesion phenomena, the mechanisms governing adhesion are still poorly understood. This is mainly because adhesion embraces a large number of notions and concepts which can vary depending on whether the phenomena is molecular or macroscopic in nature. The science of adhesion is a multi-disciplinary subject and one needs to consider aspects of surface chemistry, surface physics, rheology, polymer chemistry, stress analysis, polymer physics, and fracture phenomena.

In an adhering system, adhesion can be expressed in terms of forces or the work of attachment or detachment (Mittal, 1976). If expressed in this manner, then the correct classification should be "work of adhesion" or "basic adhesion". Basic adhesion is the interfacial bond strength and should depend only on the interfacial properties. It is defined as the free energy required to reversibly separate two phases from their equilibrium position to infinity at a constant temperature and pressure. It is simply the summation of all intermolecular or interatomic interactions. On the other hand, experimentally, adhesion is measured in terms of forces or the work of separating the adhering phases. The separation may take place at the interface, in the interfacial region (sometimes called interphase because of its thickness), or in the bulk of the weaker adhering phase. Separation in the bulk is termed cohesive failure and is related to the cohesive strength of that phase.

1.2. Wetting and Adhesion

It has been recognized for many years that the first step in the formation of an adhesive bond is the establishment of intimate molecular contact at the interface by wetting. The term wetting implies that the adhesive needs to be able to spread over the solid surface, and needs to displace air and any other contaminants that may be present on the surface. Incomplete wetting will produce interfacial defects and stresses concentrate around such defects and thereby lower the adhesive bond strength. Wetting may be quantitatively defined by reference to a liquid drop resting in equilibrium on a solid surface as shown in Fig. 1.1. The surface tensions at the three phase contact point are indicated such that γ_{LV}, γ_{SL} and γ_{SV} are the liquid-vapor, solid-liquid and solid-vapor interfacial tensions respectively. Young's equation relating these tensions to the equilibrium contact angle θ, is written as,

$$\gamma_{SV} = \gamma_{SL} + \gamma_{LV} \cos\theta \qquad (1.1)$$
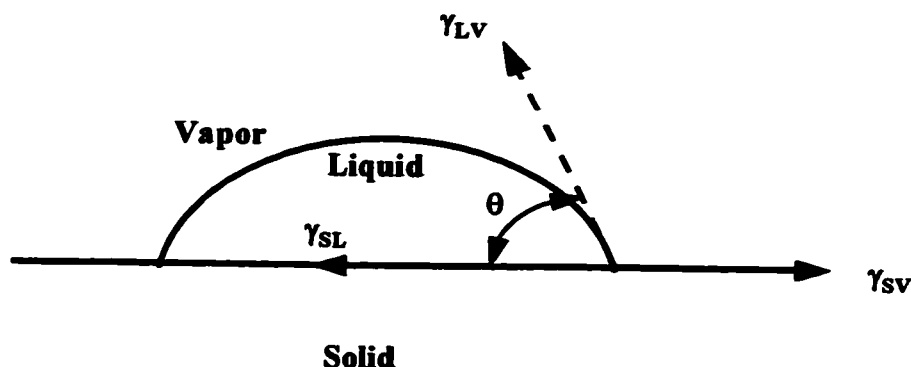
Fig. 1.1. A liquid drop resting at equilibrium on a solid surface

When $\theta > 0°$ the liquid is nonspreading on the solid substrate but when $\theta = 0°$, the liquid completely and spontaneously wets the solid and spreads freely over the surface at a rate depending on the liquid viscosity and the solid surface roughness. It is still possible for a liquid to spread and wet a solid surface even when $\theta > 0°$ but this requires the application of a pressure or force to the liquid to forcibly spread it over the solid surface.

In 1869, more than 50 years after Young's work, Dupre used Young's equation to express the work of adhesion as:

$$W_a = \gamma_{SO} + \gamma_{LV} - \gamma_{SL} \qquad (1.2)$$

where, γ_{SO} is the surface tension of the solid in vacuum. Combining Eqn. 1 and 2 provides the Young-Dupre relation:

$$W_a = (\gamma_{SO} - \gamma_{SV}) + \gamma_{LV}(1 + \cos\theta) \qquad (1.3)$$

The thermodynamic driving force for the formation of an interface is the spreading coefficient defined as (Cherry, 1981):

$$S = \gamma_{SV} - \gamma_{SL} + \gamma_{LV} = \gamma_{LV}(1 + \cos\theta) \qquad (1.4)$$

So, for similar joints using a common adhesive on a substrate, the joint strength should vary proportionately to $\cos\theta$. This was found to be the case for the adhesion of an epoxy resin to a steel adherend, where the steel surface was subjected to various surface treatments so as to obtain different contact angles (Houwink and Salomon, 1965).

4

Maximum wetting rates are achieved when the capillary pressures are the greatest and the viscosity of the adhesive is the lowest (Huntsberger, 1967). The submicroscopic topography of the solid exerts a large influence on both the capillary pressures promoting wetting and the resistance to the flow required to achieve wetting. Without sufficient time for wetting during the process of bond formation, equilibrium will not be reached. The only cases where completely wetted interfaces exhibit poor adhesive performance are (a) when the polymer conformation prevents a intimate interfacial contact and (b) when the adhesive has a low cohesive strength.

1.3. Mechanisms of Adhesion

There are various theories of adhesion but there is no single global theory or mechanism which can explain all adhesion phenomena (Kinloch,1980 and Fourche, 1995). Each of the various theories have validity for specific adhering systems. Much of the debate and confusion over which theory most comprehensively explains adhesion phenomenon arises because the test methods commonly employed to measure adhesion are not well suited to theoretical analysis. They introduce geometrical and loading factors which are difficult to analyze, and the measured joint strength includes contributions from energy losses in the adhesive and substrate. Thus, the intrinsic adhesion forces are usually obscured by other contributions, and information concerning the magnitude of such forces may only be indirectly obtained. This inability to measure the interfacial interactions has been the main obstacle to the development of a comprehensive theory of adhesion.

5

The four main mechanisms of adhesion which have been proposed are:

(a) Mechanical interlocking

(b) Diffusion theory

(c) Electronic theory

(d) Chemical bonding

Each of these mechanisms are explained in detail in the next four subsections.

1.3.1. Mechanical Interlocking

This theory proposes that mechanical interlocking of the adhesive into the irregularities of the substrate surface is the major source of intrinsic adhesion (Fig. 1.2). This interlocking phenomenon is found on porous or rough substrates such as wood, fabric, and paper. A liquid adhesive placed on such a rough substrate was found to spontaneously penetrate into the porous medium by capillarity (Fourche, 1995). It was reported that the contact area between the two materials was far larger than the apparent contact area. Another example of where mechanical interlocking may contribute significantly to the intrinsic adhesion is the metal plating of polymers. It has been argued that the adhesion of metal plating to polymeric substrates is a function of the surface topography (Kato, 1967), while others have emphasized the role of surface force interactions (Roberts et. al, 1976).

The enhancement of joint strength that may result from increasing the roughness of the substrate surface need not necessarily arise from a mechanical interlocking mechanism.
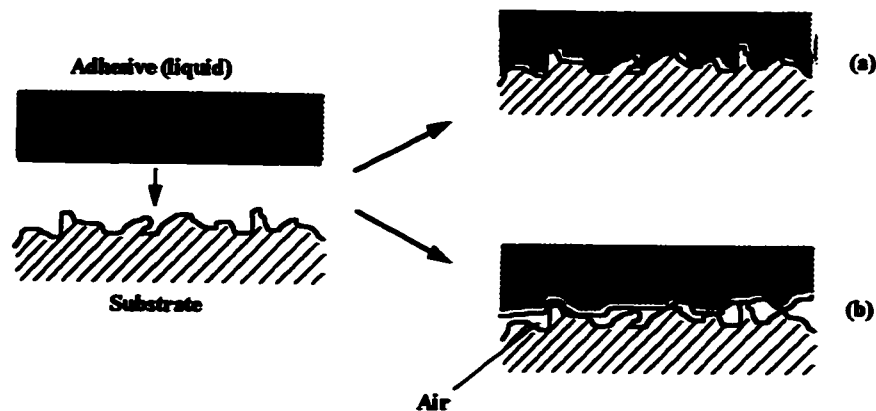
Fig. 1.2. Mechanical interlocking (a) Good adhesion; (b) Poor adhesion

The measured adhesive strength almost always reflects the value of two parameters: (a) the intrinsic adhesion and (b) the energy dissipated viscoelastically and plastically. The latter term usually dominates the measured joint strength in several commonly used tests. It has been suggested that the importance of surface roughness is to increase the energy dissipated viscoelastically and plastically during joint failure (Evans and Packham, 1979). Therefore, although in certain instances mechanical interlocking may contribute to the intrinsic adhesion forces, the frequently observed increase in joint strength with increasing roughness may be attributable to other mechanisms.

1.3.2. Diffusion theory

The diffusion theory of adhesion proposed by Voyutskii (1957) states that the intrinsic adhesion of polymers to themselves (autohesion), and to each other, is due to the mutual diffusion of polymer molecules across the interface as illustrated in Fig. 1.3. This requires that the macromolecules or chain segments of the polymers (adhesive and substrate)

possess sufficient mobility and are mutually compatible. Their compatibility can be loosely approximated by finding the difference in their solubility parameters. The lower the difference, the more compatible the system. The solubility parameter, δ, is defined as:

$$\delta = \frac{(\Delta H_v - RT)^{1/2}}{v} \tag{1.5}$$

where ΔH_v is the molar heat of vaporization, R is the gas constant, T is the temperature (K) and v is the molar volume.
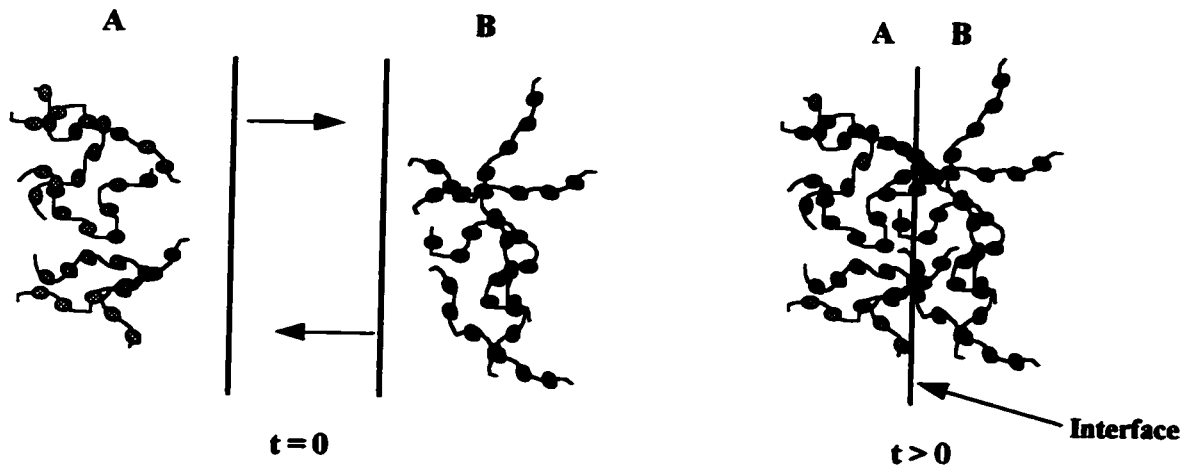
Fig. 1.3. Interdiffusion across the interface (adapted from Fourche, 1995)

In the case of polymer autohesion for polyisobutylene, it was found that the adhesion under a constant assembly pressure is a function of temperature and contact time. The average interpenetration depth, x, of one phase into another is given as:

$$x \propto \exp(-\frac{E}{2RT}) \, t^{1/2} \tag{1.6}$$

8

where, E is the diffusion activation energy, t is the contact time, R is the molar gas constant, and T is the temperature.

Dissimilar molecules are usually incompatible. Consequently, diffusion of an entire macromolecule across the interface is unlikely. However, both theory and experiment show that local-segmental interdiffusion can occur across the interface. Transmission electron micrography of the interface between dissimilar polymers has provided direct evidence for the diffusion phenomena (Van Oene and Plummer, 1977). It was shown that the interface between two polymers appears as a band, indicating intermixing of the two components in the interfacial zone. The thickness of the interface was found to increase with contact time and reaches an equilibrium value for incompatible polymers. The bond strength was also found to increase with higher bonding temperature, higher bonding pressure, higher chain flexibility, absence of bulky short side groups, and lower degree of cross-linking.

1.3.3. Electronic Theory

In this theory the adhesive-substrate system is treated as a plate capacitor whose plates consist of the electrical double layer which occurs when two materials are brought in contact, as shown in Fig. 1.4. The energy of adhesion of the system is equal to the energy of separation of the two capacitor faces, which is given as:

$$W = \frac{\delta^2 h}{2\varepsilon}$$ (1.7)

9

where δ is the surface charge density, h, the distance between the charge planes, and ε the dielectric constant of the medium.
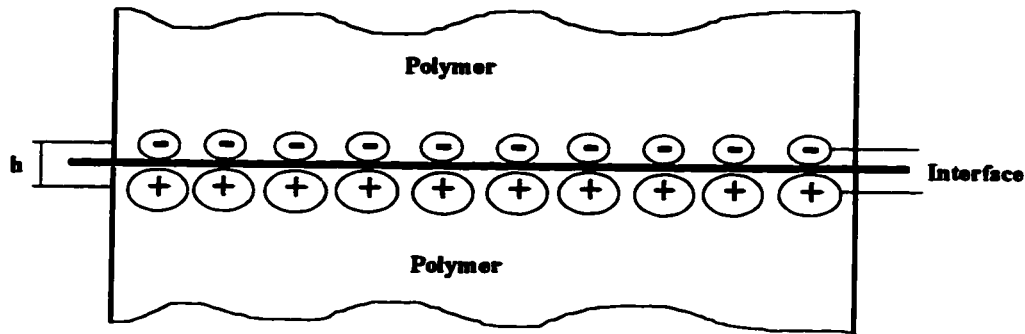
Fig. 1.4. Schematic diagram of an electrical double layer at a polymer-polymer interface (adapted from Fourche, 1995).

It had been difficult to verify the presence of an electrical double layer without breaking the adhesive bond. However, direct evidence of such a layer at the interface without rupture of the assembly was provided using scanning electron microscopy on a low-density polyethylene-aluminum assembly (Possart, 1988). The interpretation of adhesion according to the electrical theory is only applicable for incompatible polymers.

1.3.4. Chemical Bonding

Interfacial chemical bonding can increase the adhesive bond strength by preventing molecular slippage at the interface during fracture and increasing the fracture energy by increasing the interfacial attraction. Chemical covalent bonds correspond to high interaction energies, of about 60 to 700 kJ/mol and thus, the adhesion due to the formation of chemical bonds at the interface will obviously be strong.

Small amounts of appropriate reactive functional groups, when incorporated into polymers, can greatly increase the adhesive bond strength (Wu, 1982). In some cases as little as 0.001-0.01 mole fractions of functional groups can dramatically increase the adhesive strength. At such low amounts, polymer bulk properties and wettability are unchanged and the improvement in adhesion cannot be due to any of these factors. Furthermore, the functional groups are extremely specific with respect to the chemical composition of the surface. These findings suggest that the improved adhesion results from interfacial chemical bonding. The epoxy groups of an epoxy resin react with the hydroxyl groups of a cellulose at the interface and this chemical bond leads to strong adhesion between the two (Wu, 1982). Organosilanes are widely used as primers on glass fibers to promote the adhesion between the resin and the glass in fiberglass-reinforced plastics. Excess amounts of these functional groups should be avoided, as they may degrade the bulk properties and thus affect the adhesive strength.

1.4. Fracture Energy and its Measurement

As defined in §.1.1, the thermodynamic work of adhesion can only be used when the fracture process is reversible. This, however, is almost never the case in practice. In most real systems, the fracture process is irreversible, accompanied by large viscoelastic dissipation. The experimentally measured work of adhesion, also known as the fracture energy, consists mainly of the reversible work of adhesion and irreversible plastic work, i.e.

$$G = W_A + W_P \qquad (1.8)$$

where W_A is the work of adhesion and W_P is the plastic work. For a perfectly brittle material $G = W_A$ since plastic yielding does not occur. This is approximated by glass and polystyrene. The plastic work is larger in a ductile material than in a brittle one. However, even in a brittle material, the plastic work is usually several orders of magnitude greater than the reversible work of adhesion, i.e. $G \sim W_P$. Since W_P is a viscoelastic quantity, the fracture energy is thus dependent on rate, temperature, and loading geometry.

Although the fracture energy is given as the sum of the thermodynamic work and plastic work in Eqn. 1.8, an alternative relation has been proposed:

$$G = G_0 \, \psi(R) \tag{1.9}$$

where G_0 is the fracture energy at zero rate (equilibrium fracture energy), R is the rate and $\psi(R)$ a rate dependent viscoelastic function (Gent and Schultz, 1971). This relation has been confirmed experimentally and theoretically. At zero rate, viscoelastic effects are absent, and the separation process is reversible. Therefore, $\psi(R) = 1$ and $G = G_0$. The viscoelastic functions were obtained experimentally for a particular system and loading geometry.

1.5. Scope of Work

The mechanical strength of an adhesive joint is its most important property. Many different tests have been developed to evaluate it. Fracture energy tests include tensile and shear tests (Wu, 1982), peel tests (Hamed, 1966), cantilever beam tests, blister tests

12

(Williams, 1969), and cone tests (Anderson et. al, 1977). The fracture energy is dependent on the rate, temperature, and loading mode. In this work, three tests have been studied, namely, the peel test (Chapter 2), the double cantilever beam test (Chapter 3) and the microscratch test (Chapter 4). The tests are discussed in detail and experimental results obtained using these tests are presented. A more comprehensive review of tests used to measure adhesion is presented in Wu (1982) and Kinloch (1982).

The peel test is commonly used in industry for evaluating the adhesive strength of various polymeric systems. However, it has several drawbacks which makes the adhesion values obtained from this test a little suspect. Because of its popularity, we have obtained experimental results using this test and have discussed the problems associated with the interpretation of these in Chapter 2. This test is extremely versatile and can be used for a thin film/rigid substrate system, a thin film/thin film system, a fiber/matrix system, a flexible substrate/rigid substrate system and a flexible substrate/flexible substrate system. In our work we analyze two systems, a flexible substrate-rigid substrate system and a flexible substrate-flexible substrate system.

The double cantilever beam (DCB) test is used to obtain bulk adhesion values. Bulk adhesion values implies adhesion values for a system where both the substrates are extremely thick compared to the thickness of the interface. We shall show in Chapter 3 that the adhesive strength obtained using this test approaches the equilibrium value. This

test eliminates some of the problems associated with the peel test and is more representative of the strength of the interface.

After obtaining bulk adhesion values using the DCB test, we looked at the adhesion for a system of a thin film on a rigid substrate. The test used to obtain the adhesive strength for this system was the Microscratch test and results from this test are presented in Chapter 4. The films used in this test were approximately one micron thick. The adhesion of these very thin films was analyzed using a fracture mechanistic approach. Thin films are used in a variety of applications. However, these films are unstable and the mechanical integrity of the applications where they are used depends on the stability of the films. We analyze the stability of these films under various conditions in Chapter 5.

1.6. References

Anderson, G. P., Bennet, S. J., and DeVries, K. L., *Analysis and Testing of Adhesive Bonds, Academic Press*, New York (1977).

Cherry, B. W., *Polymer Surfaces*, Cambridge University Press, London (1981).

Evans, J. R., and Packham, D. E., *J. Adhesion* 10, 177(1979).

Fourche, G., *Polym. Eng. Sci.* 35, 957(1995).

Fourche, G., *Polym. Eng. Sci.* 35, 968(1995).

Gent, A. N., and Schultz, J., *Recent Advances in Adhesion*, ed. L. H. Lee, Gordon and Breach, New York (1973), p. 253.

Hamed, G. R., *Treatise on Adhesion and Adhesives*, ed. R. L. Patrick, Marcel Dekker, New York (1966), p. 33.

Houwink, R. and Salomon, G., *Adhesion and Adhesives*, eds., Elsevier, Amsterdam (1965), p. 108.

Huntsberger, J. R., *Treatise on Adhesion and Adhesives*, ed. R. L. Patrick, Marcel Dekker, New York (1967), p. 119.

Kaelble, D. H., *Physical Chemistry of Adhesion*, Wiley-Interscience, New York (1971).

Kato, K., *Polymer* 8, 33(1967).

Kinloch, A. J., *J. Mater. Sci.* 15, 2141(1980).

Kinloch, A. J., *J. Mater. Sci.* 17, 617(1982).

Possart, W., *Int. J. Adhes. Adhes.* 8, 77(1988).

Roberts, R., Ryan, F. W., Schonhorn, H., Sessler, G. M., and West, J. E., *J. Appl. Polymer Sci.* 20, 255(1976).

Van Oene, H., and Plummer, H. K., *ACS Org. Coatings Plast. Prep.* 37, 498(1977).

Voyutskii, S. S., and Margolina, Y. L., *Rubber Chem. Technol.* 30, 531(1957).

Williams, M. L., *J. Appl. Polym. Sci.* 13, 29(1969).

Wu, S., *Polymer Interface and Adhesion*, Marcel Dekker, New York (1982).

CHAPTER 2

The Peel Test

2.1. Introduction

The peel test is commonly used in industry for characterizing the adhesive strength of materials. A typical configuration of a peel test is shown in Fig. 2.1.
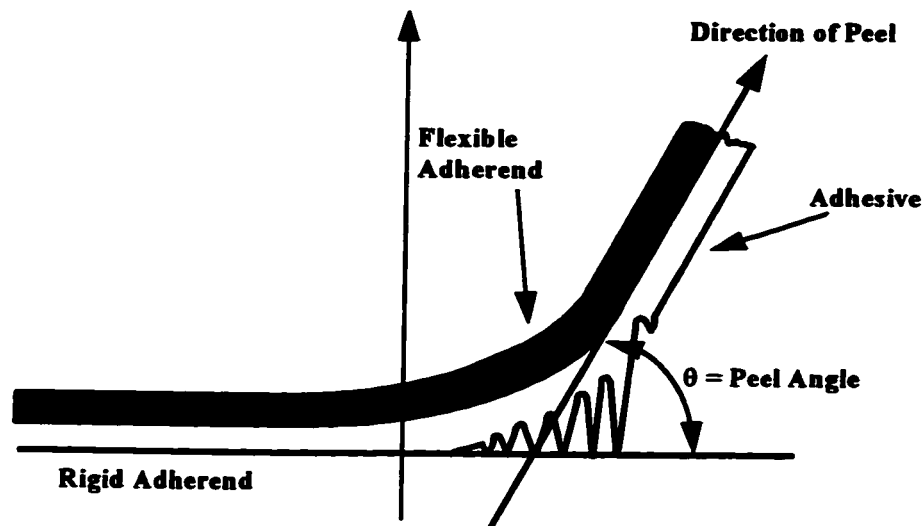
Fig. 2.1: A typical peel test configuration (adapted from Wu, 1982).

In this test, an adhesive strip is adhered onto a surface and this is peeled off at a specified rate. Quantification of peel adhesion involves measurement of the force, P, required to remove the adhesive from the surface. When the sample width, b, in a peel test exceeds about 1 cm for polymer systems, edge effects are negligible and the force/width ratio is independent of sample width (Gardon, 1965). Thus peel results are generally reported as the P/b ratio, which is reported in N/m or J/m^2.

Several factors make the peel test useful (Huntsberger, 1966 and Hamed, 1966): (1) minimal effort is required in setting up this test and it is very simple to use, (2) the test configuration allows analyses of the stresses within the materials being tested and also the work of peeling, (3) since the sample dimensions are large compared to the dimensions of the stressed regions, the area of the bond has no effect on peel data, (4) a single test yields hundreds or thousands of data points representative of the adhesive bond along the length of the sample.

$\theta = 90°$

$\theta = 180°$

(a) 90° Peel Test   (b) 180° Peel Test   (c) T - Peel Test
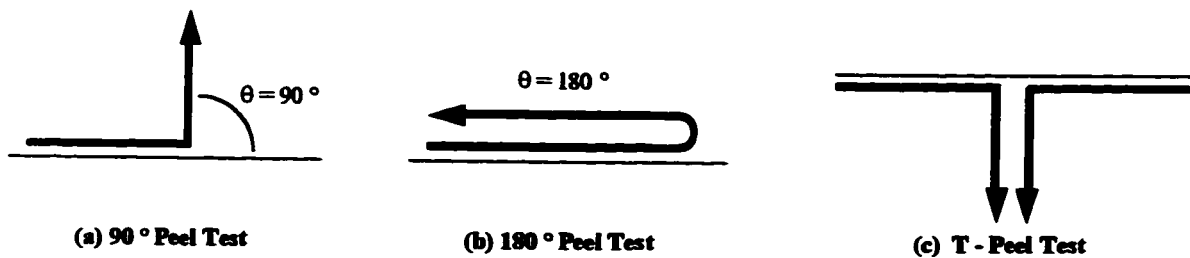
Fig. 2.2: Different peel tests.

The work of adhesion in a peel test depends upon the peel angle θ and the type of adherend. In standard peel tests, the peel angle θ is kept constant during the test. The different peel tests are classified based on angle of peel. They are the 90°-peel test, the 180°-peel test and the T-peel test as shown in Fig. 2.2. ASTM D1876 describes the T-peel test and ASTM D903 the 180°- peel test. Other configurations, such as a climbing drum peel test, a floating-roller peel test have also been developed (ASTM D1781, ASTM D3167 respectively).

The work of adhesion for the peel test is given as,

$$G = \frac{P(1-\cos\theta)}{b} \qquad (2.1)$$

In most fracture geometries (e.g., blister, scratch, etc.), the work of adhesion is the stored strain energy lost as the crack advances. To calculate this fracture energy, a stress-strain constitutive law is required. However, in the peel test, no such constitutive equation is required which makes this test advantageous for materials for which these laws are uncertain.

Conservation of energy requires that the energy supplied during peeling must equal the energy expended in the fracture processes :

Work due to peeling, E_P = surface energy expended to create free fracture surfaces, E_{Surf}

+ bulk energy dissipated within the adhesive, $E_{B,Adh}$

+ bulk energy dissipated within the stripping member, $E_{B,Strip}$

+ strain energy in the newly detached strip, E_{Strain} \qquad (2.2)

E_{Strain} is usually small and may be neglected. E_{Surf} is also called the intrinsic work of adhesion, W_A. Its value depends on the energy per unit area required only to disrupt the interactions that existed across the free surface before fracture. W_A is independent of the test rate, peeling angle, and the thickness' of the stripping members. If an adhesive bond were fractured reversibly, then the peel force would reflect only W_A. However, for normal peel testing the reversibility condition does not hold and the energy expended in fracture can be several orders of magnitude larger than W_A because of energy dissipation

18

within the adhesive and stripping member (Hamed, 1966). This is the major disadvantage of the peel test since the measurement does not give the strength of the adhesive bond at the interface and the adhesion value measured is sensitive to the test parameters.

2.2. Analysis of the Peel Test

Linear elastic analysis

Bikerman (1959) analyzed a 90°peel of a flexible ribbon adhered to a rigid substrate by a Hookean adhesive and obtained the following relation,

$$P = 0.3799b\sigma_0\left(\frac{E_r}{E_a}\right)^{1/4} t_a^{1/4} t_r^{3/4}$$

(2.3)

where P is the peel force, b the width of the ribbon, σ_0 the tensile strength of the adhesive, E_r and E_a the modulii of the ribbon and the adhesive respectively, t_r and t_a the thickness of the ribbon and the adhesive respectively. Several researchers followed up on Bikerman's analysis of the peel test with their own refinements (Kaelble, 1959; Jouwersma, 1960; Brunt, 1962 and Gardon, 1963). Kaelble's (1959) more comprehensive treatment included the dependence of peel force on the angle of peeling. Jouwersma (1960) treated the special case for the 90°peeling of an adhesive from a rigid substrate and obtained the following equation,

$$P = 0.108ebt_a E_a$$

(2.4)

where, e is the elongation at break of the adhesive and b is its width.

However, in all the analyses, the adherend and the adhesive were assumed to be linearly elastic, and the stresses were assumed to be uniform across the width and thickness of the adhesive. In a peeling experiment, both the adherend and the adhesive undergo plastic yielding and viscoelastic deformation. These provide an energy dissipation mechanism, and thus a higher peel force is required than in the purely elastic case. When the dissipations are confined to small regions in the vicinity of the locus of fracture, equations based on linear elastic behavior can still be used. However, if the deformations are substantial then they need to be accounted for.

Elastic-plastic analysis

For the case of small plastic deformations, Anderson et al. (1976) and Gent and Hamed (1977) treated the case for the peeling of an adhesive from another surface. For a 90° peel and small extensions, the work of peeling is given by,

$$W = \frac{P}{b} \qquad (2.5)$$

For zero angle peel tests, the work of peel is,

$$W = \frac{P^2}{2b^2 t_a E_a} \qquad (2.6)$$

Many practical adhesives owe their success to their ability to undergo large plastic deformations, which not only diminish stress concentration but also consume large amounts of energy. For a 90° peel and large plastic deformations, Huntsberger (1966) analyzed the peeling of a film from a rigid substrate and obtained,

20

$$P = 0.678be^{1/4}t_a\left[\frac{E_a}{\overline{\sigma}_f}\right]^{1/4}\overline{\sigma}_f \qquad (2.7)$$

where, $\overline{\sigma}_f$ is the mean stress during plastic flow.

2.3. Factors Affecting the Peel Test

2.3.1. Effect of Adhesive Thickness

Examination of Eqn. 2.4 and 2.7 shows that both elastic and highly plastic adhesive films require peel forces directly proportional to the thickness of the adhesive. This trend was confirmed at low adhesive thicknesses, for the peeling of a PET strip from a rubber substrate at a 180° peel angle (Gent and Hamed, 1977). However at higher thicknesses, the peel force was found to level off and the above equations fail to account for this. On the other hand, energy analysis correctly predicts the observed effect of the adhesive layer.

2.3.2. Effect of Adherend

Gent and Hamed (1977) studied the influence of plastic yielding within the adherend. If the adherend is linearly elastic or inextensible, no energy is dissipated in bending it. However, if it is viscoelastic, bending will cause plastic deformation of the adherend and thus increase the peel force and the fracture energy. The contribution of this additional mechanism to the peel force is complex and is influenced by a number of factors such as thickness, modulus, yield stress, and the strength of adhesion. For a PET film adhered onto a rubber covered metal plate, the PET yields plastically at a well-defined yield stress

and was used as a model elastic-plastic adherend. The maximum possible contribution to the peel strength from plastic yielding is,

$$P_{y,max} = \frac{1}{4}\sigma_y t \tag{2.8}$$

where, σ_y is the yield stress of the adherend and t is its thickness. It was shown that no contribution to the peel force from plastic flow occurs for adherends having a thickness greater than t_c :

$$t_c = \frac{12E_{ad}P_0}{b\sigma_y^2} \tag{2.9}$$

where, E_{ad} is the modulus of the adherend, P_0 is the peel force in the absence of plastic yielding.

It was found that the contribution of plastic dissipation to the total peel force was zero when the interfacial adhesion was relatively small and the adherend was sufficiently thick so that it does not undergo any plastic yielding (Gent and Hamed, 1977). Also the plastic deformation of the adherend depends upon the deformability of the adhesive. A stiffer adhesive causes a larger contribution to the peel force than a soft, deformable one. Experimentally, the peel force versus adherend thickness plot was shown to exhibit a maximum (Egan and Satas, 1966). This is in agreement with theory, which predicts that the plastic contribution is proportional to thickness at low thicknesses, but there is no contribution for thicker adherends. An indicator of extensive plastic yielding was that after peeling, the PET strip exhibited a high degree of permanent curvature and curled up on itself (Duke, 1974).

2.3.3. Effect of Temperature and Rate of Peeling

Polymers being viscoelastic materials are sensitive to deformation rate and temperature. The effects of rate and temperature on the peel force are quite complicated, causing multiple transitions in the peel force as shown in Fig. 2.3. These transitions usually arise from changes in the viscoelastic response of the adhesive, and sometimes coincide with transitions of the locus of failure from cohesive to interfacial. The effects of rate and temperature on the peel force are equivalent, and can be superimposed to give a single master curve by using an appropriate shift factor. At low rates of peel, the peel force increases with the rate (Fig. 2.3) and failure takes place entirely within the adhesive layer. At a critical rate of peel, an abrupt transition takes place to interfacial failure, i.e., clean separation of the adhesive from the adherend, at much smaller peel forces.

This transition occurs when the rate of deformation of the adhesive layer at the peeling front becomes so high that the adhesive molecules are unable to disentangle and flow apart like a liquid but remain intertwined as a coherent elastic solid. At low rates (or high temperatures) the work expended in ductile flow is large and the peel force, which measures the energy spent in peeling, is correspondingly high (Fig. 2.3). In the elastic state, the work of separation is expended mainly near the interface and it is small. The entire force-rate curves in Fig. 2.3 at different temperatures can be superimposed to give a single master curve by using the universal form of the WLF shift factor (Eqn. 2.10).

$$\log a_T = c_1 - \frac{c_2(T - T_g)}{c_3 + (T - T_g)} \tag{2.10}$$

where, c_1, c_2 and c_3 are constants and T_g is the glass transition temperature of the polymer. For many polymers $c_2 = 17.44$ and $c_3 = 51.6$ K. The WLF equation (Eqn. 2.10) is used extensively to make master curves of viscoelastic data.
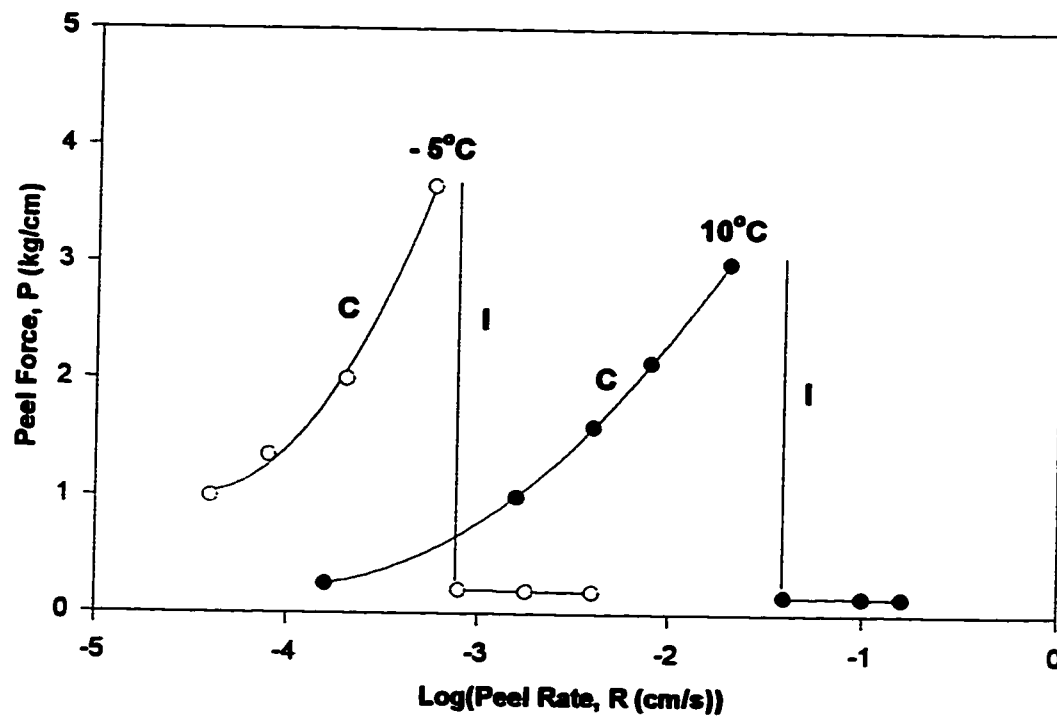
Fig. 2.3: Peel force P versus peel rate R for an un-crosslinked butadiene-styrene adhering to a PET polyester film. The symbols C and I denote cohesive failure and interfacial failure, respectively (adapted form Gent and Petrich, 1969).

Comparison of the tensile modulus of the adhesive with the peel strength shows that the transition at low rates is associated with liquid-to-rubber transition.

2.3.4. Effect of Peel Angle

Theories predict that the peel force varies inversely with $(1-\cos\theta)$ (Eqn. 2.1). Thus, the peel force should be the highest for $0°$ peel and the lowest for $180°$ peel. This has been confirmed for weak brittle joints, where dissipative processes are small (Kendall, 1976). However for stronger joints, at high peel angles near $180°$, the peel force tends to be greater than at $90°$. This was attributed to additional energy dissipation due to plastic yielding of the adherend as it bends through $180°$ (Gent and Hamed, 1977).

2.3.5. Effect of Annealing Time

Setz et al. (1996) investigated blends of polypropylene (PP) and poly(styrene)-*block*-poly(ethylene-*co*-butyl-1-ene)-*block*-poly(styrene) (SEBS). They used a $180°$-peel test configurations to obtain the interfacial bond strength between the two dissimilar phases. It was found that the peel strength increased with the annealing time and finally reaches a plateau. The levelling off was reported to be due to a saturation of the interface. Similar results were reported for the adhesion of a butadiene-acrylonitrile rubber to a poly(vinyl alcohol) (Wu, 1982). Manoj and De (1994) showed that for the adhesion of poly(vinyl chloride) to nitrile rubbers below a certain annealing temperature, annealing time has no effect on the bond strength. However, above this temperature, the bond failed at the interface for short contact times and cohesively for longer times.

2.3.6. Effect of Annealing Temperature

The effect of the bonding or annealing temperature on adhesion has been studied by several researchers (Manoj and De, 1994; Heuschling, et. al, 1994 and Sung, 1979). Manoj and De found that the adhesion increased with increasing temperature, which was due to an increase in the extent of wetting and interdiffusion, thereby leading to the formation of a strong interface. For the adhesion of polyolefins to butyl rubbers, Sung (1979) observed that the peel strength increased sharply near the melting point of the polyolefins, accompanied by a transition of the failure mode from interfacial to cohesive. This sharp increase was thought to be due to the formation of a diffuse interface. However, according to Heuschling (1994), for the adhesion of polypropylene to aluminum, the peel strength decreases with increasing annealing temperature. Heuschling suggested that low-molecular weight species present in polypropylene diffuse to the interface and form a weak boundary layer. The failure then occurs within this boundary layer instead of at the interface. This diffusion was believed to increase with temperature and thus the reduction in bond strength with temperature.

2.4 Experimental

2.4.1 Materials

Polymer systems studied using the peel test were polycarbonate (PC) with ethylene-vinylacetate copolymer (EVA) and poly(ethylene terephthalate) (PET) with EVA. The PC was provided in pellet form by GE Plastics. The PET was provided by AT Plastics as a roll of film ~0.05 mm thick. This roll had a very thin layer of a proprietary primer coated

onto one of its sides to improve adhesion between the PET and the other substrate. The ethylene-vinylacetate copolymers were also provided by AT Plastics. EVA copolymers with 10%, 16% and 29% vinylacetate content and having a melt flow index (MI) of 7, 15 and 10 (g/10min) respectively, were used in this study.

2.4.2. Sample preparation

Ethylene-vinylacetate copolymer sheets

The EVA copolymers with different VA content were provided in pellet form. They were extruded through a Killion single screw extruder to obtain sheets which were collected as rolls. The thickness of the sheets was controlled by changing the roll speed. The conditions inside the extruder were different for the different EVA's and are as reported in Table 2.1.

	10%EVA	16%EVA	29%EVA
Screw Speed (rpm)	40	40	40
Melt Temperature (°C)	181	145	160
Barrel Zone Temperatures (°C)			
Number 1	155	125	145
Number 2	160	135	150
Number 3	165	145	155

Table 2.1: Operating conditions inside the Killion single screw extruder

Polycarbonate sheets

A rectangular mold was cut out from a sheet of aluminum foil using a knife. Polycarbonate pellets were placed into this mold and the mold was placed between steel plates (30 cm × 30 cm × 6 cm) and covered with aluminum foil. A Wabash Hydraulic Plate Press, Model #:30-1212-HMBX, was heated to 200°C using hot oil as the heating medium. The steel plates with the mold between them was placed into the press. The press was closed and heating was carried out at 200°C with minimal pressure for 3 minutes. The pressure was increased to 10 tons and this was maintained for 10 minutes. After this heating cycle, the press opened automatically, the mold was taken out and left to cool in air. The PC sheet was taken out of the mold and cut up into rectangular pieces, 7 cm wide and 10 cm long.

Annealing and preparing PC and EVA sheets for peel testing

An EVA sheet (30 × 15 cm^2) was cut out from the roll of film obtained using the extruder. The smaller rectangular PC sheet (10 cm × 7 cm) was placed in the center of this sheet. Teflon sheets were placed on either side and provided smooth, non-stick surfaces. The sample was placed between the platens of a Carver Model C laboratory press at the desired temperature for a certain amount of time. Minimal pressure was applied onto the sample while annealing. The sample was taken out and placed between aluminum plates to cool. After about 5 mins, the aluminum plates and the Teflon sheets were removed. The annealed PC/EVA sample was cut up into smaller pieces approximately 25 mm wide. Since the EVA sheet is longer than the PC sheet, some EVA was hanging from both sides.

One side of the EVA was cut off, while the other was peeled back a short distance so as to expose a little of the PC sheet. The sample obtained was as shown in Fig. 2.4a and is ready for peel testing.

Annealing and preparing PET and EVA sheets for peel testing

PET and EVA sheets (30×15 cm^2) were cut out from their respective rolls. The EVA was placed onto the primed side of the PET sheet and Teflon sheets were placed on either side. A small piece of Teflon tape was placed between the PET and EVA sheets so as to provide a short unadhered part. This arrangement was placed into a Carver Model C laboratory press for annealing at a fixed temperature. Minimal pressure was applied. After a pre-determined amount of time (which will be referred to as the annealing time in the following text), the sample was placed between aluminum plates and air-cooled for about 5 min. The PET/EVA sample was cut up into smaller samples approximately 25 mm wide. The sample obtained was as shown in Fig. 2.4b and is ready for peel testing.

2.4.3. Peel Testing

An INSTRON Model #1130 tensile tester was used for peel testing. This machine was equipped with pneumatic grips, where the lower grip was fixed while the upper grip could move at a fixed rate. The speed of the crosshead could be controlled by changing drive gears. The slowest speed possible in this machine was 50 mm/min and this was the speed used for our testing. The loadcell was a 500N tension load cell. As the test progresses, the force required during peeling is continuously recorded by the chart recorder.

For the PC/EVA system (Fig. 4a), the exposed part of the PC sheet was inserted into the lower grip. The hanging EVA was pulled back and clamped into the upper grip so that the EVA would be peeled off the PC at an angle of ~180°. The test was started and the EVA was peeled off at a rate of 50 mm/min as shown in Fig. 2.4a. For the PET/EVA system (Fig. 4b), the EVA is clamped into the lower grip, while the PET is clamped into the upper one. The peeling is carried out at a rate of 50 mm/min. and the peel configuration is like a "T" as shown in Fig. 2.4b.
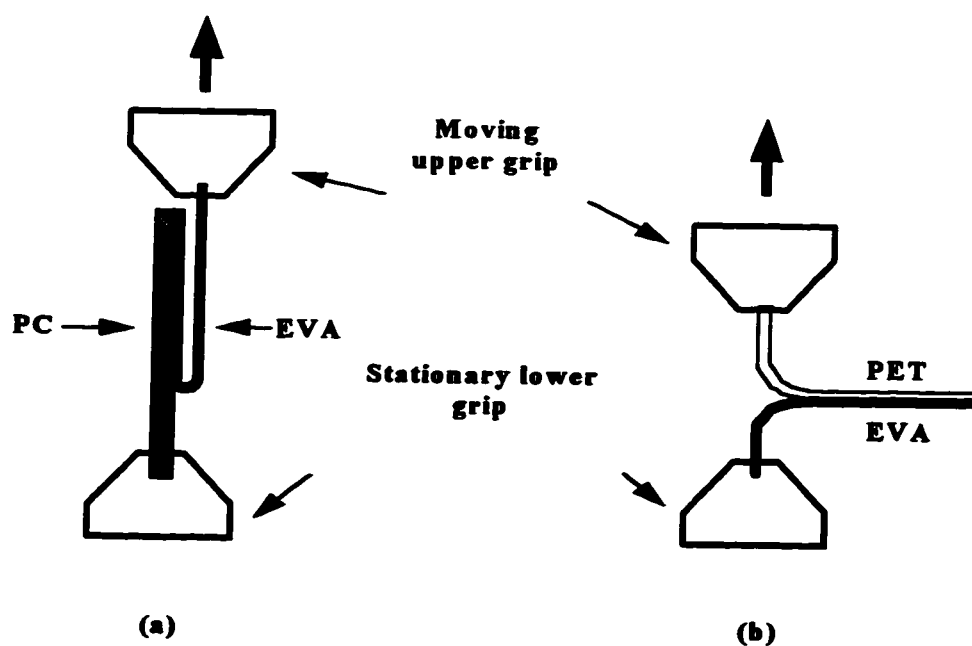
Fig. 2.4. Schematic of the peel test configuration. (a) PC/EVA system with a 180°-peel configuration, (b) PET/EVA system with a T-peel configuration.

2.5. Results

2.5.1. Calculation of the Work of Adhesion

The force required for peeling is measured along the length of the sample and this force is representative of the adhesion at the interface. Typical curves obtained during peeling, as recorded by the chart recorder, are shown in Fig. 2.5. The x-axis is the distance traveled by the crosshead while the y-axis is the load in Newtons. The load increases initially and then stays fairly constant as shown in Fig. 2.5a. However, in Fig. 2.5b the fluctuations in the load are large and these indicate non-uniform adhesion along the sample length. These fluctuations will be discussed in detail later in this chapter.
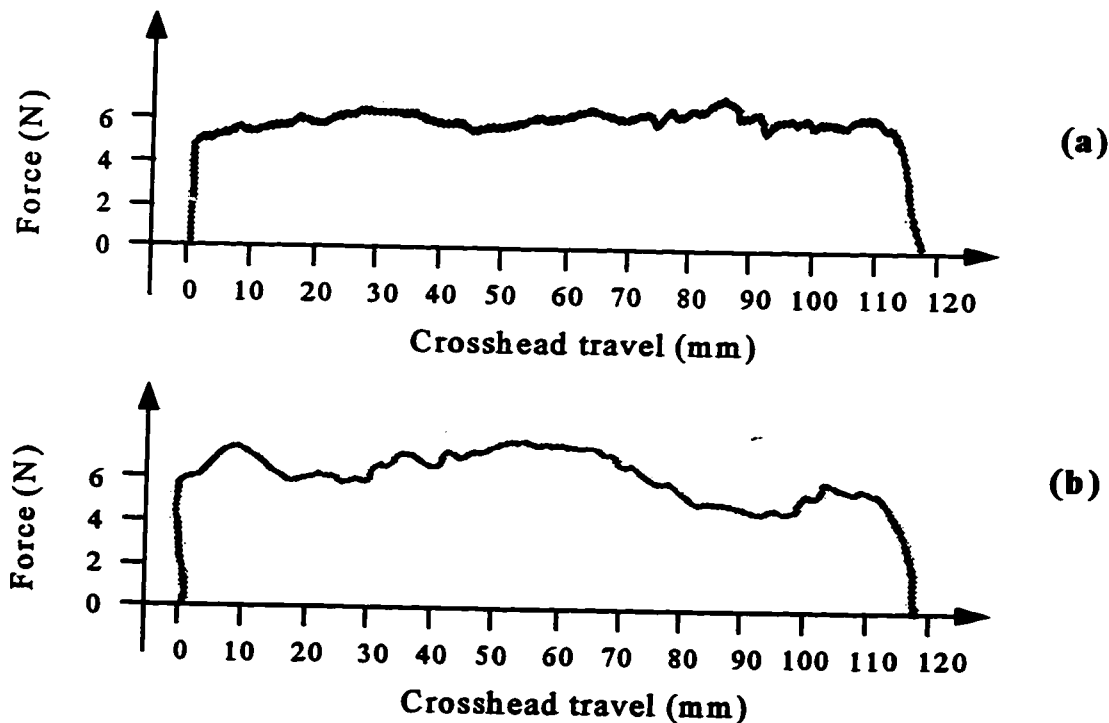
Fig. 2.5. Force or load versus the distance traveled by the crosshead on the INSTRON Model #: 1130. (a) Load stays fairly constant (PC/16% EVA system annealed at 150°C for 15 minutes). (b) Load fluctuates (PC/10% EVA annealed at 100°C for 20 minutes).

To calculate the average force during peeling, the area under the load versus crosshead motion (F vs. x) curve was found and divided by the total displacement:

$$\overline{F} = \frac{\int F dx}{\int dx} = \frac{Area \ under \ curve}{Distance \ moved \ by \ crosshead} \tag{2.11}$$

To measure the area, NIH Image Analysis software Version 1.57 was used. The curves obtained from the chart recorder were scanned and then analyzed using this software.

For the PC/EVA system, since the configuration was a 180° peel, from Eqn. (2.1), the work of adhesion was calculated as:

$$G = \frac{2\overline{F}}{b} \tag{2.12}$$

where, b is the width of the sample. However, for the PET/EVA system, since the configuration was a T-peel, the work of adhesion is given by:

$$G = \frac{\overline{F}}{b} \tag{2.13}$$

In the peel test, due to the large amount of energy dissipated during testing, the interfacial bond strength is usually not expressed as the work of adhesion. Rather, it is represented as the peel strength and we shall use this terminology. This peel strength has the units of J/m^2. The data for average force and the peel strength for the two systems are summarized in Appendix 2.

2.5.2. Effect of Annealing Time

A study was performed on the effect of the annealing time on the adhesion between PC and the different EVA's and between PET and the EVA's. Annealing time was expected to yield better adhesion between the phases due to increased wetting and interdiffusion of the polymer molecules. As explained in §.1.3.2., in immiscible polymers, it is local segmental diffusion occurring across the interface that leads to an improvement in adhesion.

Polycarbonate / Ethylene-vinylacetate copolymer
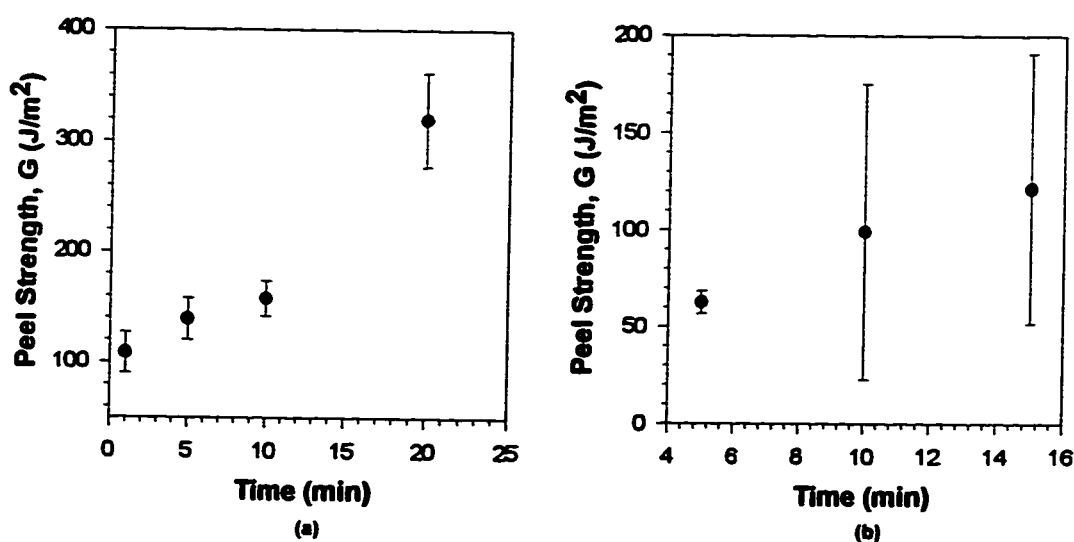
Fig. 2.6. Peel strength versus annealing time for the adhesion of polycarbonate to (a) 16% EVA and (b) 29%EVA, the annealing temperature for both was 100°C.

For the adhesion of the PC to the EVA's, results were obtained for the systems of PC/16%EVA and PC/29%EVA. The adhesion between PC and the 10%EVA was too

weak to be detected. For the PC/16%EVA and PC/29%EVA systems annealed at 100°C the peel strength increases with annealing time as shown in Fig. 2.6. On visually examining the surfaces of the peeled strips after the test, it was concluded that the failure was interfacial in all cases since there were no discontinuities on the sample surfaces.

For the 16% EVA the peel strength increases sharply after 10 minutes of annealing. This could be due to the fact that for an annealing time of less than 10 minutes, the 16% EVA does not wet the surface of the PC completely. After sufficient time has been provided for wetting, interdiffusion of the 16% EVA and PC may occur, thus improving the adhesion. On the other hand, for the 29% EVA, the time required for wetting the PC seems to be shorter. It has been shown that the optimum condition for wetting and adhesion is the matching of the polarities of the two phases (Kaelble, 1971 and Wu, 1982). An increase in the vinylacetate content in the EVA's results in increased polarity of the copolymer, due to the polar nature of the acetoxy side chain. Thus, the reduction in the time required for wetting with vinylacetate content could be because the polarity of the 29% EVA is much closer to that of the PC than the 16% EVA.

Poly(ethylene terephthalate)/Ethylene-vinylacetate copolymer

For this system, the EVA's used were 10%, 16% and 29%. The results are as shown in Fig. 2.7 for the adhesion of 10% and 29% EVA. These results also show the same trend as that observed for the PC/EVA system. For the 10% EVA, around 55 minutes are required to obtain a substantial improvement in adhesion with time, whereas for the 29% EVA, only around 1 minute is required. This may again be due to the effect of polarity.

34
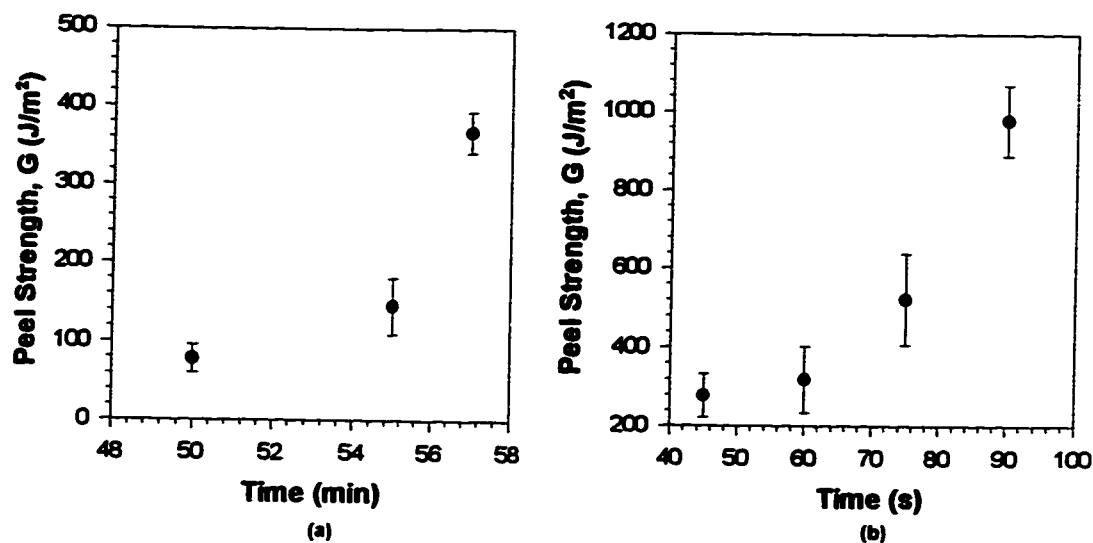
Fig. 2.7. Peel strength versus annealing time for the adhesion of poly(ethylene terephthalate) to (a) 10% EVA and (b) 29%EVA, the annealing temperature for both was 100°C.

2.5.3. Effect of Annealing Temperature

Polycarbonate / Ethylene-vinylacetate copolymer

The peel strength results for two annealing temperatures are shown in Fig. 2.8. For the 16% EVA, there does not seem to be any significant effect of the annealing temperature on the peel strength over the temperature range studied. A larger range of annealing temperatures was not tried since below 100°C there was no detectable adhesion and above 150°C, the EVA flowed extensively causing the sample to deform. However, for the 29% EVA, there is some improvement in adhesion after a contact time of 10 minutes for the sample annealed at 150°C compared to that annealed at 100°C.
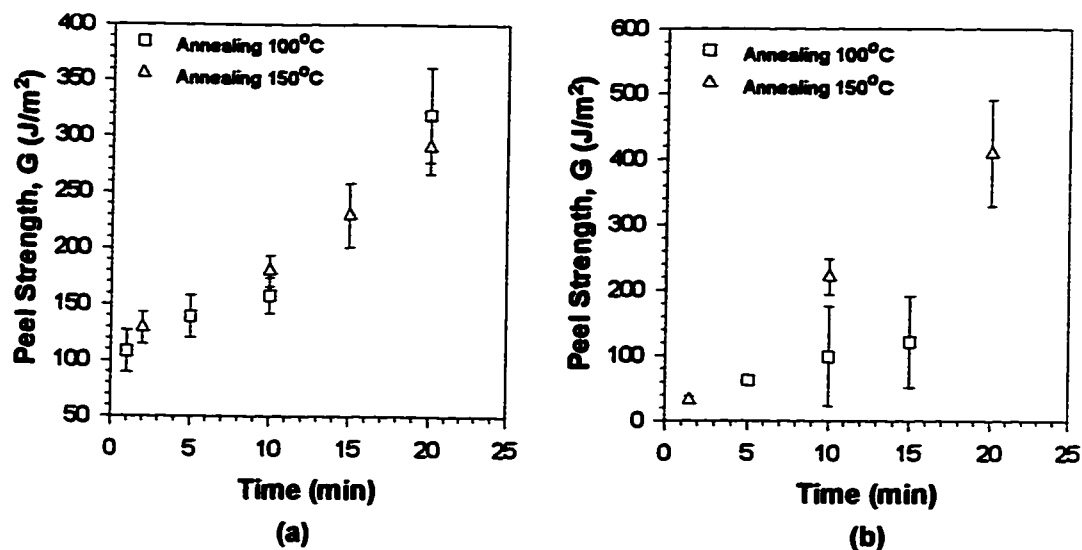
Fig. 2.8. Peel strength versus annealing time at two different annealing temperatures for the adhesion of PC to (a) 16% EVA and (b) 29% EVA.

Poly(ethylene terephthalate) / Ethylene-vinylacetate copolymer

The effect of annealing temperature on the PET/EVA system is as shown in Fig. 2.9. The peel strengths for the 10% and 29% EVAs adhered to PET could not be measured for the same contact time range since at low times the adhesion between the 10% EVA and the PET was too low to be detected and at high times, the 29% EVA flowed excessively. From Fig. 2.9, we can see that for the same peel strength, the annealing time required at 100°C is much greater than those annealed at 150°C. Approximately 1 minute is required to get detectable values for the 29% EVA/PET samples annealed at 100°C; while for samples annealed at 150°C, there is measurable adhesion at 2 seconds.
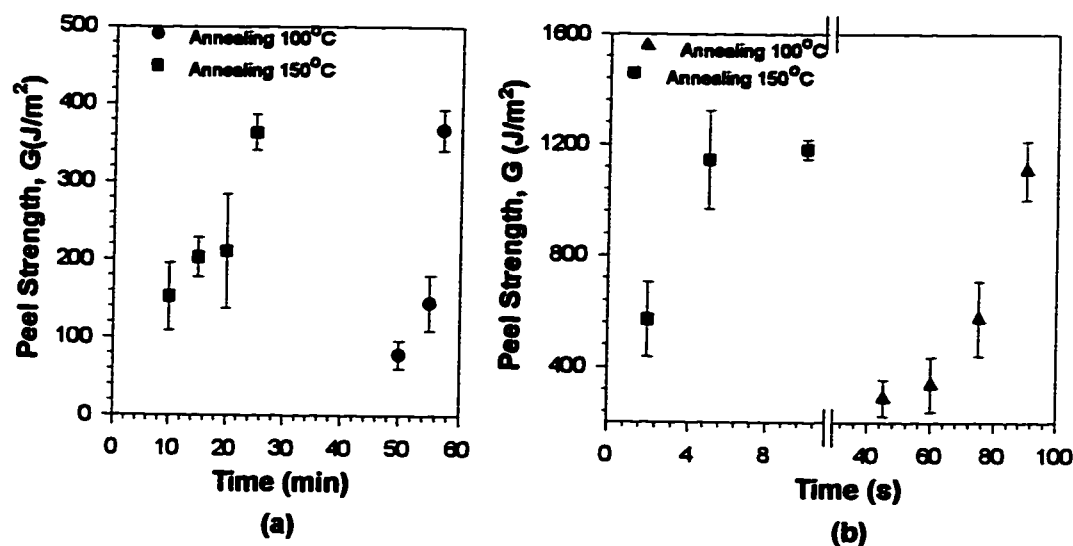
Fig. 2.9. Peel strength versus annealing time at two different annealing temperatures for the adhesion of PET to (a) 10% EVA and (b) 29% EVA.

2.5.4. Effect of Thickness of EVA

As mentioned in §. 2.4.2, a number of smaller samples were cut out from the PET/EVA sample obtained after annealing. After testing these samples an average of the peel strengths was taken. Although these samples were cut out from the same sample, they had slightly different thicknesses. This was because while annealing in the Carver Model C laboratory press, the slight pressure applied may not have been uniform across the sample. Due to this, the EVA was thicker on one side. On testing the above samples, some dependence of the peel strength on the thickness of the EVA was noticed. This can be seen in Fig. 2.10, where each point represents one sample. We see that the peel strength decreases with increasing thickness of the EVA. This prompted us to look at the effect of thickness of the EVAs on the adhesive strength. Not only was there a difference

in thickness between individual samples, but each sample varied in thickness across its length. However, this variation was marginal when compared to the difference in thickness between two samples.
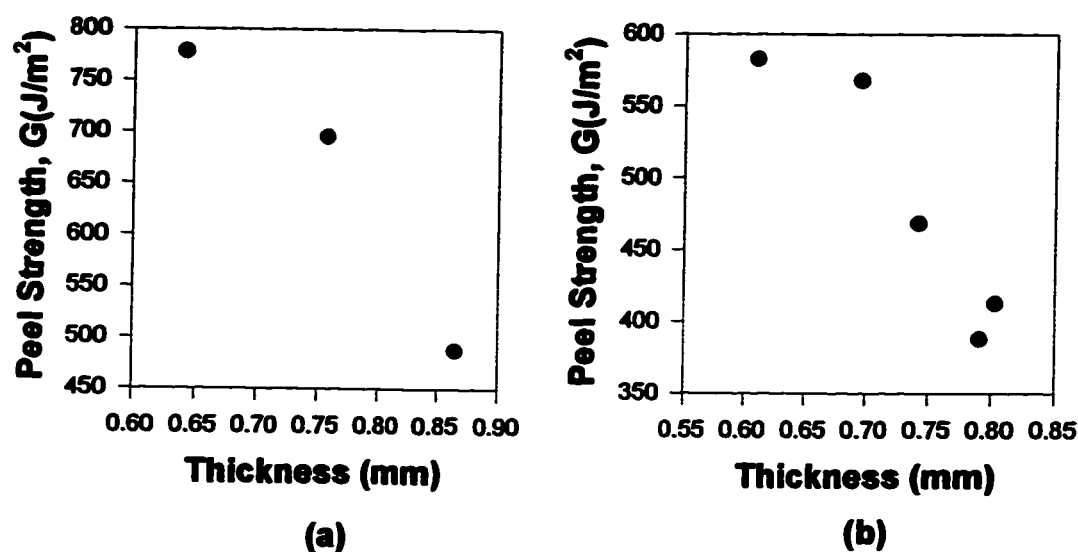
Fig. 2.10. Peel strength versus thickness of the 16% EVA for the adhesion of 16% EVA and PET. Samples annealed at 100°C.

EVA sheets of different thicknesses were produced using the Killion single screw extruder by changing the screw speed. Samples of the EVAs were adhered onto the PET sheets and these were tested following the same procedure as outlined in §. 2.4.2. The results obtained are as shown in Fig. 2.11 for the 16% and 29% EVAs. As can be seen in Fig. 2.11, for both the 16% and 29% EVAs, there is a critical EVA thickness for the highest peel force.
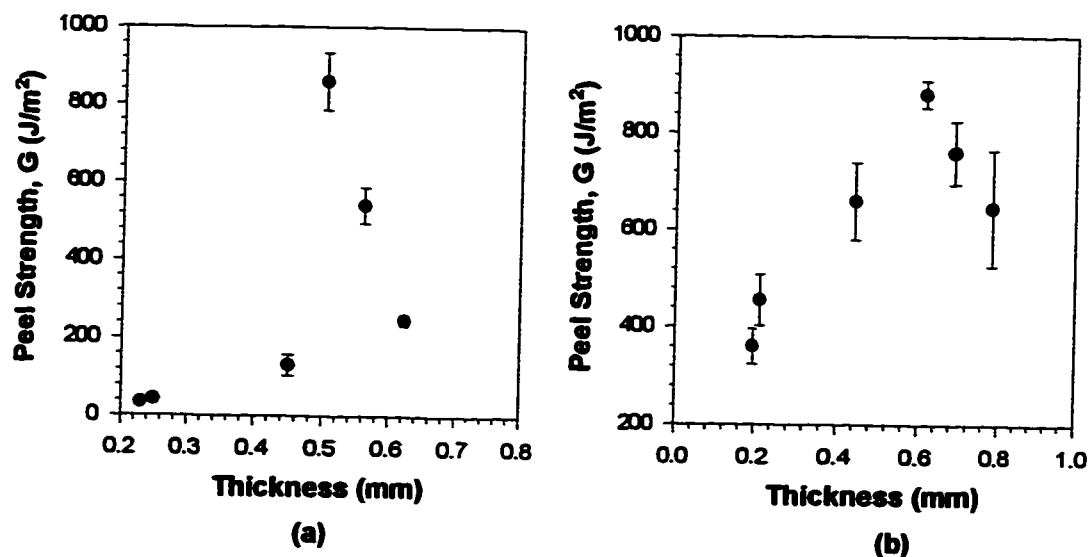
Fig. 2.11. Peel strength versus thickness for the adhesion of PET to (a) 16% EVA and (b) 29% EVA. Samples annealed at 100°C.

Although theory predicts that the peel strength should increase as the thickness of the adhesive layer is increased (Eqn. 2.4 and Eqn. 2.7), the phenomena of a maximum peel strength at a critical thickness has been reported by a number of workers (Egan and Satas, 1966; Gent and Hamed, 1977; Kinloch et. al, 1994). For a sufficiently long peeling strip, no energy is dissipated within the adherend provided that the strip is elastic. However, if the adhesion is very strong, or if the peeling strip is sufficiently thin, bending stresses may lead to the plastic deformation of the strip during the course of peeling. As explained in §.2.3.2, Gent and Hamed (1977) proposed an additional force, P_y, due to this plastic yielding. Also, P_y is greater the thicker the peeling strip (Eqn. 2.8).

Since in our system, the adhesion of PET to the EVAs is extremely good, the phenomenon seen in Fig. 2.11 is explained on the basis of plastic deformation of the EVA strip. This can be understood by refering to Fig. 2.12.
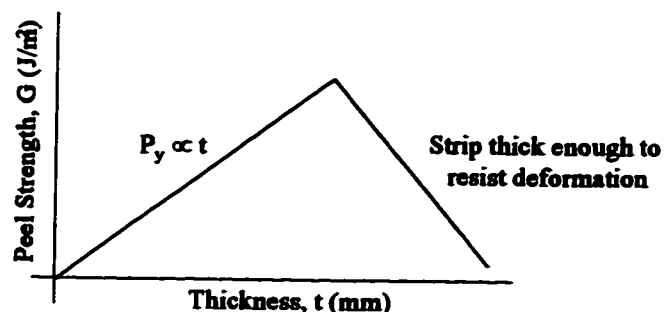
Fig. 2.12. Dependance of peel strength on thickness of peeled strip

For a given degree of adhesion the very thin strips of the EVAs will undergo complete plastic yielding on peeling. However, the total energy dissipated in this way is small as the thickness of the peeling strip is small. Hence, both the additional force P_y and the total peel strength will be small at these low thicknesses as seen in Fig. 2.12. As the strip thickness is increased, more energy will be dissipated in yielding and P_y will rise. The peel strength consequently rises and reaches a maximum. However, beyond a certain thickness (approximately 5 mm for 10% EVA and 6 mm for 29% EVA) as the thickness increases, the backing will not experience sufficiently large bending stresses to cause yielding so that the peel strength decreases. Additionally, one can see from Fig. 2.11 that the maximum obtained in the peel strength is sharper for the adhesion of the 10% EVA to PET as compared to that for the 29% EVA. The 29% EVA has a lower modulus than the 10% EVA. As the strip thickness increases, the 10% EVA cannot withstand large bending stresses and undergoes a more sudden change than the 29% EVA. As already mentioned

above, one of the conditions for a maximum in peel strength with increasing thickness is strong adhesion between the adherends leading to plastic deformation of the peeling member. The adhesion for the PC/EVA system was weak compared to the PET/EVA system and hence no maximum is observed for this system.

2.5.5. Fracture Surface Analysis

Microscopy was used to observe the various surface characteristics of the peeled samples. A HITACHI S-2700 scanning electron microscope (SEM) was used to examine selected surfaces. The fracture surfaces for the PC/EVA system were smooth and had no structure. This led to the conclusion that the failure for this system was purely interfacial. However, for the adhesion of the EVAs to the PET, some of the fracture surfaces exhibited striations and deformities on the surface. This indicated cohesive failure within the EVA. Micrographs of the surface of 16% EVA for its adhesion to PET annealed at 100°C are shown in Fig. 2.13. Fig. 2.13 shows the difference in the structure of the fracture surface depending on the annealing time. The samples were being peeled from the right to the left. On annealing the 16% EVA to the PET for 15 s., the surface was smooth and there was no detectable adhesion (Fig.2.13a). On increasing the annealing time to 20 s., the fracture surface showed thumbnail shaped cracks, all of which pointed in the same direction (Fig. 2.13b). This is the direction in which the PET was peeled off from the surface of the EVA. As the annealing time increased to 30 s., the EVA surface became rougher (Fig. 2.13c) and the size of the cracks increased, indicating extensive plastic deformation of the EVA.
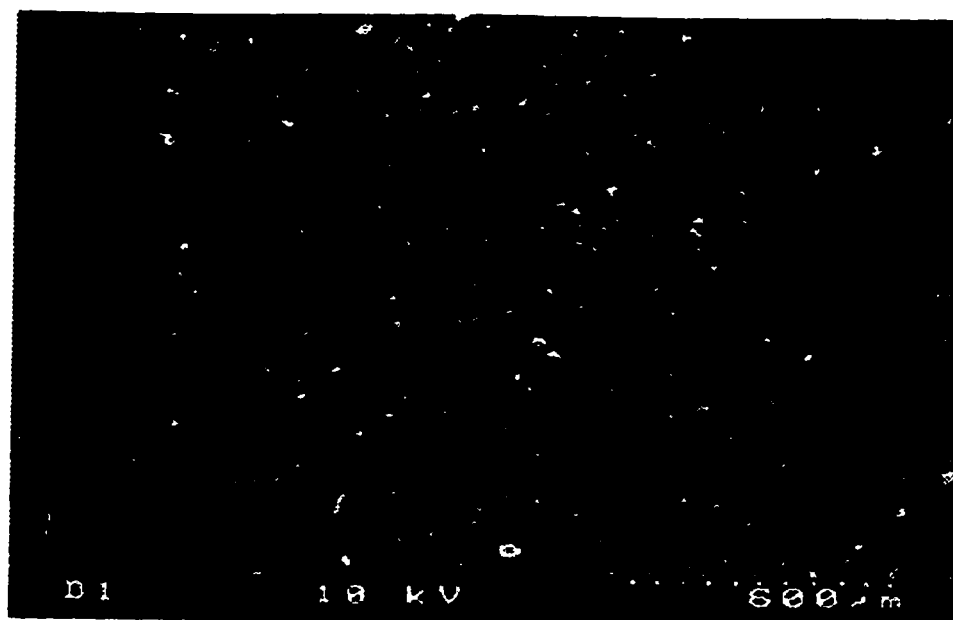
(a)
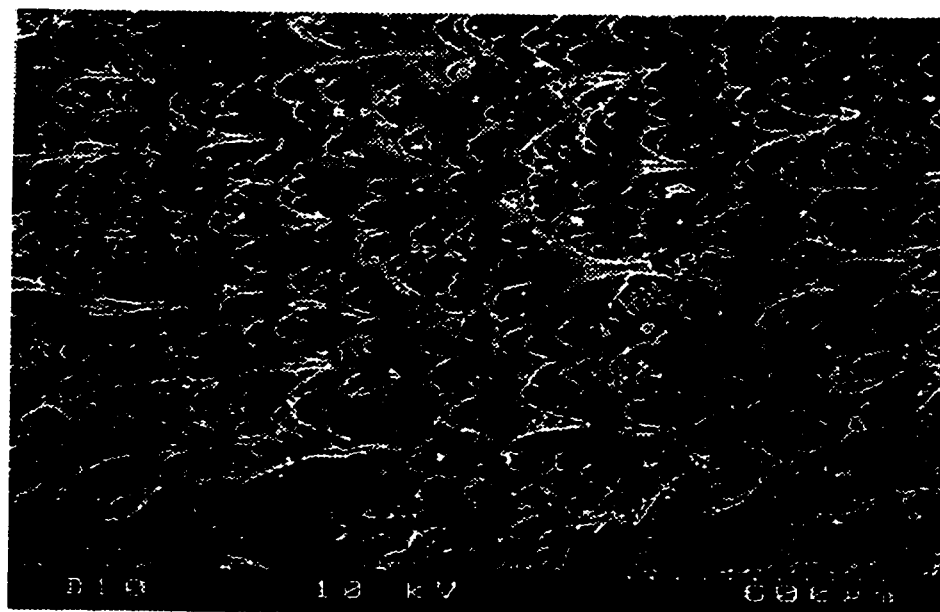
(b)

Fig. 2.13. Fracture surfaces of 16% EVA strips after peeling from
the PET at a rate of 50 mm/min. Samples annealed for (a) 15 seconds,
(b) 20 seconds, (continued on next page......)
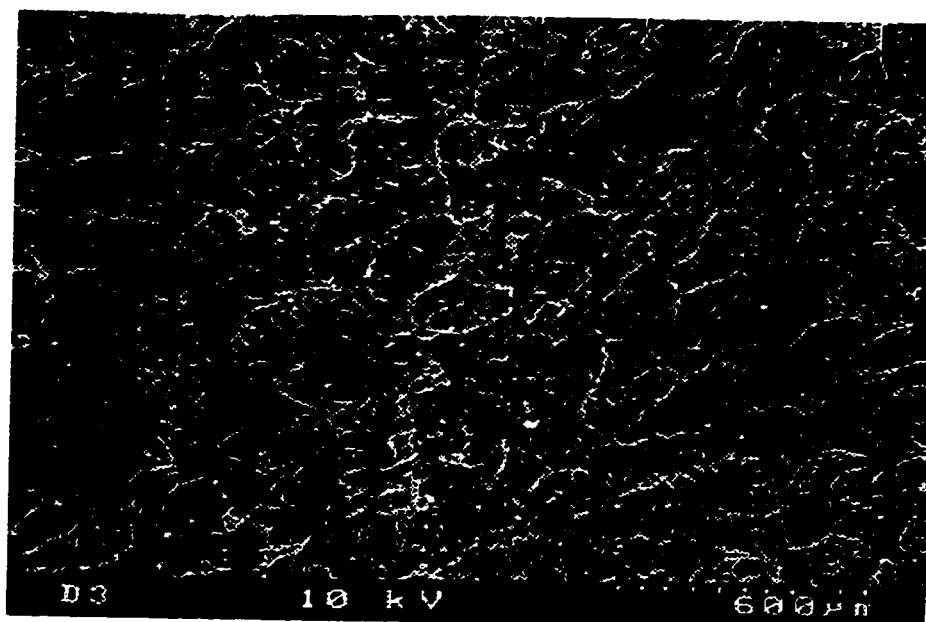
(c)
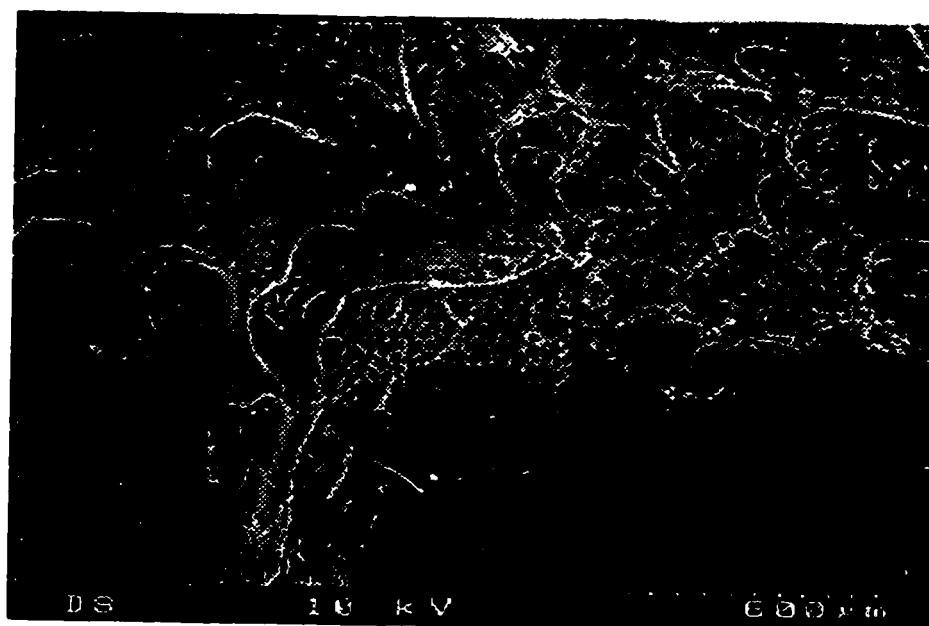
(d)

Fig. 2.13. (...continued) Fracture surfaces of 16% EVA strips after peeling
from the PET at a rate of 50 mm/min. Samples annealed for (c) 30 seconds,
(d) 45 seconds.

For an annealing time of 45 s., the cracks are large (~ 0.2 mm) and the surface is extremely rough. Additionally, as the annealing time increases, the peel strength for the adhesion of the 16% EVA to the PET increases, as shown in Fig. 2.14. This increase in peel strength may partly be a result of improved adhesion, but may also be due to the extra energy being dissipated in plastically deforming the EVA.
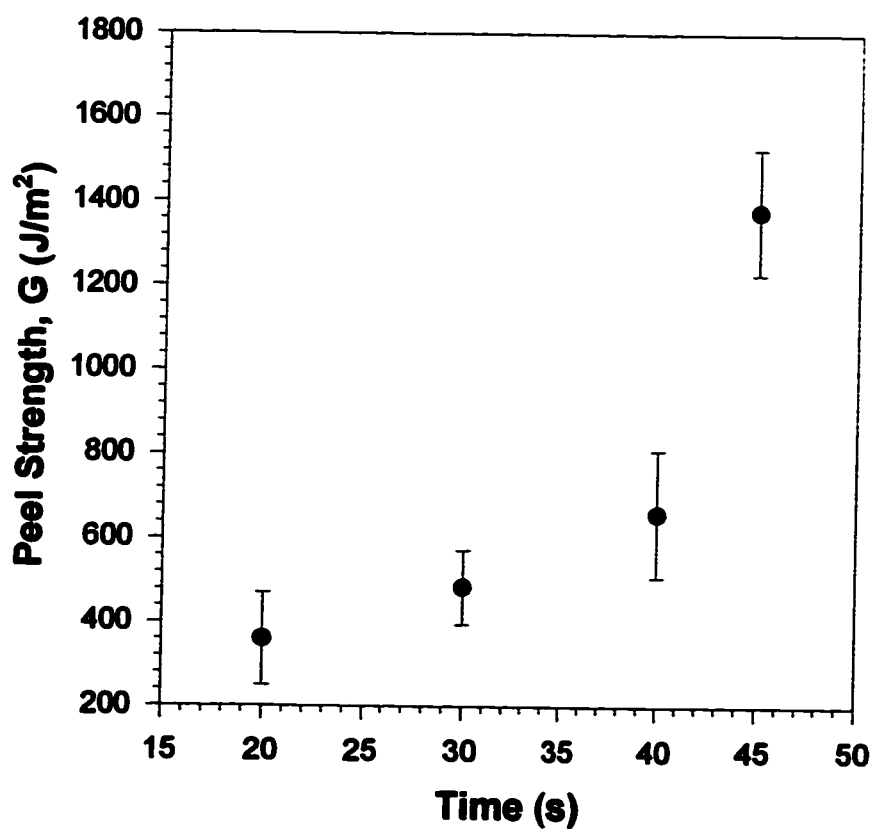
Fig. 2.14. Peel strength versus the annealing time for the adhesion of the 16%EVA to PET annealed at 100°C.
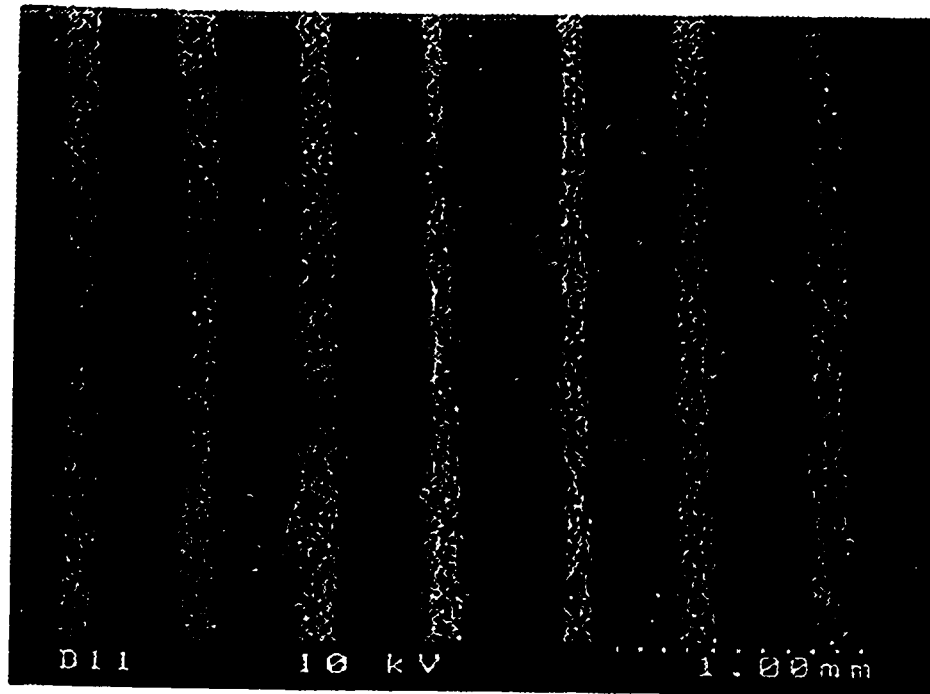
(a)
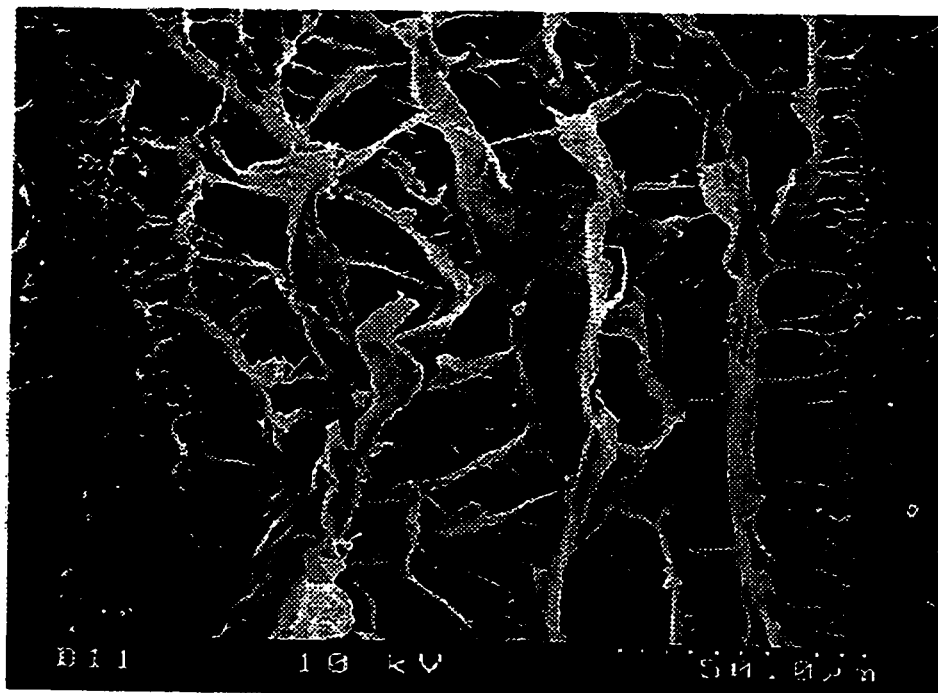
(b)

Fig. 2.15. Fracture surface of 10%EVA after peeling from the PET at a
rate of 50 mm/min. (a) regularly spaced striations on the surface,
(b) magnified view of inside of one of the striation.

For the adhesion of the 10% EVA to the PET, the fracture surface of the sample annealed at 100°C consisted of regularly spaced striations on the surface as shown in Fig. 2.15. On observing one of these at higher magnifications (Fig. 2.15b), it was observed that each of these striations had some structure within it. This structure could be due to the EVA tearing off in these regions. The load curve obtained for this system is shown in Fig. 2.16. The peel force fluctuates wildly with alternate peaks and valleys which are regularly spaced. It was speculated that the force fluctuations correspond to the striations.
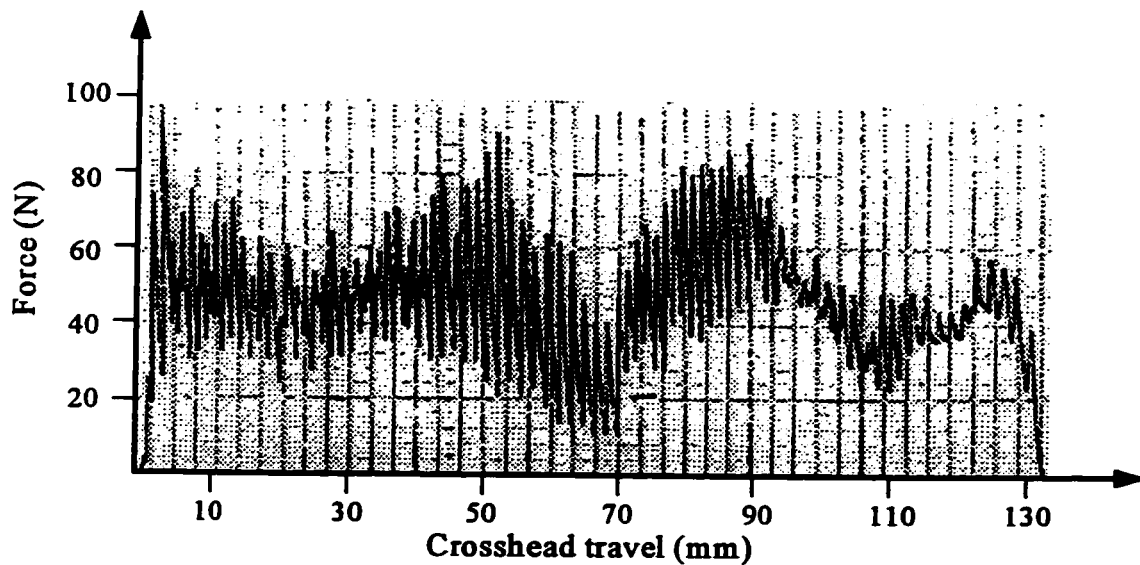
Fig. 2.16. Force versus crosshead displacement curve for the adhesion of 10%EVA to PET at an annealing temperature of 100°C for 15 minutes showing fluctuations in the peel force.

To verify if each striation on the fracture surface represents a peak, the distance between alternate striations on the surface of the 10% EVA was calculated and compared with the distance between successive peaks on the peel force curve. It was found that the distance between the centers of alternate striations was 0.503 mm while the distance between successive peaks was 0.489 mm. This confirms the fact that the peel force rises sharply

46

and this rise corresponds to a striation on the surface of the 10% EVA. Between these striations were regions of poor adhesion and these corresponded to the valleys in the force curve. The reason for these striations is not clear. Racich and Koutsky (1975) found striations on the surfaces of their peeled samples. However, these striations were not as prominent and regular as the ones obtained in this work. They theorized that the striations were due to substrate roughness effects. This led to the examination of the surface of the extruded 10% EVA in more detail under a BHSM Metallurgical optical microscope. It was found that there appeared to be regular marks running perpendicular to the direction of peel on the surface and could be an artifact of the extrusion process.

2.5.6. Comparison of the EVAs

For the adhesion of the PC to the EVAs (16% and 29%) it was found that as a function of the annealing time the adhesion for the PC/29% EVA system was higher than that for the PC/16% EVA system, as shown in Fig. 2.17. In both systems, the adhesion increased with annealing time. For the PET/EVA system, the 10%, 16% and 29% EVAs were compared and the results are shown in Fig. 2.18. The time required to get a detectable adhesion value was the lowest for the 16% EVA while it was the highest for the 10% EVA. Also the maximum peel strength that could be obtained was the highest for the 16% EVA and the lowest for the 10% EVA. The large differences between the two systems in the time required to obtain good adhesion and in the measured peel strength was attributed to the higher polarity of the 16% EVA over the 10% EVA.

47
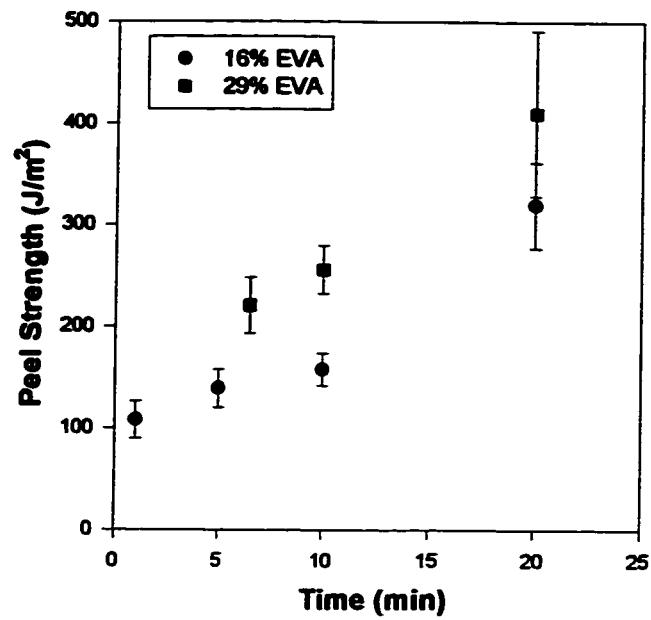
Fig. 2.17. Peel strength versus annealing time for the adhesion of PC to two different EVAs, i.e. 10% EVA and 29% EVA.
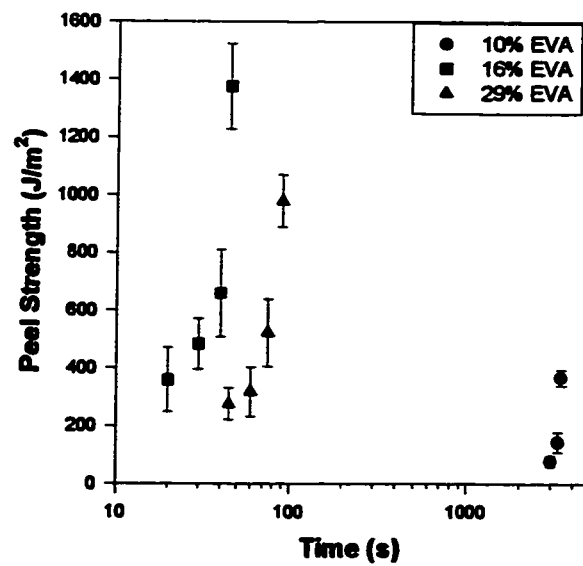
Fig. 2.18. Peel strength versus annealing time for the adhesion of PET to 10%, 16% and 29% EVA. Samples annealed at 100°C.

However higher adhesion was obtained for the 16% EVA versus the 29% EVA though the latter has a higher polarity. Although the increase in polarity probably resulted in improved compatibility between the PET and the EVA and therefore better adhesion, this effect may be overshadowed by the higher melt flow index (MI) for the 16% EVA (15 g/10min) versus the 29% EVA (10 g/10min). A higher MI implies a lower molecular weight and lower viscosity. This means that the polymer molecules are more mobile than those for the lower MI polymer. Increased mobility of the 16% EVA molecules leads to better wetting of the surface and faster diffusion of the molecules to the interface, and thereby leads to the formation of a strong bond at the interface.

2.6. Conclusions

The peel test is a convenient test to quantify the adhesion between polymers. It is fast and easy to set up. However, this test depends on many variables and therefore it is unsuitable for product development purposes. It should be used primarily as a quality control tool to distinguish between the adhesive performance of different batches of an established product.

It was found that for both the PC/EVA and PET/EVA systems, the peel strength increases with the annealing time. This increase was due to the better wetting achieved by the EVA on the substrate surface. The effect of annealing temperature on peel strength was weak for the PC/EVA system. This could be due to the small temperature range

studied (100°C-150°C). However, for the PET/EVA system an increase in temperature reduced the time required to get a detectable adhesion value. For the 10%EVA, the annealing time was reduced from 50 min. to 10 min. as the temperature was increased from 100°C to 150°C. For the 29%EVA, the reduction in annealing time was from 40 s. to 2 s. when the temperature was increased from 100°C to 150°C.

The effect of thickness on the adhesion between PET/EVA was studied and it was found that there was a maximum in the peel strength as the thickness was increased. For the 16%EVA, a maxima in peel strength was found at ~ 0.5 mm, while for the 29%EVA, this maximum occurs at ~ 0.6 mm. The maximum was thought to be a result of the plastic deformation of the EVA strip as the sample was peeled. There was a critical thickness beyond which the EVA strip was thick enough to resist these deformations. Thus, for testing of the PET/EVA system, the thickness of the EVA strip should be greater than this critical thickness.

The surfaces of the strips after peeling were analyzed for cohesive or interfacial failure. Failure was interfacial for the PC/EVA system. But, for the PET/EVA system, the failure was mostly cohesive. The surfaces of the EVAs for the PET/EVA system showed deformities which were thumbnail shaped and were all pointing in the direction of peel. These were thought to be a result of the phenomenon of stick-slip which takes place as the peeling progresses. The surface of the 10%EVA for the PET/10%EVA system, showed regular striations on the surface which corresponded to fluctuations in the peel

force. These striations were thought to be a result of asperities on the surface of the 10% EVA.

On comparing the different EVAs in their adhesion to PC, it was found that the adhesion increased with VA content. This increase in peel strength with VA content was attributed to the increase in polarity of the EVA as the VA content is increased. An increase in polarity makes the 29% EVA more compatible with the PC than the 10% EVA. On comparing the PET/EVA system, it was found that for the PET/10%EVA system, the peel strength was the lowest and also the time required to get detectable adhesion was large. The PET/16%EVA had better adhesion compared to the PET/29%EVA and in addition, the time required for adhesion of the 16% EVA was lower than that for the 29% EVA. This was attributed to the fact that the 16% EVA has a higher MI than the 29% EVA which led to better wetting and interdiffusion and therefore better adhesion. The effect of MI overshadows the effect of the increase in polarity on the adhesion. Thus, while the VA content plays a role in determining the compatibility of the EVAs, it is also important to consider the MIs or molecular weights of the EVAs.

2.7. References

Anderson, G. P., DeVries, K. L., and Williams, M. L., *Expmtl. Mechanics* 16, 1(1976).

Aubrey, D. W., Welding, G. N. and Wong, T., *J. Appl. Polym. Sci.* 13, 2193(1969).

Bikerman, J. J., *J. Appl. Polym. Sci.* 2, 216(1959).

Bonnerup, C., and Gatenholm, P., *J. Adhesion Sci. Technol.* **7**, 247(1993).

Brunt, N. A., *J. Appl. Polym. Sci.* **23**, 548(1962).

Chnsirikul, W., Chung, T. C., and Harrison, I. R., J. *Thermplastic Comp. Mat.* **6**, 18(1993).

Duke, A. J., *J. Appl. Polym. Sci.* **18**, 3019(1974).

Egan, F. L. and Satas, D., *Adhes. Age* **9**, 22(1966).

Gardon, J. L., *J. Appl. Polym. Sci.* **7**, 625(1963).

Gardon, J. L., *Treatise on Adhesion and Adhesives*, ed. R. L. Patrick (Marcel Dekker, New York., 1966), Vol. 1, pp. 269.

Gent, A. N. and Hamed, G. R., *J. Appl. Polym. Sci.* **21**, 2817(1977).

Gent, A. N. and Hamed, G. R., *Polym. Eng. Sci.* **17**(7), 462(1977).

Gent, A. N. and Hamed, G. R., *Rubber Chem. Technol.* **55**, 483(1982).

Hamed, G. R. and Shieh, C. H., *Rubber Chem. Technol.* **55**, 1469(1982).

Hamed, G. R., *Treatise on Adhesion and Adhesives*, ed. R. L. Patrick (Marcel Dekker, New York, 1966), Vol. 6, pp. 33.

Huntsberger, J. R., *Treatise on Adhesion and Adhesives*, ed. R. L. Patrick (Marcel Dekker, New York, 1966), Vol. 6, pp. 1.

Jouwersma, C., *J. Polym. Sci.* **45**, 253(1960).

Kaelble, D. H., *Trans. Soc. Rheol.* **3**, 161(1959).

Kinloch, A. J., Lau, C. C., and Williams, J. G., *Int. J. Fracture* **66**, 45(1994).

Manoj, N. R., and De, P. P., *J. Elast. Plast.* **26**, 265(1994).

Racich. J. R. and Koutsky, J. A., *J. Appl. Polym. Sci.* **19**, 1479(1975).

Setz, S., Stricker, F., Kressler, J., Duschek, T., and Mulhaupt, R., *J. Appl. Polym. Sci.* **59**, 1117(1996).

Sung, N. H., *Polym. Eng. Sci.* **19**, 810(1979).

Whang, W., and Cheng, W., *Polym. Eng. Sci.* **35**, 666(1995).

Wu, S, *Polymer Interface and Adhesion*, Marcel Dekker, New York, 1982.

CHAPTER 3

The Double Cantilever Beam Test

3.1. Introduction

One of the areas where adhesion is particularly important is in blends of polymers. There has been significant effort in recent years to produce improved materials through blending commercially available polymers rather than through the synthesis of new polymers. The inherent thermodynamic incompatibility of the polymers results in blends having a microphase separated structure in which the interfaces between the blended polymers are sharp and mechanically weak. The mechanical performance of these blends is strongly dependent on both the morphology of the blend and on the adhesion between the polymers. Generally, only morphological features of the blends have been examined due to the relative ease of examining blend structures using microscopy. The adhesion between the matrix phase and the dispersed phase is not so readily measurable. The Double Cantilever Beam test has been used to characterize the adhesion at the interface between two dissimilar polymers.

The Double Cantilever Beam test can also serve as a good quality control test and to test the performance of new polymers. Most mechanical tests of adhesion result in adhesion values which are reliable only to an order of magnitude and cannot be used to detect small changes in adhesive performance. This large scatter in adhesion data is due to the large deformations in the polymer samples being tested. The DCB test not only

minimizes these deformations but is also sensitive to small changes in polymer quality which affects their adhesive performance.

Cantilever beam tests are analytically and experimentally simple, and can be used to measure the fracture energy. Fig. 3.1 shows two typical cantilever-beam configurations used in measuring adhesive fracture energy.
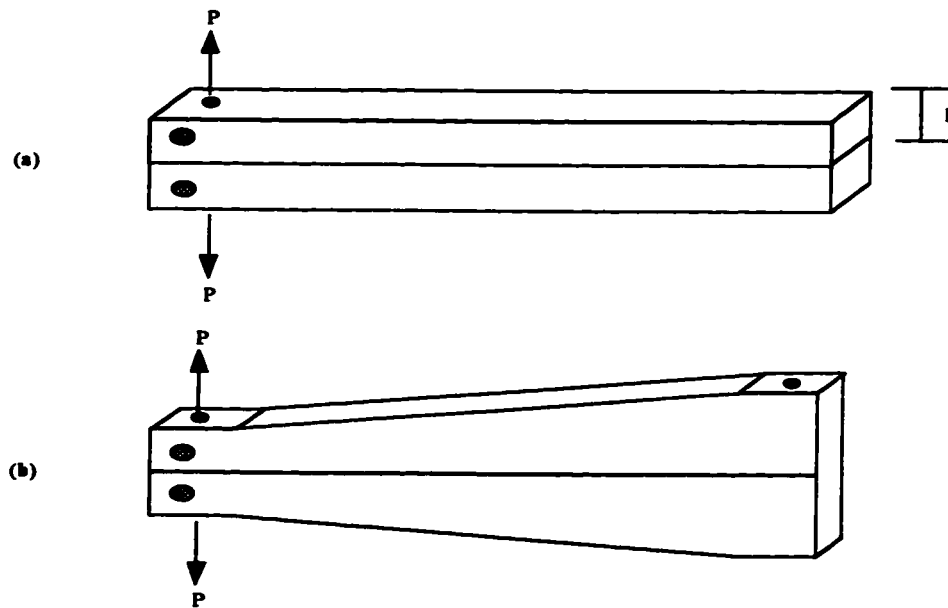
Fig. 3.1. Cantilever beam configurations: (a) double cantilever beam; (b) tapered double-cantilever beam.

In these tests, two dissimilar polymers are bonded together at an elevated temperature. The polymers are then pulled apart resulting in the propagation of a crack at the interface. The length of this crack can be used characterize the adhesion in the system. The process of crack growth in a stressed body is often described in terms of energies and leads to a decrease in the total energy of the body. If the total energy of the system is U,

then for a body of uniform thickness B, the energy release rate, G, is defined as (Williams, 1980),

$$G = -\frac{1}{B}\frac{\delta U}{\delta a} \tag{3.1}$$

δa is the small change in crack length which results in the energy change δU. The negative sign is used since a reduction in system energy results in an increase in energy available for external work. For the double cantilever beam specimen shown in Fig. 3.1a, the fracture energy calculated using beam theory and Eqn. 3.1 for a homogeneous material is (Williams, 1980),

$$G = \frac{3}{16}\frac{Eh^3\Delta^2}{a^4} \tag{3.2}$$

where E is the elastic modulus of the material, h is the thickness of each block, Δ is the deflection of the beam when it is pulled apart and a is the length of the crack formed. In terms of the load, P, applied to pull the blocks apart, the expression for the fracture energy can be written as,

$$G = \frac{12P^2a^2}{EB^2\Delta^3} \tag{3.3}$$

The above equation indicates that G increases as the crack length, a, increases for a fixed load (Williams, 1980). In this method, both P and a must be considered. For practical purposes, there is considerable advantage in a geometry in which G does not change with a, and this can be achieved by using the geometry shown in Fig. 3.1b. The taper to this geometry ensures that the fracture energy remains constant irrespective of the length of the crack.

When a crack propagates, the crack tip is subjected to three major loading modes. These are (Fig. 3.2):

Mode I: Opening mode or tensile mode, where the crack surfaces move directly apart.

Mode II: Sliding mode, where the crack surfaces slide over one another.

Mode III: Tearing mode, where the crack surfaces move relative to one another.

To determine the magnitude of the local stress for a given specimen configuration and applied stress, the parameters K_I, K_{II} and K_{III} are used. These parameters are called "stress intensity factors" for the three corresponding loading modes. In general $K = f(\sigma$, crack length) where σ is the stress and the function f depends on specimen configuration and loading mode. In some cases, the crack propagation may involve a mixture of loading modes. This mode mixity is characterized by the ratio of the stress intensity factors, e.g. the ratio of K_I and K_{II}.
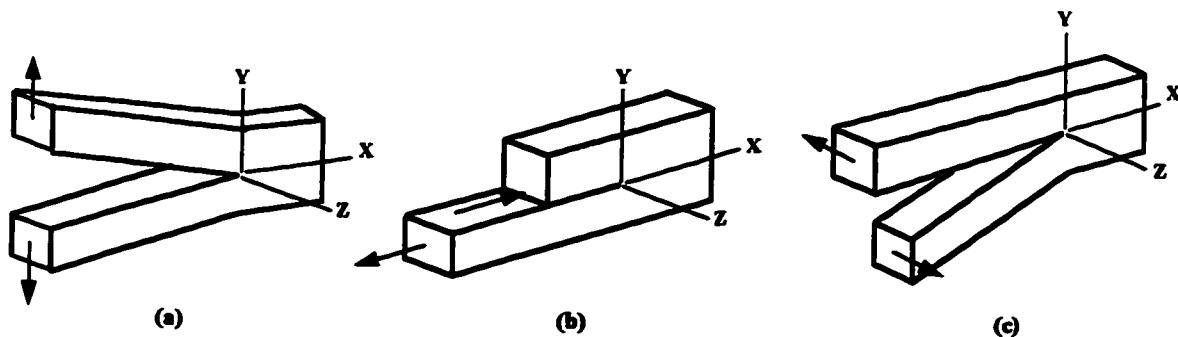
Fig. 3.2. Three basic fracture modes, (a) Mode I; (b) Mode II and (c) Mode III.

An important distinction between an interface crack and a crack in a bulk material is that in the former, a crack traveling at an interface between two dissimilar materials is

subjected to a mixture of both Mode I and Mode II opening conditions. This is in contrast to a crack in a bulk material which normally grows in such a direction that it experiences a pure opening mode, which means that K_{II} equals zero. In addition, the mathematical separation into Mode I and II is not possible. It has been pointed out by Rice (1988) that under certain conditions, a complex stress intensity factor, K^* may be used to describe the stress pattern at the tip of a crack for a bimaterial problem. As the differences in the elastic constants of the two materials becomes small, K^* may be related to the more common stress intensity factor, $K=K_I + iK_{II}$, with the mode mixity described by the phase angle, $\psi=\tan^{-1}(K_I/K_{II})$. Hence, according to Brown (1990), for interfacial failure it is necessary to consider the effects of varying the ratio of Mode I to Mode II loading on crack propagation.

Brown (1990) was the first to use the double cantilever beam test to study the toughness of the interface between two polymers. He studied a polystyrene/polymethylmethacralate (PS/PMMA) system where both the polymers are incompatible. He observed that the interface between the PS and PMMA was extremely tough and obtained a value for G_c of about 200 J/m^2. On examining the fracture surfaces of the PS/PMMA samples, it was observed that crazes grew into the PS from the interface and the crack tended to follow one such craze and then jumped back to the interface. This phenomenon of crazing can be better understood with reference to Fig. 3.3. Crazing occurs predominantly in glassy polymers like PS, PMMA and polycarbonate (PC). However no crazing is found in systems containing very strong interfaces in ductile

polymers where gross plastic deformation suppresses crazing and very weak interfaces where crazes never form (Brown, 1991).
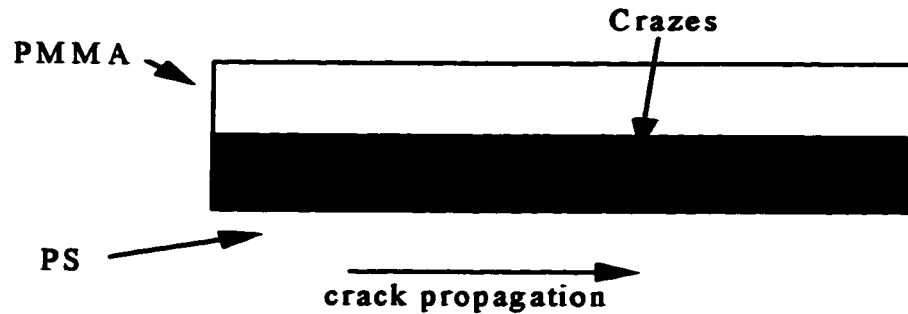
Fig. 3.3. Failure of the PS/PMMA interface by the phenomenon of crazing

In a regular or symmetric configuration where the strips of both polymers are of the same thickness, the double cantilever beam loading geometry would create a K_{II} component in the stress intensity factor at the crack tip causing the crack to swerve towards the more compliant material. If the more compliant material also has a lower crazing stress, small crazes will grow at an angle from the plane of the main crack. As the PS has a lower crazing stress than the PMMA, the crazes result and contribute significantly to the fracture energy of the system resulting in the very high interface toughness. In order to prevent crazing in a DCB test, Brown (1990) suggested that the sample be made asymmetric. This asymmetry can be achieved by bonding the sample to a substrate that is stiff with respect to the polymer beams or by changing the thickness of the beams, such that the material with the lower crazing stress is thicker. The toughness of the PS/PMMA interface was measured using two different forms of the DCB test. In one form, a razor blade was inserted into the interface, while in the other, the beams were

pulled apart using an Instron testing machine. Three orientations of the samples were studied: the sample free-standing (normal DCB test); PMMA adhered to a rigid substrate; and PS adhered to the substrate. The free-standing sample gave a G_c of 60 to 100 J/m^2; the PMMA adhered sample interface was too strong and the crack propagated into the PS upper layer; the PS adhered sample cracked at the interface and gave a G_c of 5 to 10 J/m^2. Clearly the asymmetry caused by bonding the sample to a rigid substrate had a very significant effect on the values of fracture energy obtained.

A number of researchers have used the asymmetric DCB test to study the adhesion of polymers (Brown, 1990; Constantino et al., 1992; Char et al., 1993; Reichert and Brown, 1993; Cho et al., 1994; Creton et al., 1994; Lee and Char, 1994; Beck-Tan, 1994 and Norton et al., 1995). However, most of the work has been done for polymer interfaces reinforced with block copolymers. These studies have shown that large improvements in interfacial adhesion result directly from copolymer addition. Experimental investigations into the interfacial properties of PS/poly(2-vinylpyridine) (PVP) (Constantino et al., 1992), poly(phenylene oxide) (PPO)/PMMA (Brown and Reichert., 1992) and PS/PMMA (Char et al., 1993) have all demonstrated a 100-fold increase in interfacial fracture energy via compatibilization using a copolymer.

The simplest approximation for the critical energy release rate, G_c, for the interfacial failure is to consider that the only contribution comes from the bending of the

two beams and no energy is stored ahead of the crack tip. In this case G_c is obtained from simple beam theory as (Tada,1973):

$$G_c = \frac{3\Delta^2 h_1^3 E_1 h_2^3 E_2}{8a^4[E_1 h_1^3 + E_2 h_2^3]} \tag{3.4}$$

where h_1 and h_2 are the thicknesses, E_1 and E_2 are the elastic modulii of the two polymer strips, Δ is the thickness of the razor blade and a is the crack length. This relation is a good approximation as long as the crack is long relative to the thickness of the beams but overestimates G_c for the shorter crack lengths typical of stronger interfaces (Creton et al.,1992). A better description of our experimental situation is given by a model of a cantilever beam on an elastic foundation derived by Kanninen (1973). In this model one of the beams is adhered onto a rigid substrate. Using this model, the following equation for G_c, was obtained

$$G_c = \frac{3\Delta^2 h^3 E}{8a^4(1+0.64h/a)^4} \tag{3.5}$$

where h and E are the thickness and elastic modulus of the unadhered strip respectively. Thus, the strip adhered to the rigid substrate was no longer important in calculating the fracture energy.

3.2. Experimental

3.2.1. Materials

Systems studied using the DCB test were polystyrene (PS)/ethylene-vinylacetate copolymer (EVA) and polycarbonate (PC)/EVA. Thus, both the systems studied were of

a brittle, glassy polymer (PS and PC) adhered to a rubbery polymer (EVA). The PS used throughout this work was provided in pellet form by the Dow Chemical Company. The PC was provided by GE Plastics. A number of different EVAs provided by AT Plastics were used in this study. The EVAs differed in their vinylacetate content and are listed in Table 3.1.

EVA Copolymer (% vinylacetate)	Melt Index (MI) (g/10 min)	Young's Modulus (GPa)
9%	3	0.016
15%	5	
16%	15	0.019
18%	150	0.010
28%	2.4	0.0058
28%	40	0.0049
28%	400	0.0035

Table 3.1. List of ethylene-vinylacetate copolymers used in this study

3.2.2. Sample Preparation

The pellets of the polystyrene, polycarbonate and the EVA were stored in an oven at 80°C prior to use. This removed any volatiles present in the pellets. The pellets of the glassy polymers (PS and PC) were compression molded in a Carver Model C laboratory press under a pressure of 1 ton using a square aluminum mold into sheets 6.5 cm × 6.5 cm. Stainless steel sheets covered with Teflon sheets were placed on either side of the mold.

The molding temperature for PS and PC were different and depended on the glass transition temperature (T_g) of the polymer used. The temperature used for the PS was 200°C while that for the PC was 250°C.

The dry pellets were taken directly from the storage oven at 80°C and the mold was filled with a layer of these. After these pellets had melted, another layer was placed above the melted pellets. The press was then closed and pressure was applied. This pressure was maintained for around 5 minutes and then the mold was water cooled. The above molding procedure prevented the formation of bubbles within and on the surface of the polymer sheets. The sheet of polymer was then removed from the mold and stored. Different thicknesses of these sheets could be obtained by using different thickness molds. These sheets were cut up into strips 6 cm × 1.5 cm using a band saw. The edges of these strips were smoothened using sand paper and the surface of the strips was cleaned using compressed air and a low lint wiping cloth. The above procedure was used for making both PS and PC strips. The EVA was molded in a similar manner except that the mold was made of Teflon. Teflon sheets were placed on either side of the mold and the molding temperature used was 150°C. Teflon was used because it does not stick to most polymers. The EVAs are often used in adhesive applications and stick to any metal. The EVA sheets were also cut into strips 6 cm × 1.5 cm with a pair of scissors and wiped clean with low lint wipes.

The strips of the PS obtained were annealed and bonded to the EVA. The PS was put into an oven maintained at 100°C. The corresponding EVA strip, which needed to be bonded to the PS was placed by its side. After about 1 minute, any traces of moisture present on the surface of the strips were removed and the EVA was then placed onto the PS. The glassy polymer was always placed at the bottom, so that the EVA wetted the surface of the glassy polymer. If the glassy polymer strip was placed on top, it would sink into the liquid-like EVA. The sample was annealed for a predetermined amount of time, after which it was removed and cooled in air. The PC was bonded to the EVA in a similar manner. The sample was now ready for DCB testing.

3.2.3. Apparatus

Manual DCB Test
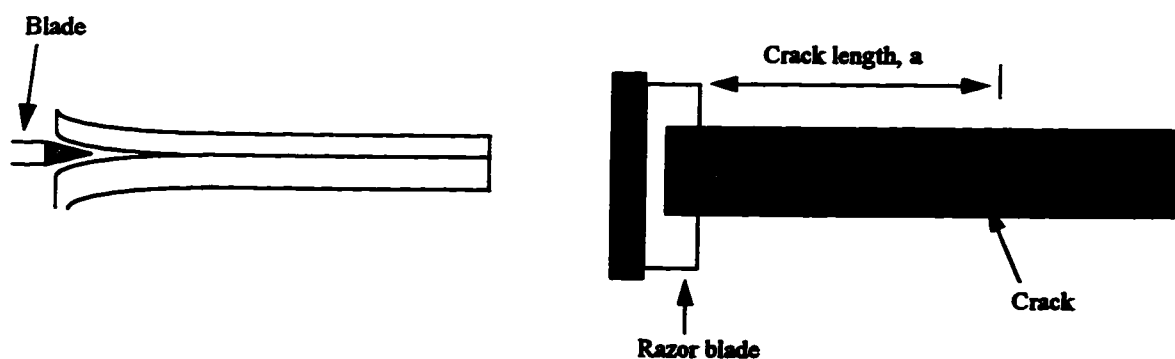
Fig. 3.4. Schematic of the double cantilever beam test

The EVA side of the above sample was glued onto an aluminum plate (5.5cm × 2.5cm). The presence of the metal backing stiffened the EVA and ensured that the razor blade was

pushed into the interface and not into the EVA. A razor blade with a known blade thickness was inserted by hand into the interface between the PS and the EVA which caused a crack to propagate at the interface as shown in Fig. 3.4. A major problem with this type of testing was the lack of standardization in the test which led to scattered data. To control and standardize the test, we automated it.

Automated DCB Test

An Instron Universal Testing Machine (Model 1011) was used in the automated test and the test apparatus is as shown in the Fig. 3.5.
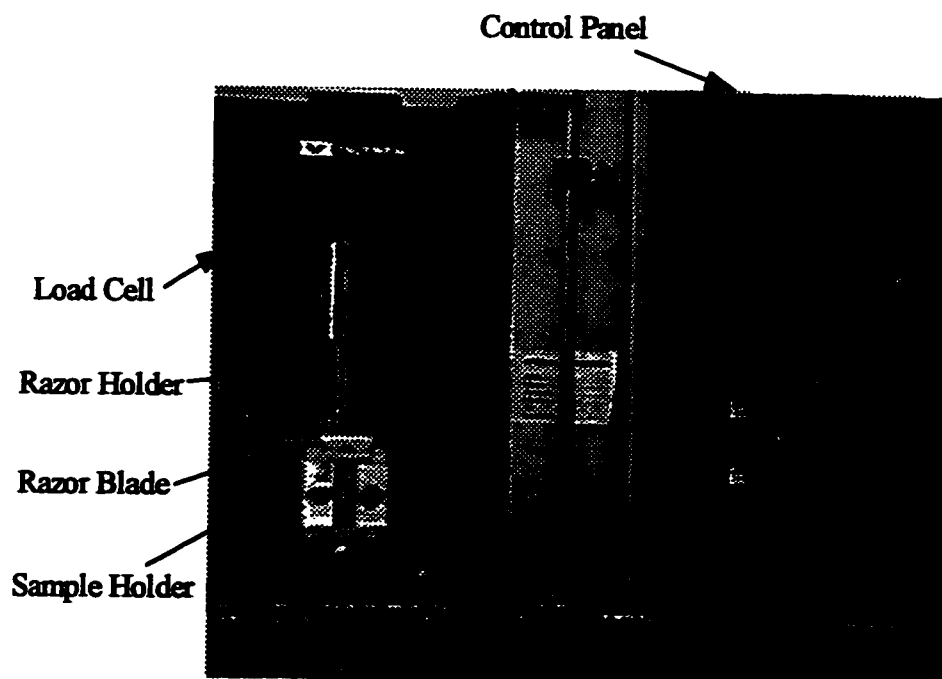
Fig. 3.5. Schematic of the double cantilever beam apparatus.

It comes equipped with a LCD display panel that is used for setting up the test conditions and for reading the data from test results. A leveling pad is attached to each corner of the base of the machine. A strip chart recorder was connected to the Instron. The crosshead of the Instron could be set to move at any speed between 1 to 500 mm/min. and the machine can be operated in either tension or compression mode. The apparatus consisted of the following units, (a) the sample holder, (b) the razor blade holder; (c) the loadcell on the Instron; and (d) a video recording unit.

The sample holder was specially designed to be stable and versatile. A schematic is shown in Fig. 3.6. Its base was a black anodized aluminum translation stage (Melles Griot, Model # 07TAC504). The drive motion of the stage was imparted by a metric chrome plated micrometer and the stage motion was protected from backlash by a spring which loads the stage against the micrometer. The stage is supplied with a lock which holds the stage and helps maintain its position after it has been set. The sample holder made of aluminum was mounted on top of this stage. Using the translation stage, the sample holder could be precisely positioned in the horizontal direction.
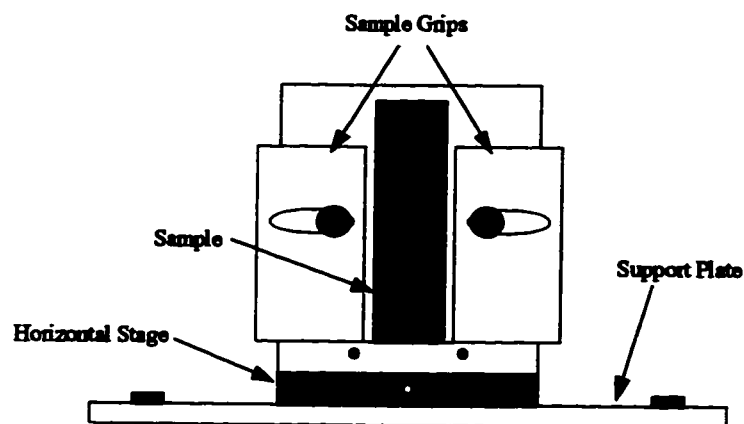
Fig. 3.6. Schematic of the sample holder used on the Instron.

During the test, the sample was held in place by two sample grips. This assembly was mounted onto a support plate which was bolted to the bottom of the Instron.

The razor blade holder assembly was also specially designed to fit into the Instron Model #1101 and is shown in Fig. 3.7. It consisted of a load cell attachment which fitted into the load cell of the Instron, so that any force experienced by this attachment was transmitted to the load cell and consequently to the load recording system of the Instron. The blade clamping mechanism was connected to this attachment by a holding pin. The clamping mechanism for the razor blade was made extremely rigid and the blade could be tightened between the clamps as shown in Fig. 3.7. Care was taken to ensure that the blade was not overtightened as this caused the blade to bend.
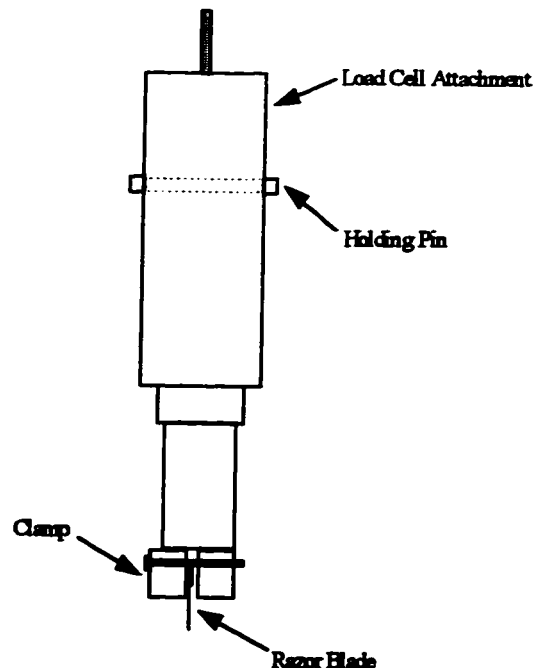
Fig. 3.7. Schematic of the razor blade holder

The load cell or load transducer attached to the Instron 1101 had a maximum capacity of 5 kN and could be used for both tension and compression testing. The load transducer contained a Linear Variable Differential Transformer (LVDT). This is a very sensitive device that measures minute deflections of the load transducer. The load transducer was connected to the moving crosshead of the Instron by screws. The entire test was recorded by a Hitachi Model VM-H710A 8 mm Video Camcorder. The camcorder is equipped with a 24X zoom option and image stabilization. As the crack grows at the interface of the sample, it is recorded at a certain zoom setting, which helps in accurate measurement of the final crack length.

3.2.4. Testing Procedure

Manual DCB Test

For the tests done manually, a razor blade was inserted into the interface between the polymers. Since the failure of polymeric materials is time-dependent, the sample was left free-standing and the crack length was measured 24 hours after the razor was inserted. Before measuring the crack length, the blade was pushed in such that the crack moved a little. When the crack stopped moving, the distance from the edge of the razor blade to the end of the crack was noted as the crack length. The polymer strips were taken apart and the thickness of the upper, unglued strip was measured. For very tough systems, it was difficult to insert the razor blade into the interface. While inserting the razor blade, sometimes the blade would dig into the softer EVA and the sample was discarded. The fracture energy G_c was calculated using Eqn. 3.5.

Automated DCB Test

For the automated test, the sample preparation procedure was different from that given in § 3.2.2. The procedure was modified so that the razor blade could be introduced at the interface and positioned such that it did not dig into any of the polymer strips and was driven along the interface. Before annealing the strips together, a small piece of Teflon tape was placed on one edge of the glassy polymer (PS and PC) strip so that it covered about 0.5 cm on the end of the strip. The EVA was then placed on top of this strip and the sample was annealed as before. After annealing for the required amount of time, the sample was cooled. The presence of the Teflon tape prevented the EVA from adhering to the PS at that end.

Similar to the manual test, the EVA side of this sample was glued onto an aluminum plate (5.5 cm × 2.5 cm) covered with masking tape using epoxy glue. The masking tape was used to make the resulting crack optically clear. Once the glue dried, the Teflon tape was removed which resulted in a small groove between the EVA and the glassy polymer. The razor blade was placed in this groove and was aligned by hand to ensure that it is driven into the interface. While placing the razor blade into the groove, care was taken that the blunt side of the blade was into the interface. Avoiding the sharp side was necessary as this side was striated and this could cause part of the blade to dig into the EVA.

The sample glued to the metal backing was placed within the sample holder, which is shown in Fig. 3.6. The sample was held in place by tightening the grips. The crosshead of the Instron was moved down such that the blade that had been placed in the sample was within the gap of the razor blade holder. The translation stage was moved so that the blade was exactly at the center of this gap. The screws of the blade holder were tightened making sure that the blade did not bend. The Instron was now ready to push the blade through the interface at a rate of 1 mm/min. This was the minimum speed possible on the Instron Model 1101. The blade should be inserted at the slowest speed possible to minimize any deformation of the polymers. After the blade had penetrated around 5 mm into the interface, the motion of the crosshead was stopped. The crack propagation was continuously recorded onto the Hitachi Model VM-H710A which was connected to a TV. This allowed for a more accurate measurement of the crack length since it can be magnified onto the TV screen. The crack propagation was monitored until the crack stopped moving. The average crack length was measured form the edge of the razor blade to the end of the crack. The sample was removed from the sample holder and the thickness of each polymer strip was measured.

3.3. Results and Discussion

For the PS/EVA system, the samples were tested manually. The crack obtained is shown in Fig. 3.8 and is thumbnail shaped. For some of the samples, the crack was not uniform across the width of the sample. For such samples, an average crack length was calculated by taking a number of points along the end of the crack.
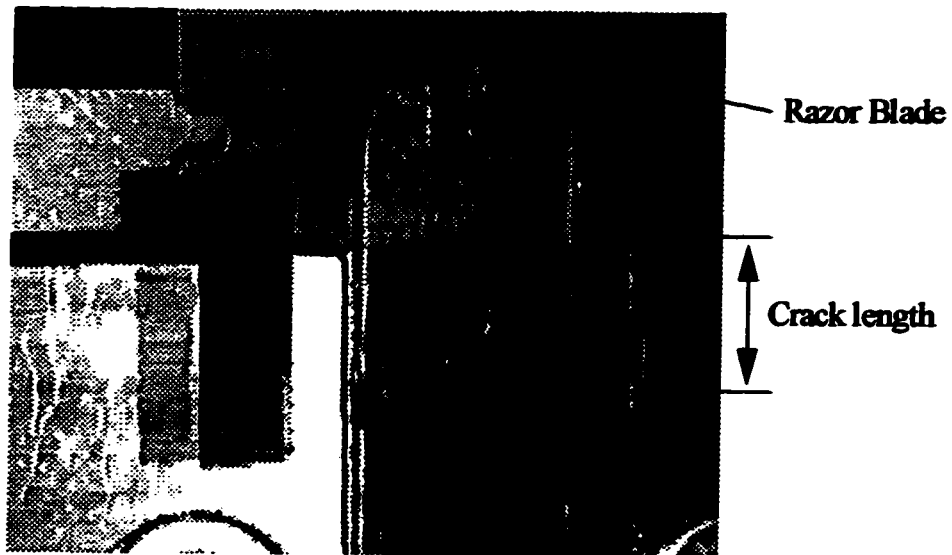
Fig. 3.8. Crack obtained at the interface in the DCB test.
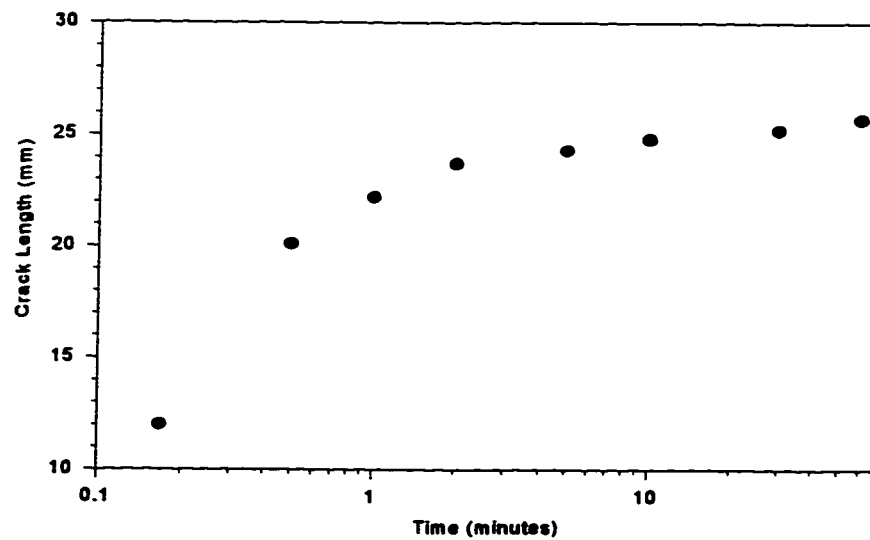
Fig. 3.9. Crack length versus time for the PS/15%EVA system annealed at 100°C for 1 hour.

The crack took around 10 minutes to reach equilibrium as shown in Fig. 3.9 for the system PS/15%EVA. The length of the crack was measured at this point and the fracture energy was calculated using Eqn. 3.5.

For the PS/EVA system, the effect of changing the VA content on adhesion was investigated. The EVAs studied were 9% (20MI), 15% (8MI) and 28% (2.4MI). It was found that as the VA content in the EVA copolymers increases, the adhesion of the copolymer to PS decreased. The results are shown in Fig. 3.10.
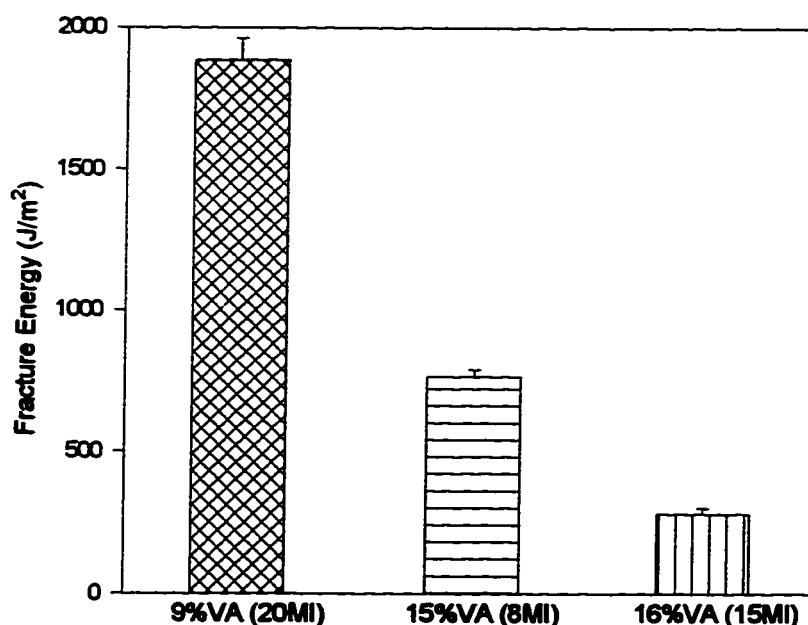
Fig. 3.10. Fracture energy, G_c versus %vinylacetate for the PS/EVA system annealed at 130°C for 50 minutes. The vertical lines above the bars represent positive standard deviations.

As shown in §2.5.6 for the adhesion of PC/EVA using the peel test, the 29% EVA gave better adhesion than the 10% EVA and this increase in adhesion was believed to be

due to a matching of polarities between the 29% EVA and the PC as compared to the 10% EVA and PC. For the PS/EVA system using the DCB test, the effect of VA content on the adhesion is the opposite of that observed using the peel test (Fig. 3.10). For the PS/EVA system, this opposite effect could be due to the fact that a very large difference in polarities may exist between the EVAs and the PS. So, a change in the VA content may not substantially affect the polarity between the PS and the EVAs and thus, would not bring about an improvement in adhesion with increasing VA content.

The decrease in the work of adhesion with the VA content for the PS/EVA system could then be qualitatively explained based on the diffusion theory of adhesion of polymers (Wu, 1982 and Kaelble, 1971). According to this theory, segments of polymer molecules diffuse across the interface to various extents and form an interfacial layer. The extent of this diffusion determines the strength of the interface and is a function of the properties of the polymers, the time of contact between the polymers, temperature of bonding, molecular weight, viscosity, etc. For the EVA copolymers, increasing the vinyl acetate content increases the steric hindrance due to the acetoxy group and as a result the chain stiffness increases. It has been shown that an increase in the rigidity of the polymer chains lowers the diffusivity of the polymer molecule across the interface and hence decreases the bond strength. The molecules of the 28% EVA are more rigid and are not able to diffuse into the polystyrene as effectively as those of the 9% and the 15% EVAs. Therefore the interfacial adhesion strength is lower for the 28% case. The chemical architecture of the different EVAs may also affect the adhesion at the interface between the PS and the EVA.

In manual testing, where the razor blade was introduced into the sample interface by hand, the rate at which the razor blade was inserted could not be controlled nor could the blade be kept at the interface. To reduce the uncertainty involved with performing the DCB test manually, an automated version of this test was devised and is shown in Fig. 3.5. For automated testing also, Eqn. 3.5 was used to calculate the fracture energy.

3.3.1. Effect of Vinylacetate Content

Fig. 3.11 shows the effect of vinylacetate content on the work of adhesion for the adhesion of PS to different EVAs using the automated test.
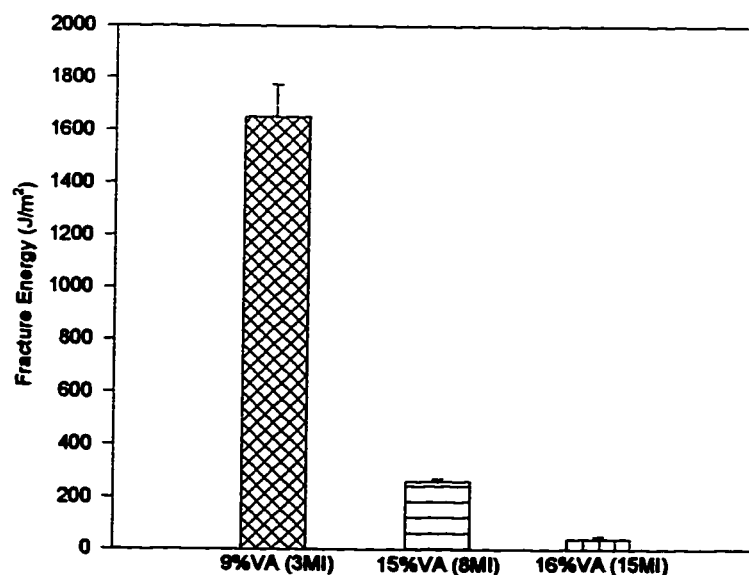
Fig. 3.11. Effect of vinylacetate content on the fracture energy for the PS/EVA system using the automated DCB test. The samples were annealed for 50 minutes at 130°C.

Like the results for the manual DCB test (Fig. 3.10), the fracture energy decreases with increasing vinylacetate content. This dependence of the fracture energy on the VA content was explained on the basis of the diffusion theory of adhesion. The automated test eliminated some of the uncertainties associated with the manual test and standardized the testing procedure. Thus, the automated test yielded reasonably accurate values and could be used to detect changes in product quality.

3.3.2. Sensitivity of the DCB Apparatus

The ultimate purpose of developing the DCB test was to obtain a method to detect small differences in adhesion between different EVAs and to quantify the adhesion in new multilayer products. The differences in adhesion could be due to contaminants present in the product, differences in product quality obtained during processing operations, or environmental factors like humidity, aging, etc. To measure these differences, we needed to develop a standardized test which was sensitive to small changes in the adhesion.

In § 3.3.1, the effect of the VA content on the work of adhesion was studied. As mentioned in this section, a significant reduction in scatter of the results was obtained by using the automated DCB test. It was concluded that the results obtained using the automated test were more reliable than those for the manual test. To investigate if the automated DCB test was sensitive to small changes in product quality, we tested two samples of the same EVA, one contaminated and the other pure. These samples were obtained from AT Plastics and the nature of the contaminant was not known. The sample

was a 16% EVA (28MI) and its adhesion to polycarbonate (PC) was measured. The results are shown in Fig. 3.12. The contaminated EVA had a much lower adhesion to the PC as compared to the uncontaminated EVA. Since, the nature of the contaminant was not known, we could only speculate about the mechanism causing this loss in adhesion. During the annealing process, the contaminants in the 16% EVA may have diffused to the interface between the EVA and the PC leading to a weaker interface.
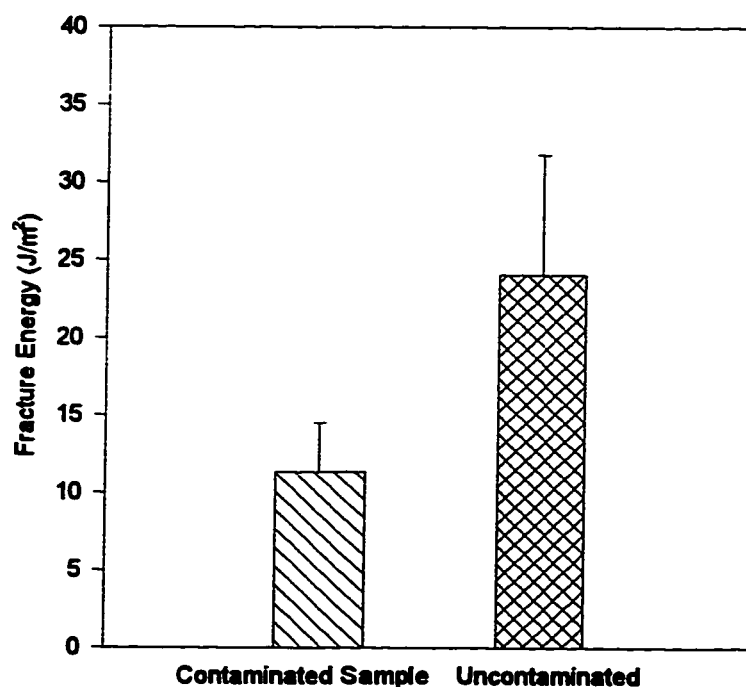
Fig. 3.12. Effect of contaminant on the adhesion of a 16%EVA (28MI) to PC, annealed at 130°C for 15 minutes.

This phenomenon has been reported by Wu (1982), who found that commercial polyethylenes exhibited weak adhesion due to the presence of low molecular weight

fractions which were rejected to the surface when the polymer melt freezes and crystallized. This was one possible mechanism for the contaminant causing a reduction in adhesion. Thus, the automated DCB test was able to detect the loss in adhesion characteristics due to the presence of the contaminant in the 16% EVA.

3.3.3. Effect of Annealing Time

The effect of annealing time on the work of adhesion was measured and is shown in Fig. 3.13 for the PC/28%EVA (2.4 MI) system.
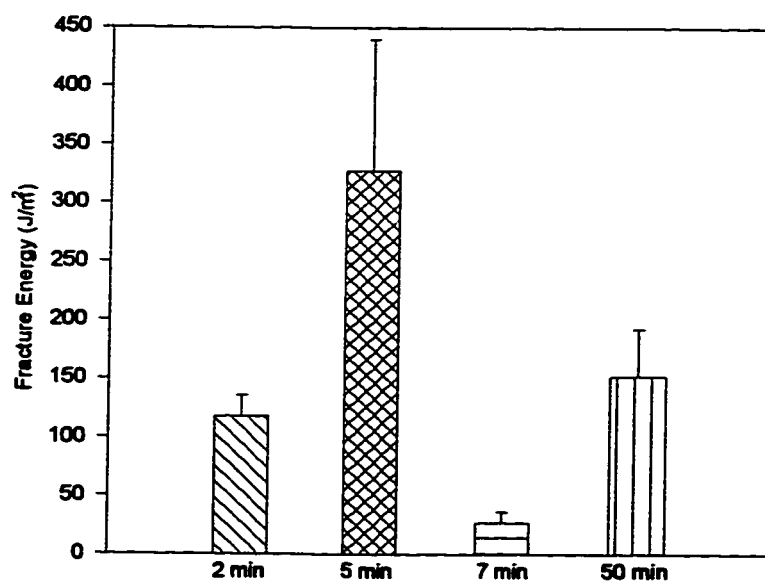
Fig. 3.13. Fracture energy versus annealing time for the adhesion of 28%EVA (2.4MI) to PC, annealed at 130°C.

Fig. 3.13 shows that the fracture energy shot up on increasing annealing time from 2 to 5 minutes. However, it dropped on annealing the samples for 7 minutes and then increased

again. On closely examining the surfaces of the samples used for the test, it was observed that the surfaces of the PC samples used for the 2 min. and 5 min. tests were rougher than those of the 7 min. and 50 min. samples. This difference in roughness occurred because, while molding the PC sheets in the plate press, the Teflon sheets placed on either side of the mold had different surface roughness. The rougher surface Teflon sheets used during molding gave a rougher PC sample surface.

3.3.4. Effect of Surface Roughness

The effect of surface roughness was studied in more detail by deliberately using PC samples with different surface roughness and the results are shown in Fig. 3.14.
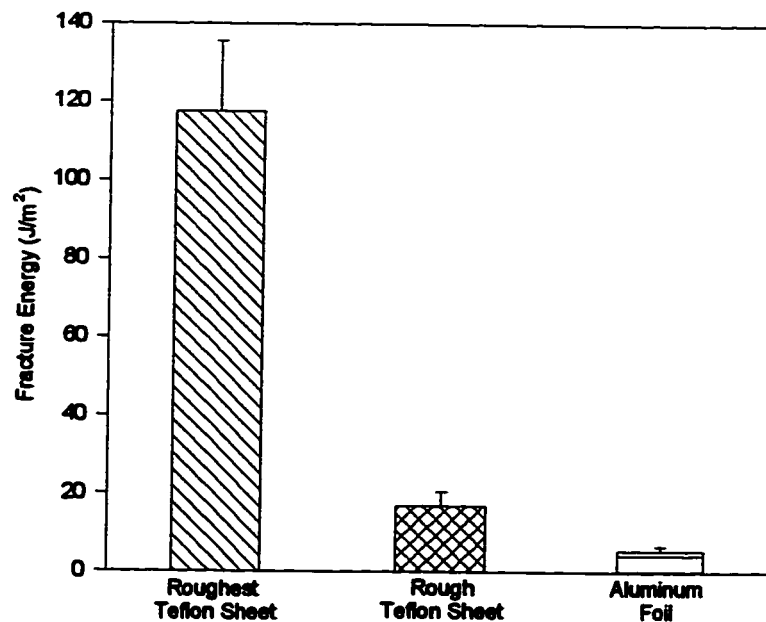
Fig. 3.14. Fracture energy as a function of surface roughness of PC samples for the adhesion of 28% EVA to PC. The samples were annealed for 2 minutes at 130°C.

As seen from Fig. 3.14, the fracture energy drastically dropped as the surface of the PC sample becomes smoother. As explained in § 1.3.1, the mechanical theory of adhesion proposes that the adhesion increases with increasing surface roughness. This increase however, may not be entirely due to an increase in the mechanical interlocking mechanism. It was mentioned in § 1.3.1 that besides this mechanism, a rougher surface may cause increased viscoelastic and plastic dissipation of energy. Since, the surface roughness was found to affect the adhesion measured using the DCB test, care was taken to ensure that samples being tested had similar surface roughness by using the same roughness Teflon sheets during sample preparation.

3.3.5. Effect of Mechanical Properties on Adhesion

The effect of the following mechanical properties on the adhesion was studied : (1) the tensile or elastic modulus and (2) the toughness. The adhesion of PC to EVA was studied and the mechanical properties were obtained using a tensile test.

3.3.5.1. Tensile Testing

The samples for tensile testing were prepared in the same way as for the DCB test given in § 3.2.2. The only difference was that the EVA sheets obtained were cut into rectangular sections 1 cm wide and 9 cm long.

The same Instron Universal testing machine (Model 1011) used for the DCB test was used for tensile testing. However, in place of the sample holder and razor blade

holder shown in Fig. 3.5, pneumatic grips operating at a pressure of 60 psig were installed. The testing procedure given in the Instron manual was followed. The rectangular EVA strips were placed into the grips and the Instron was programmed to pull the polymer at a speed of 300 mm/min. This speed was recommended for tensile testing of elastomers in the manual provided with the Instron. A chart recorder attached to the Instron continuously recorded the data in the form of a tensile curve shown in Fig. 3.15.
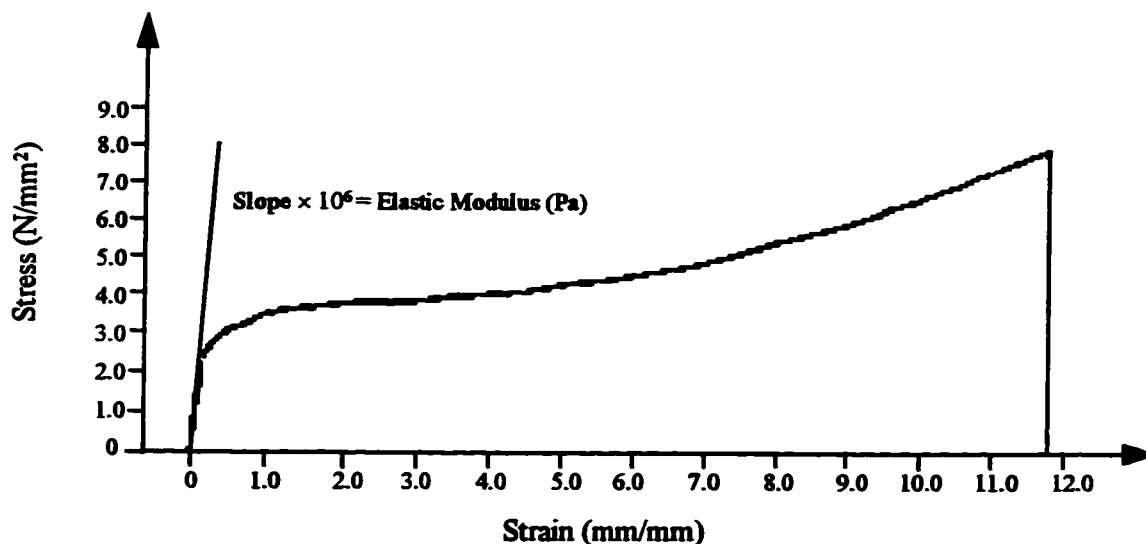
Fig. 3.15. A typical stress versus strain curve obtained for the tensile testing of the 28% EVAs.

The elastic modulus was obtained by drawing a line from the origin at a tangent to the initial part of the curve i.e. at very small stress and strain. The slope of this line was calculated and this was the tensile or the elastic modulus of the polymer. The toughness of the sample was obtained by measuring the area under the stress-strain curve.

3.3.5.2. Results of Tensile Testing

It was believed that the mechanical properties of the EVAs would depend on the VA content and the melt flow index (MI). To study this, the EVAs chosen were 9% EVA (20MI), 16% EVA (15MI), 18% EVA (28MI) and 28% EVA (40MI). The elastic modulus and toughness were calculated as illustrated in the previous section. The effect of VA content on the elastic modulus and the toughness are shown in Fig. 3.16 (a) and (b) respectively. The results indicate the presence of a maximum in the elastic modulus and the toughness for the 16% EVA (15MI). But, this maximum may not be entirely due to the VA content. The 16% EVA had the lowest MI amongst the EVAs studied and this could also result in the mechanical properties of this polymer being higher than the rest. Ideally, to study the effect of the VA content on the adhesion, EVAs having the same MI should be compared. However, this was not possible as EVA copolymers with the same MI were not available. But, the effect of MI on the mechanical properties could be studied in more detail as copolymers with different MI's for the 18% EVA and the 28% EVA were available. The results are shown in Fig. 3.17 for the effect of MI on the elastic modulus.
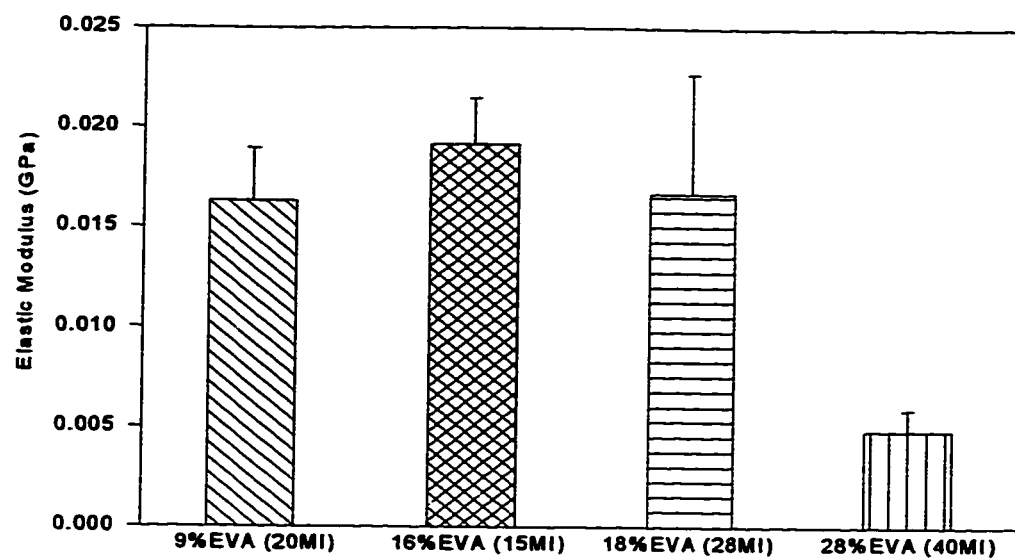
(a)
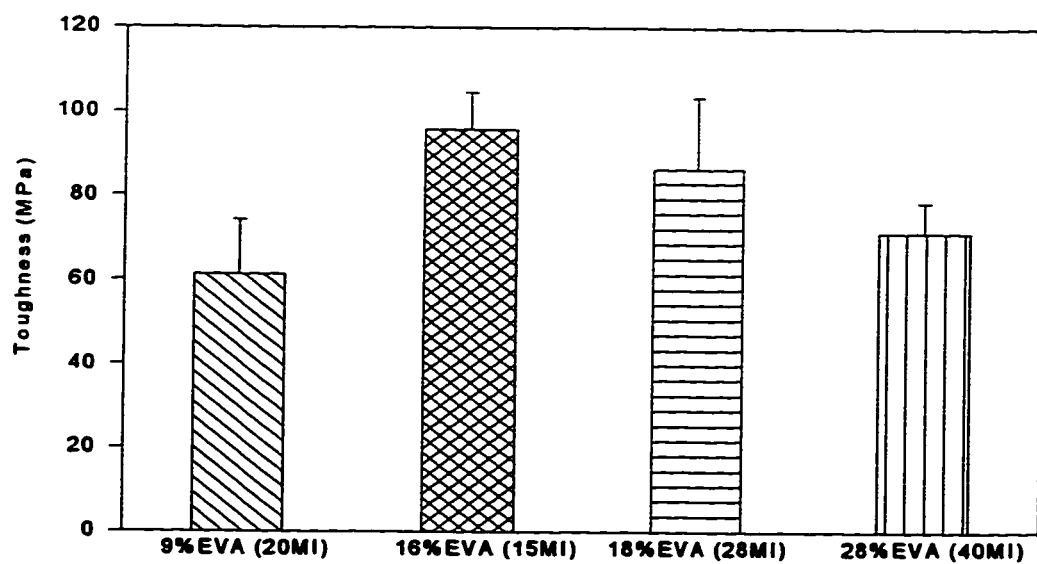
(b)

Fig. 3.16. Effect of VA content on the following mechanical properties of the EVAs, (a) elastic modulus and (b) toughness.
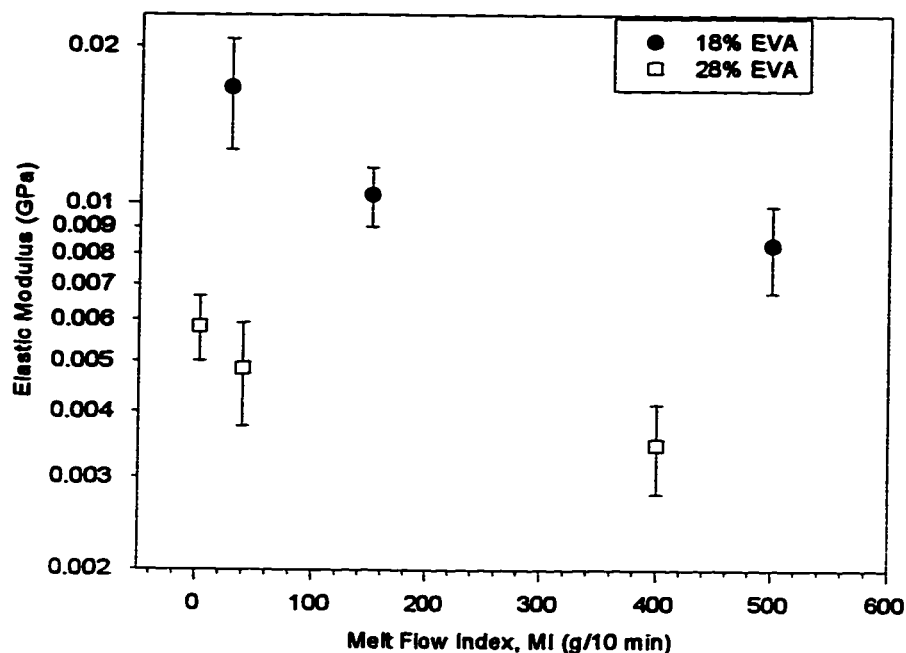
Fig. 3.17. Effect of the melt flow index (MI) on the elastic modulus of the EVA copolymers.

From Fig. 3.17, it is clear that the modulus decreases with MI, which is expected since an increase in MI implies a decrease in molecular weight of the copolymer which makes it more compliant. Thus, the elastic modulus which is a measure of the stiffness of the polymer, would decrease. Another important feature of Fig. 3.17 is that the elastic modulus for the 28% EVA is always lower than for the 18% EVA. This decrease in the modulus with increasing VA content is due to a decrease in the degree of crystallinity of the copolymers. This effect is due to the relatively bulky nature of the acetoxy side chain resulting from the copolymerized vinylacetate. This reduces the ability of the polymer chains to pack closely together and form crystalline regions. It has been reported that between about 40 and 50% vinylacetate, the copolymer becomes completely amorphous.

The effect of the elastic modulus on the work of adhesion is as shown in Fig. 3.18. The work of adhesion decreases as the elastic modulus increases.. This has two implications. It could mean that as the EVA copolymer becomes stiffer, it becomes difficult for the EVA molecules to flow over the surface of the PC leading to poor wetting and consequently lower adhesion.
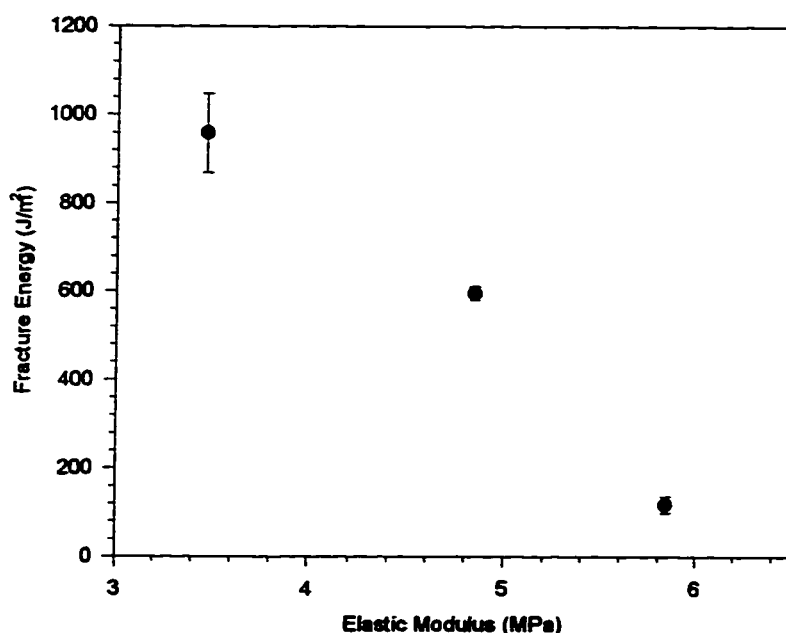
Fig. 3.18. Effect of elastic modulus on the fracture energy for the adhesion of 28% EVA and PC annealed for 5 minutes at 130°C.

The other reason could be related to the viscoelastic response of the polymer. A material with a lower elastic modulus is more deformable causing more viscoelastic dissipation within the sample. If most of the energy is dissipated viscoelastically, very little of this energy would be available for the formation of the crack in the DCB test. Consequently,

the crack formed would be smaller than expected leading to a high fracture energy as calculated by Eqn. 3.6. Thus the work of adhesion for the EVA with a lower modulus would be higher than an EVA with a higher modulus.

3.4. Conclusions

The double cantilever beam (DCB) test was used to measure the adhesion of ethylene-vinylacetate copolymers (EVA) to different substrates. In this test, a thumbnailed shaped crack was formed at the interface and this crack required some time to reach equilibrium. A manual DCB test was used which suffered from a lack of standardization of testing parameters and large scatter in the results obtained. This test was used to measure the effect of the vinylacetate (VA) content on the work of adhesion for a EVA/Polystyrene (PS) system annealed at 130°C for 1 hour . The adhesion decreased with increasing VA content due to a diffusion mechanism, where the diffusivity of the EVAs decreased with increasing VA content. The decrease in the diffusivity was a result of the EVA chains becoming stiffer as the VA content was increased.

To overcome the shortcomings of the manual DCB test, an Instron Universal Testing Machine was used to automate this test. As these machines are commonly used in industrial laboratories for the testing of polymers, this test could be easily adapted to an industrial requirement. The effect of the VA content on the adhesion for a PS/EVA system annealed at 130°C for 50 minutes was measured using the automated test and the adhesion was qualitatively similar to that obtained from the manual test. The test could

detect a difference in adhesion between a contaminated and an uncontaminated 16% EVA (28MI). It was found that the contaminated EVA had a fracture energy which was about half that of the uncontaminated EVA. Thus, the automated test was sensitive to small changes in product quality and could be used as a product development or quality control tool.

The work of adhesion increased with annealing time. However, besides the annealing time it was found that the roughness of the sample surfaces played a critical role in determining the adhesion values. As the roughness of the surface of the sample increased, there was better adhesion. This was due to a combination of increased mechanical interlocking at the interface and viscoelastic dissipation caused by the rough surface. Thus, sample preparation is a critical step when comparing different systems.

The mechanical properties of the EVAs were measured using a tensile test. On comparing the mechanical properties of 9% EVA (20MI), 16% EVA (15MI), 18% EVA (28MI) and 28% EVA (40MI), it was found that the 16% EVA (15MI) had the highest elastic modulus and highest toughness amongst the copolymers. It was concluded that this was due to a combination of the VA content and the melt flow index (MI). On investigating the effect of these factors on the mechanical properties of the 18% EVA and the 28% EVA in more detail, it was found that the elastic modulus decreased with increasing MI and increasing VA content. The decrease in modulus due to increasing MI was due to the material becoming more compliant as the MI was increased. The negative

effect of VA content on the modulus was due to a decrease in the degree of crystallinity of the copolymer as the VA content was decreased.

Finally, the fracture energy for a PC/28%EVA system annealed at 130°C for 5 minutes was measured as a function of the elastic modulus. The fracture energy decreased from a maximum of 1000 J/m^2 to a minimum of 100 J/m^2 as the modulus was increased from about 3.5 MPa to 6 MPa. It was concluded that this large drop in fracture energy could be due to two factors. An increase in the elastic modulus, either, led to decreased wetting causing a loss in adhesion or led to a decrease in the amount of energy dissipated viscoelastically.

3.5. References

Beck-Tan, N. C., Ph.D. Thesis, University of Maryland, USA (1994).

Brown, H. R., and Reichert, W. F., *Macromolecular Reports* **A29**, 201(1992).

Brown, H. R., *J. Mater. Sci.* **25**, 2791(1990).

Brown, H. R., *Macromolecules* **24**, 2752(1991).

Char, K., Brown, H. R., and Deline, V. R., *Macromolecules* **26**, 4164(1993).

Cho, K., Kressler, J., and Inoue, T., *Polymer* **35**, 1332(1994).

Constantino, C., Kramer, E. J., Hui, C., and Brown, H. R., *Macromolecules* **25**, 3075(1992).

Creton, C., Brown, H. R., and Deline, V. R., *Macromolecules* **27**, 1774(1994).

Creton, C., Brown, H. R., and Shull, K. R., *Macromolecules* **27**, 3174(1994).

Kaelble, D. H., *Physical Chemistry of Adhesion*, Wiley-Interscience, New York (1971).

Kanninen, M. F., *Int. J. Frac.* **9**, 83(1973).

Lee, Y., and Char, K., *Macromolecules* **27**, 2603(1994).

Norton, L. J., Smigolova, Pralle, M. U., Hubenko, A., Dai, K. H., and Kramer, E. J., *Macromolecules* **28**, 1999(1995).

Reichert, W. F., and Brown, H. R., *Polymer* **34**, 2289(1993).

Rice, J. R., *J. Appl. Mech.* **55**, 98(1988).

Washiyama, J., Kramer, E. J., Creton, C. F., and Hui, C., *Macromolecules* **27**, 2019(1994).

Williams, J. G., *Stress Analysis of Polymers*, John Wiley & Sons, New York (1980).

Wu, S., *Polymer Interface and Adhesion*, Marcel Dekker, New York (1982).

CHAPTER 4

The Microscratch Test

4.1. Introduction

Polymer films deposited on rigid substrates have found special significance in the electronic packaging industry, in magnetic recording media, multilayer substrates and capacitors. They are used to provide resistance to abrasion, erosion, corrosion, wear, radiation damage, or chemical resistance; reduce friction or electrical resistance, provide lubrication, prevent sticking; and also to provide special magnetic or dielectric properties. These films may be thin ($<1\mu m$), thick ($>1\mu m$), or bulk coatings The adhesion of these films to substrates determines to a large extent the durability, longevity, and wear of the film-substrate system. Whenever thin films of polymers are used as protective overcoats (paints, coatings) for environmental protection, adhesion is very important (Mittal, 1976). If the adhesion is poor, the extent of deterioration of the substrates by environmental factors (humidity, corrosive gases, etc.) is greatly accelerated. Polymeric substrates are metallized to reduce their permeability to gases, and again for these applications adhesion becomes important. In the case of multilayer structures, adhesion between the individual layers is crucial. In the case of thin-film deposition (for example by evaporation), adhesion plays an important role in governing the kinetics of the growth and structure of the films, which in turn determines their functional performance. Thin films of dental gold are used in artificial teeth, and the adhesion of the coating to the tooth surface is very important.

Mittal (1976) has reviewed comprehensively the adhesion measurement techniques for thin and thick films and bulk coatings. Several existing methods along with a few evolving ones are discussed in detail here. The methods for the measurement of adhesion are:

1. Nucleation methods. In this method the nucleation behavior of depositing thin films is studied and this is used to determine basic adhesion.

2. Mechanical methods. All mechanical methods use some means of removing the film from the substrate. These methods can be broadly classified into two categories depending upon the mode of detachment of the film : (a) methods involving detachment normal to the interface like the direct pull-off, moment or topple, ultracentrifuge and ultrasonic, and (b) methods involving the lateral detachment of the film from the interface like the scotch tape method, the peel test, tangential shear or lap shear, the scratch test, and the blister test.

3. Miscellaneous methods. This category includes those techniques which are either of very limited applicability or those which are still in the process of being developed

The mechanical methods which yield values for the adhesion between a film and a substrate, though widely used, do not provide a quantitative measure of the strength of the bond between the film and the substrate. Most tests are really engineering tests of the durability of a thin film in a particular fracture mode. Except for the ultracentrifuge and the ultrasonic vibration tests, the other tests are all destructive and sample deformation leads to a grossly overestimated value for the strength of the interface..

The characterization of adhesion strength by scratch testing is commonly used in the hard coatings industry for films several microns thick. In this test, a smoothly rounded chrome steel, tungsten carbide, or diamond tip is drawn across the film surface and a vertical load, applied to the tip, is gradually increased until the film is completely removed. The load at which a clear track is formed is taken as a measure of adhesion (Ahn et. al, 1974). However, because thin films only a fraction of a micron thick are required by the electronic packaging and magnetic recording industries, new specifications are imposed on scratch test apparatuses. Also when testing polymer thin films, the test is dependent on many variables and this makes such testing more difficult. Hence a new generation of micromechanical testing apparatus has been developed to characterize the adhesion of thin films.

Such a micromechanical device was developed by Wu (1991) at IBM and was called a microindenter. It was used for microindentation testing on metal and ceramic thin films. Microindentation is used to measure the hardness of thin film samples and is popular because of its simplicity and versatility. Samples can be tested in the same configuration as used in service conditions and it can perform different types of testing via different testing modes and in turn allows for other mechanical properties, in addition to hardness, to be acquired. On the microindenter developed by Wu, four types of testing, namely microindentation, microscratch, load relaxation, and indentation fatigue tests could be conducted.

The microscratch test has been used to evaluate the adhesion strengths of metal/metal, metal/ceramic and metal/polymer systems (Venkataraman et. al, 1993; Venkataraman et. al, 1992; Venkataraman, 1992; Wu, 1991; Weaver, 1975; Benjamin and Weaver, 1963). This test is particularly useful for testing the adhesion of thin films to substrates as sample deformation is confined to a very small region and is therefore at a minimum. Since the microscratch test requires small amounts of materials, this test is useful in characterizing minute amounts of expensive, specialty polymers which are synthesized in the laboratory. Although some work has been done with polymers using the microscratch test (Venkataraman et. al, 1993) only the strength of bulk polymers was examined. The purpose of this research was to use the microscratch test for estimating the work of adhesion of a polymer thin film on a polymer substrate. The system chosen was a polystyrene (PS) film (E=3.5 GPa.) on a ethylene-vinyl acetate copolymer (EVA) substrate (E=0.045 GPa).

A typical microscratch test is as shown in Fig. 4.1. A conical diamond indenter scratches into and across the polystyrene film. As the indenter moves into the film the forces at the tip of the indenter are measured. There are two such forces, one parallel and the other perpendicular to the surface of the film. When the indenter reaches the interface between the PS film and the EVA substrate, a drop in the loads occurs and these are taken as a measure of the strength of the interface. A detailed description of the test and the apparatus is given later on in this chapter.
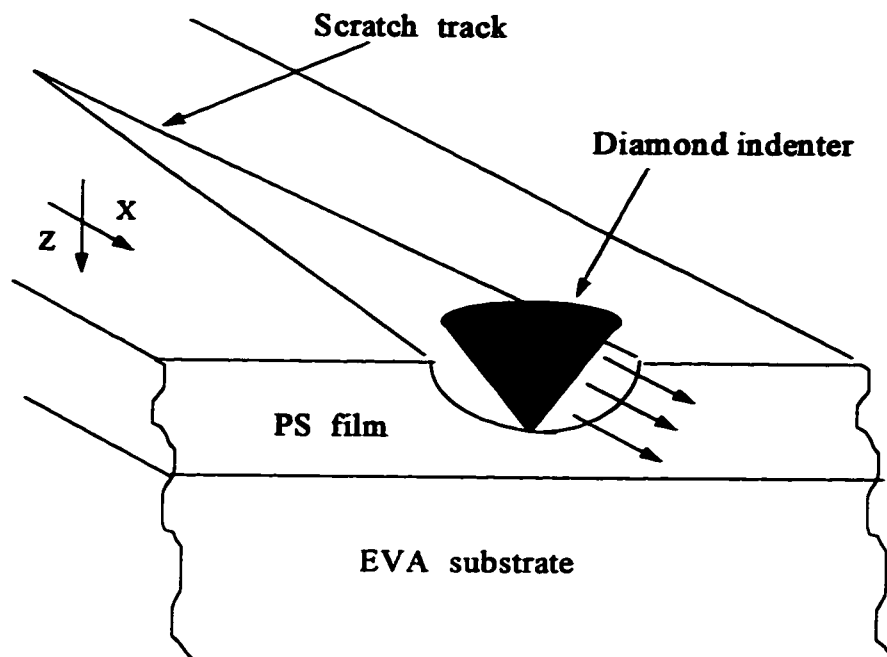
Fig. 4.1. Schematic of a microscratch test

4.2. Experimental

4.2.1 Materials

The polystyrene used throughout the work was PS-666D produced by The Dow Chemical Co. with a viscosity average molecular weight, M_v of 2×10^5 as determined by capillary viscometry. The ethylene-vinyl acetate copolymer was provided by AT Plastics, Edmonton, Alberta, Canada. EVA copolymers with 9%, 15% and 28% vinyl acetate content (Code no. 30-43644, 02-17144 and 20-45512 respectively) and having a melt flow index (MI) of 20, 8.3 and 43 (g/10min) respectively, were used in this study.

4.2.2. Sample Preparation

Discs of the ethylene-vinyl acetate copolymer (EVA) ($T_m \approx 50°C$) were compression molded in a Carver Model C laboratory press at 150°C. An aluminum mold was filled with EVA pellets and Teflon sheets were placed on either side to provide smooth surfaces. Prior to sample preparation the EVA pellets had been stored inside an oven at around 80°C so as to remove traces of moisture. The mold along with the Teflon sheets was placed between the platens of the press which was maintained at 150°C. As soon as the pellets started melting some more EVA pellets were placed on the melted ones. After these too had melted the press was closed and a pressure of approximately 1 ton was applied to the sample. This procedure prevented the formation of bubbles within the samples. Each disc obtained had a diameter of 10 mm and was 0.8 mm thick.

A thin film of polystyrene (PS) ($T_g = 100°C$) was spun cast from a 5% solution of PS in toluene onto a glass slide at 1000 rpm using a Laurell Model WS-200-4T2 spincaster. The glass slide was stuck onto the chuck of the spincaster using double sticking tape. The 5% PS solution was taken in a dropper and the entire slide was covered with this solution. The slide was spun for 2 minutes at 1000 rpm. The thickness of the film obtained depends on the concentration of the PS solution and the speed of spincasting. To obtain this thickness the spincaster was calibrated using films cast at different speeds and the thickness of these films was obtained using a DEKTAK surface profilometer. The calibration curve is shown in Fig. 4.2 and the general trend in the film

thickness as a function of the speed of rotation is qualitatively as reported by Bornside et al. (1989). From Fig. 4.2, for a 5% PS solution in toluene at a speed of 1000 rpm, the thickness of the PS film obtained is approximately 0.55 μm.
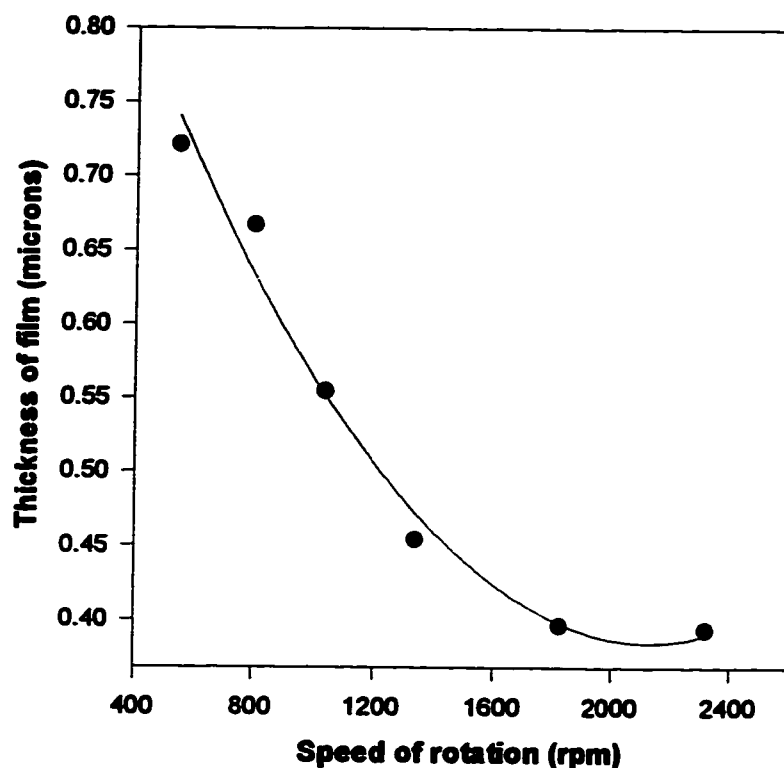
Fig. 4.2. Calibration curve of the Laurell Model WS-200-4T2 spincaster for the 5% PS solution in toluene.

It has been shown that films cast from solvents are constrained by adhesion to the substrate and this leads to the development of internal shrinkage stresses within the film (Croll, 1979 and 1983). Therefore, the glass slide with the PS film on it was kept in an oven at 100°C (at the T_g of PS) for 1 hour to not only remove traces of toluene, but also

to relax any internal stresses which might have been built up during the spin-casting process. The PS film was then floated off on water and was picked up on the EVA disc as shown in Fig. 4.3.
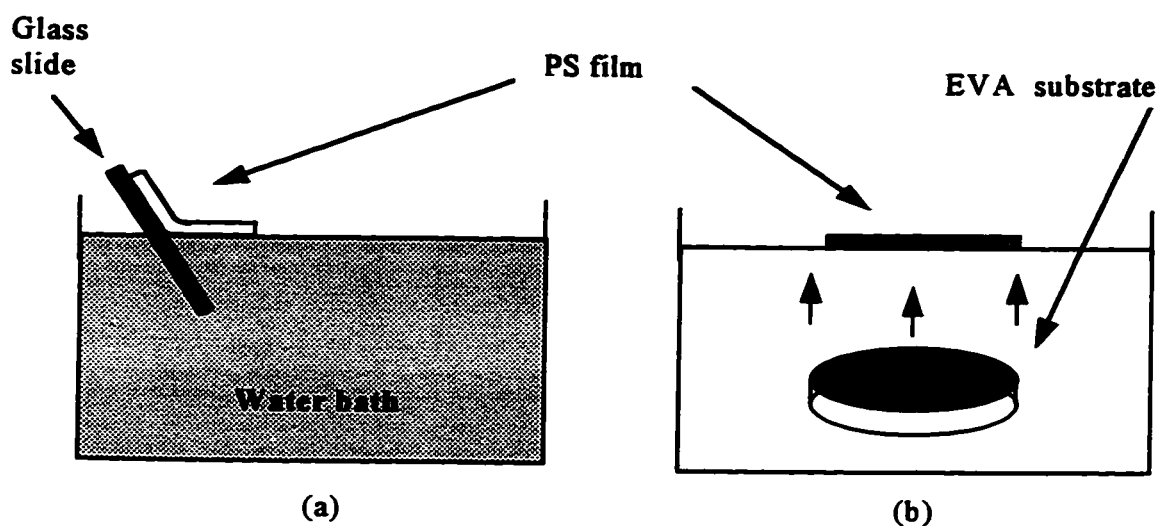
Fig. 4.3. Introduction of PS film on the EVA substrate. (a) Floating off PS film from glass slide into water, and (b) picking up PS film on EVA substrate.

Since the film was floated off in a relatively flat configuration, the development of any residual stresses was minimized. The sample was annealed in an oven at 100°C for 10 minutes to evaporate any water remaining and to promote adhesion between the film and the substrate. Samples which were annealed for longer times showed cracks on the film surface. This could be due to residual toluene evaporating during annealing and due to internal stresses which developed during the spin-casting of the film and which were not relieved in the earlier stage where the glass slide with the film on it was kept in the oven. The presence of these cracks on the film surface makes it unsuitable for the microscratch test.

4.2.3. Apparatus
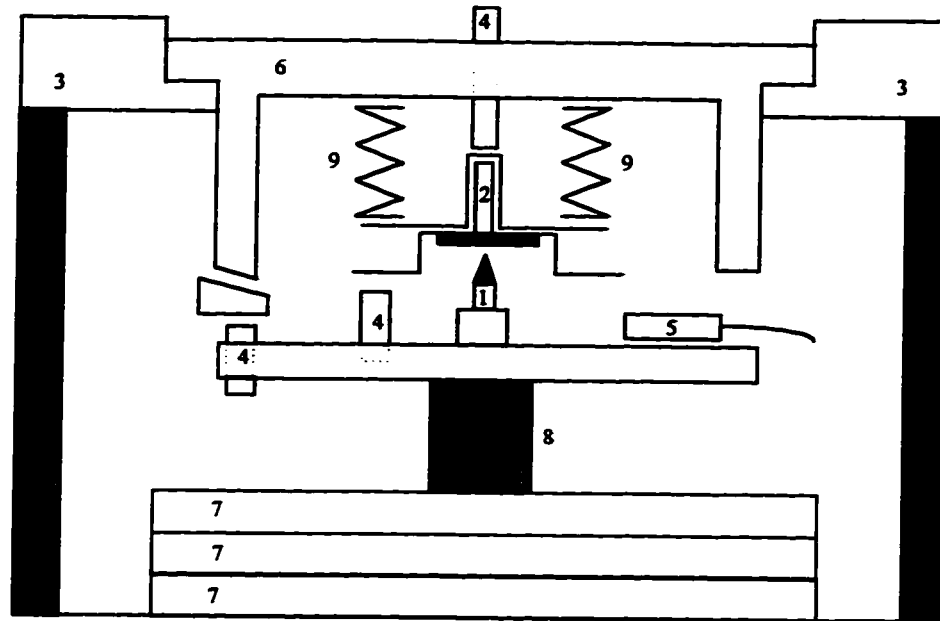
Fig. 4.4. Schematic diagram of the continuous microindenter (adapted from Wu,1991) where:
1. Indenter, 2. sample holder, 3. equipment housing, 4. capacitance probes, 5. tangential load cell, 6. normal load cell assembly, 7. XYZ precision translation stage, 8. PZT stack, 9. Be-Cu diaphragm springs.

A high resolution continuous microindenter (Fig. 4.4), developed initially by Wu (1991) and subsequently by Venkataraman (1992, 1993) was used to determine the adhesion strength of our system. The indenter tip is chosen by the user and may be conical, pyramidal or some special shape. A conical diamond indenter with a tip radius of 1μm was used. The microindenter consists of four basic units, 1. an indenter assembly, 2. a normal loadcell, 3. a fully automated precision XYZ translation stage and, 4. a tangential load cell assembly. The scratch test can be treated as a combination of two operations. One is the normal indentation process carried out by the indenter assembly; the other is a horizontal motion executed by the precision translation stage.

The automated precision translation stage consists of a stepper motor used for coarse displacement of the indenter on the order of microns in the X, Y and Z directions and a piezoelectric transducer (PZT) stack used to drive the indenter in the Z direction on the nanometer scale. PZT material is known for its rigidity, precise dimensional control, as well as the large force it can withstand. These qualities allow a PZT driven indenter assembly to be built with excellent rigidity and stability. The PZT stack is driven by a voltage amplifier to follow a predetermined pattern and is monitored by a closed loop PID controller. Either the indenter displacement output (IND) or the normal loadcell output (LC) can be employed as a servo input signal.

The specimen is mounted on the normal load cell which has a loading range from 10 μN up to 0.9 N with a load resolution of 16 μN. The tangential load cell has a loading range up to 750 mN with a resolution of 15 μN. Both the normal and the tangential load cells are constructed from Be-Cu double diaphragm springs. This design ensures that the motion of the indenter is exactly vertical and provides rigidity in the X-Y plane. Rigidity is critical for the microscratch test. Any abrupt changes in the applied load can be detected instantaneously by the load cells. This abrupt change in load can be induced by any sudden surface morphology change e.g., film cracking, film delamination, etc.

Capacitance probes are used to determine the depth of penetration of the indenter into the sample, the x- and z- position of the indenter tip, and the deflection of the normal

and tangential load cell springs. From the deflection of the load cell springs, using Hooke's law, the forces acting on the indenter tip are calculated. Each capacitance probe has a reference surface parallel to itself. These reference surfaces are attached to the sample holder so that they move with it. Each capacitance probe outputs a voltage proportional to the distance from its reference surface and this helps to keep track of the position of the sample with respect to the capacitance probes. The output from the capacitance probes is fed into the servo-feedback loop of the PZT which keeps the indenter tip at the desired location.

The major electronic attachments include a PID control circuitry for precise control of the PZT motion, a multichannel data acquisition system, and a closed loop TV camera attached to a TV monitor for viewing the interface between the indenter tip and the sample surface. A 486 computer was used for data acquisition purposes. Generally three channels were used for data acquisition and the rate of data collection can be preset. The camera speeds up the task of repositioning the indenter tip just 1 or 2 μm below the sample surface, as well as reducing the risk of damaging the indenter tip due to an accidental impact.

4.2.4. Testing Procedure

The sample was adhered onto an aluminum stub and then fixed into place with a set screw on the stub mount. The stub mount was fixed to the normal load cell by a set screw. A conical diamond indenter having a 1 μm tip radius and 90° included angle was set into the

indenter assembly. While mounting the tip into the indenter assembly, it was important to keep it visible in the TV monitor. The normal load cell was placed over the top of the indenter so that the sample surface was now just above the indenter tip. While placing the load cell, care was taken that the sample surface does not hit the tip as this would break it. If the sample surface was near the tip, it could be seen on the monitor. If it was not visible, the indenter was moved up using the stepper motors and the PZT drive, adjusting the camera to keep the tip in view. Both the sample surface and the tip appearing together in the TV monitor showed that the two were now close to each other. The normal and tangential load cells were screwed into place and the entire apparatus was then leveled with the help of leveling gauges.

After adjusting the reference surfaces and the capacitance probes, the apparatus was sealed in a sound proof box. The tip was driven a few microns into the sample surface and then withdrawn. The machine was allowed to stabilize for around 15 min. The scratch was made in the X direction with the indenter simultaneously moving up in the Z direction. The scratch length was 120 μm and the indenter moved in the X direction at a speed of 0.5 μm/s. The motion of the X stage was started and then the PZT was activated to drive the indenter into the sample at a predetermined rate called the "loading rate". The normal load, the tangential load and the indenter displacement at each point along the scratch length were recorded on the 486 computer as a data set of voltages. These were converted into forces and displacement using a program called ANALYZE.

A series of scratches were made on the same sample at different loading rates and the resulting scratch tracks were then examined using scanning electron microscopy. From the images obtained, the length, the area and the width of the debonded region were calculated using image analysis software. The critical load at which the film delaminates along with the dimensions of the debonded region were used to determine the adhesion strength of the film.

4.3. Analysis of the Microscratch Test

The strength of the interface is characterized in terms of the work of adhesion. The work of adhesion for thin film adhesion is the strain energy released when the film delaminates due to the increasing shear stresses ahead of the sliding indenter tip (Venkataraman et. al, 1993). Several researchers have attempted to analyze the scratch test in terms of the forces and stresses acting on the indenter and various models have been developed for determining the interfacial work of adhesion (Venkataraman et. al, 1992; Coghill and St. John, 1990; Laugier, 1989; Burnett and Rickerby, 1988; Bull et. al, 1988 and Benjamin and Weaver, 1963).

To obtain an expression for the shear stress at the interface as a function of the pressure under the indenter tip, Benjamin and Weaver (1963) analyzed the forces acting in a scratch test. Their expression, which is valid for soft metal films, was derived for a smoothly rounded point moving across the film surface. An important assumption in their analysis is that the radius of the indenter tip is large compared to the thickness of the film.

This assumption is not valid in our case as the film being tested is extremely thin. Burnett and Rickerby (1988) and Bull et al. (1988) modeled the stresses generated during a scratch test using an elastic-plastic indentation analysis in order to relate the critical load and the friction between the indenter and the coating to the work of adhesion. This analysis considers very thin films but is applicable only to cases where the tensile stresses normal to the interface are responsible for film detachment. Laugier (1989) used the applied normal stresses generated ahead of the indenter tip to determine the work of adhesion. However, the drawback of this theory is that it applies only to hard coatings and that only normal stresses are used rather than shear stresses along the interface. In a more recent study, Coghill and St. John (1990) related the horizontal force exerted against the indenter tip to the maximum shear stress in the film. The work of adhesion was then calculated from this maximum shear stress. But, plastic deformation of the film at the interface was not considered in their analysis. A model developed by Venkataraman et al. (1992) uses an elastic contact mechanics approach to relate the stresses acting in a scratch experiment to the strain energy released during film delamination. Using this model, the work of adhesion and hence the interfacial fracture toughness have been determined for metal/ceramic systems. In a subsequent paper (Venkataraman et al. 1993) metal/polymer interfaces were tested and the same model was used to obtain the work of adhesion.

All of the above models were for brittle films on brittle substrates or for ductile films on brittle substrates. No such model is available for brittle polymer films on ductile polymer substrates, which can account for the elastic-plastic deformation of the film and

the substrate, and the viscoelastic behavior of polymer systems. Thus, instead of using any of the above models for our complex system, we tried to use a linear elastic fracture mechanistic approach to solve our problem.

Using Dundurs parameters for the PS and EVA (28%), one can show that the α parameter approaches unity. The phase angle, important to mixed mode loading in the bi-material case, is given by,

$$\psi = \phi + \omega = \tan^{-1}\left(\frac{k_2}{k_1}\right) = \tan^{-1}\left(\frac{k_{II}}{k_I}\right) + \omega(\alpha,\beta) \qquad (4.1)$$

where k_{II} and k_I are the applied Mode II and I stress intensities and ω is the phase shift due to the bi-material constants (α, β) being different. With $\beta \sim 0$ and $\alpha \rightarrow 1$, it can be shown that the phase shift is much greater than $10°$. Thus, even though no suitable model is available which accounts for all the complexities of our system (elastic, plastic, viscoelastic deformations) the bi-material interface problem should be addressed.

As a first approximation, the interfacial strength in our system was found using a linear elastic fracture mechanics (LEFM) analysis developed for cracks at the interface between two bonded dissimilar media. Several authors have considered problems of a similar nature (Williams, 1959; Sih and Rice, 1964; England, 1965; Erdogan, 1965; Rice and Sih, 1965; Malyshev and Salganik, 1965; Comninou, 1978; Comninou and Schmueser, 1979 and Rice, 1988). Williams (1959) considered the plane problem of a

semi-infinite crack in dissimilar materials. He found for the first time that the stresses possess an oscillatory character of the type,

$$\sigma \sim r^{-1/2} \sin\left(\varepsilon \ \log r\right) \tag{4.2}$$

where r is the distance from the crack tip and ε is a bielastic constant. Although Williams analysis predicted the behavior of the stresses in the vicinity of the crack tip, it did not give quantitative results. Rice and Sih (1965) solved the problem of a crack at the interface between dissimilar elastic bodies by using a complex-variable method combined with eigenfunction expansion. The solution for the problem of an isolated force having components in the x and y-direction, applied at an arbitrary location has been reported and is used to analyze our system.
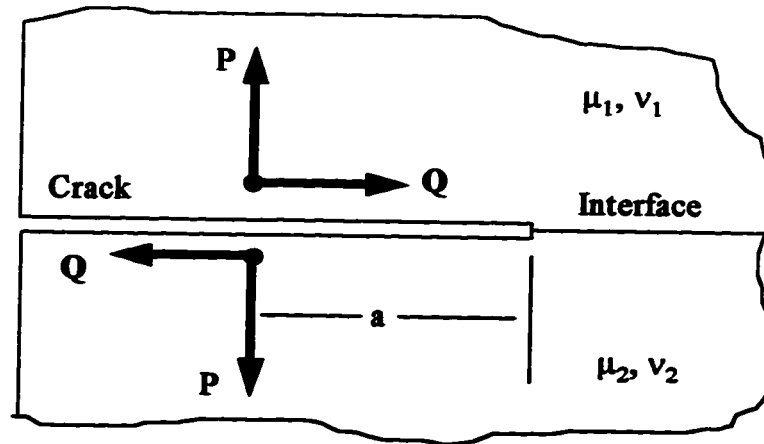
Fig. 4.5. Linear Elastic Fracture Mechanics (LEFM) model used to estimate the interfacial work of adhesion. (adapted from Rice and Sih, 1965)

In this analysis (Rice and Sih, 1965), we consider a line crack situated at the interface and this crack is subjected to a complex force $R=Q+iP$ on each side of the crack

at a distance 'a' from the crack tip (Fig. 4.5). Here, Q is the force parallel to the crack and P the force perpendicular to the crack and these are measured as the tangential load and the normal load respectively in the microscratch test. The stress-intensity factors k_I and k_{II} depend quantitatively on the external loads P and Q and the dimensions of the crack. A complex solution was obtained for the above problem by Rice and Sih (1965) and k_I and k_{II} at the crack tip were obtained from this solution. These stress-intensity factors are used to analyze our system and are given as,

$$k_I = \frac{1}{\pi}\left(\frac{2}{a}\right)^{1/2}\left[P\ \cos(\varepsilon\ \log a) + Q\ \sin(\varepsilon\ \log a)\right] \tag{4.3}$$

$$k_{II} = \frac{1}{\pi}\left(\frac{2}{a}\right)^{1/2}\left[Q\ \cos(\varepsilon\ \log a) - P\ \sin(\varepsilon\ \log a)\right] \tag{4.4}$$

In the above equations ε is a bielastic constant and is defined as,

$$\varepsilon = \frac{1}{2\pi}\log\left[\frac{C_{EVA}}{C_{PS}}\right] \tag{4.5}$$

where, $C_{EVA} = \dfrac{\eta_{EVA} + 1}{\mu_{EVA}}$, $C_{PS} = \dfrac{\eta_{PS} + 1}{\mu_{PS}}$,

$\eta_{EVA} = 3 - 4\gamma_{EVA}$ and $\eta_{PS} = 3 - 4\gamma_{PS}$ (for plane strain)

In the above equations, μ is the shear modulus and γ is the Poisson ratio of the two polymers.

Using these stress-intensity factors k_I and k_{II} the work of adhesion or the energy release rate per unit area is calculated using a method proposed originally by Malyshev and Salganik (1965) and then modified in terms of complex variables by Rice (1988).

$$G_i = \frac{(C_{EVA} + C_{PS})K\overline{K}}{16 \; \cosh^2(\pi \; \varepsilon)} \qquad (4.6)$$

Here, K is a complex stress-intensity factor and is related to k_I and k_{II} by:

$$K = (k_I + ik_{II})\sqrt{\pi} \; \cosh(\pi\varepsilon) \qquad (4.7)$$

Thus, the work of adhesion is given as:

$$G_i = \frac{\pi}{16}(C_{EVA} + C_{PS})(k_I^2 + k_{II}^2) \qquad (4.8)$$

Eqn. 4.8 is used to estimate the interfacial work of adhesion for our system of a thin PS film on an EVA substrate. The above equation utilizes the material constants for the two polymers and the stress intensity factors which are calculated from Eqn's 4.3 and 4.4.

4.4. Results and Discussion

Scratches were made on the PS film supported by 9%, 15% and 28% EVA discs. However film delamination corresponding to a critical load drop was observed only for the 28% EVA ($T_g = -33°C$). This suggests that the PS/28% EVA system had the weakest interface, while in the case of the 9% and 15% EVA, the interface was too strong to see any significant failure under the loading rates used. This qualitative result was confirmed using the Double Cantilever Beam (DCB) test from Chapter 3. A detailed description of the test and the theory behind it can be found elsewhere in Chapter 3. In this test, strips of two polymers are annealed together at a temperature above the glass transition of one of

the polymers for a fixed amount of time. A razor blade is inserted at the interface between the polymers. A crack results which is allowed to equilibrate and then its length is noted. The work of adhesion is calculated using the crack length, the thicknesses of the polymer strips and the modulii of the polymers. EVA strips with 9, 15 and 28% vinylacetate content were annealed onto PS strips and the system was tested as explained above. The effect of the vinylacetate content on the work of adhesion is as shown in Fig. 4.6.
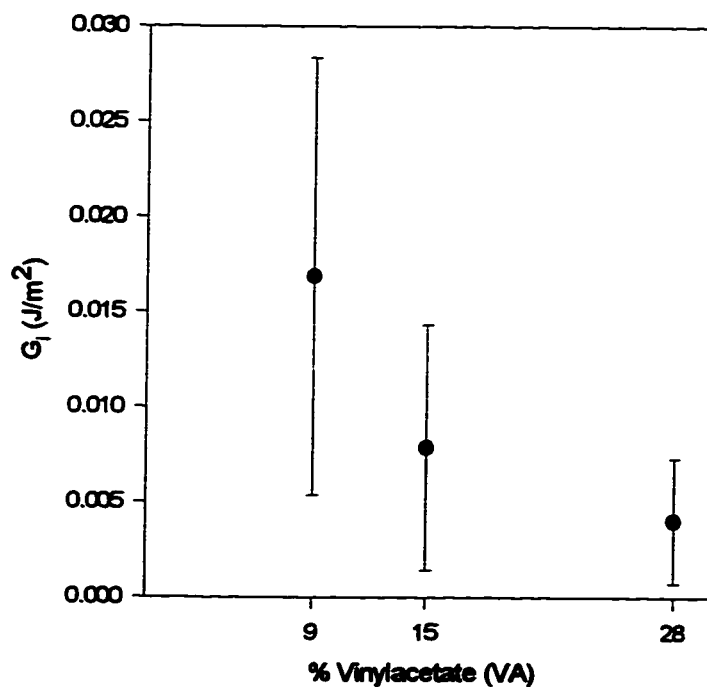
Fig. 4.6. The work of adhesion versus the % vinylacetate in the EVA copolymer for the PS/28%EVA system using the DCB test.

The results show that the work of adhesion decreases with increasing vinylacetate content and confirm the qualitative observations made about the effect of the vinylacetate content using the microscratch test.

The explanation for this decrease in the work of adhesion with the vinylacetate content is similar to that given in § 3.3 based on the diffusion theory of adhesion of polymers (Wu, 1982 and Kaelble, 1971). According to this theory the strength of the interface depends on the diffusion coeeficient of the polymers forming the interface. The molecules of the 28% EVA are more rigid and are not able to diffuse into the polystyrene as effectively as those of the 9% and the 15% EVAs. Therefore the interfacial adhesion strength is lower for the 28% case. Also, the 28% EVA has a lower molecular weight than the 9% and 15% EVAs (due to its higher melt flow index). Although the effect of molecular weight on the adhesion is variable, in our case, the lower molecular weight led to low cohesive strength of the sample and thus reduced the strength of the bond between PS and the EVA. The chemical architecture of the different EVAs may also affect the adhesion at the interface between the PS and the EVA.

For the 28% EVA/PS system annealed for 10 min. at 100°C, a series of load versus scratch distance curves are shown in Fig. 4.7. Each curve has been offset by 100 μm from one another for clarity. In each run, the value of the critical tangential load drop is consistent at 15.0 $\pm$ 0.5 mN. Using the LEFM analysis, the stress-intensity factors, k_I and k_{II}, and the work of adhesion, G_i, were determined and are listed in Table 4.1. Appendix B details the calculation procedure and the other parameters used to determine the stress-intensity factors and hence the work of adhesion.
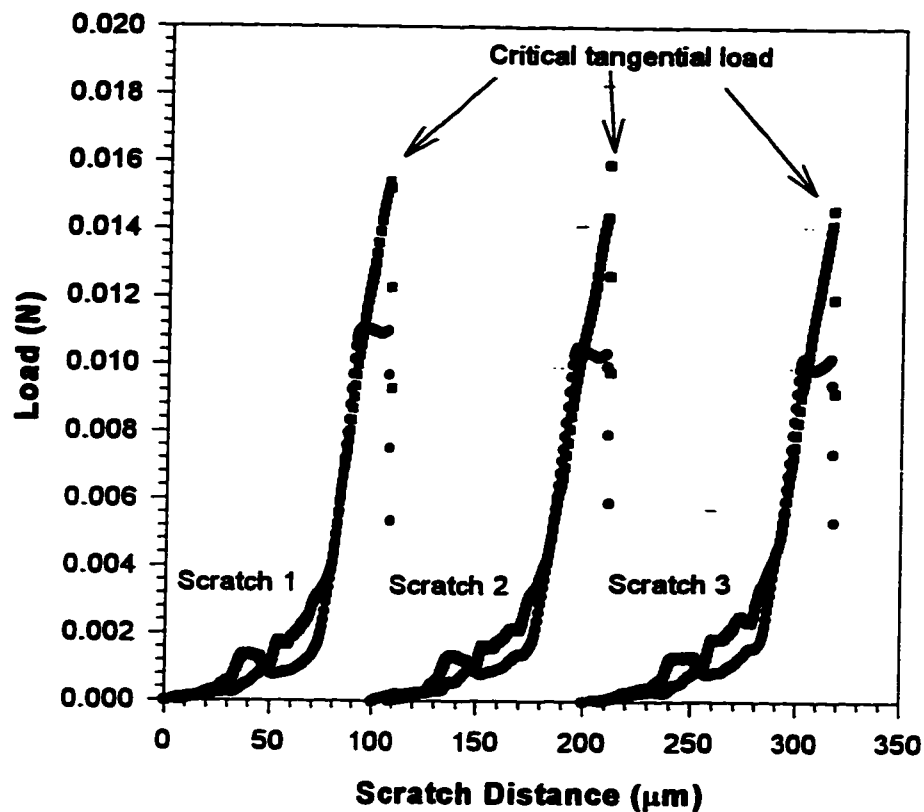
Fig. 4.7. Scratch distance versus load curves for the 0.55 μm PS film on the 28%EVA substrate. The film substrate system was annealed for 10 minutes at 100°C.

Scratch	a (μm)	P (N)	Q (N)	k_I (MPa.m$^{1/2}$)	k_{II} (MPa.m$^{1/2}$)	G_i (J/m^2)
1	15	0.011	0.0155	-282.9	287.8	0.0044
2	15	0.0105	0.016	-295.2	279.2	0.0045
3	15	0.01	0.0145	-265.7	263.1	0.0038
					Average	0.0042

Table 4.1. Stress intensity factors and the work of adhesion for the 0.55 μm PS film on the 28%EVA using the LEFM model at a loading rate of 75 μm/s.

F: 110 μm

E: 95 μm

D: 80 μm

C: 50 μm ⎤
B: 40 μm ⎬ -Stick -Slip
A: 30 μm ⎦
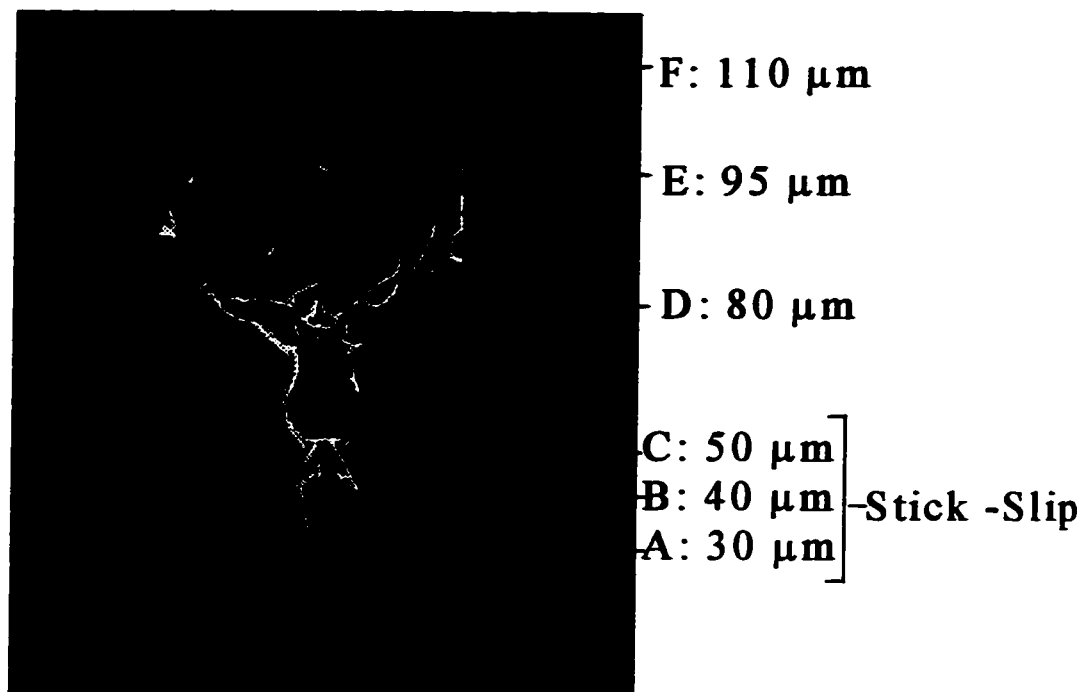
Fig. 4.8. A scanning electron micrograph showing the morphology and sequence of events occurring during the scratch test on a 0.55 μm PS film on 28%EVA.

The scanning electron micrograph of the scratch track is as shown in Fig. 4.8 for the 28%EVA/PS system. The scratch track is 120 μm long and the indenter was traveling across the film at 0.5 μm/s and into the film (loading rate) at 75 μm/s. The micrograph indicates some features which are characteristic of this polymer/polymer system. One of the features seen here and which has also been reported by Venkataraman et al. (1993) are the very symmetrical gouges in the initial portion of the scratch track (30-50 μm). Fig. 4.9 shows the load versus scratch distance curve for the scratch shown in Fig. 4.8.
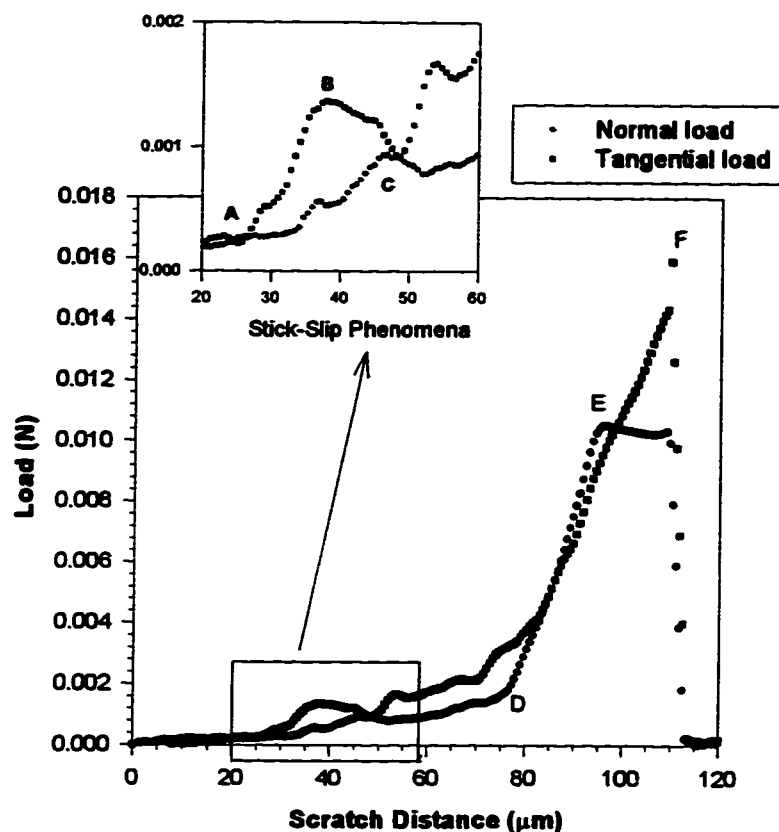
Fig. 4.9. A scratch-loading curve for the 0.55 μm PS film on 28%EVA showing the sequence of events occurring during the scratch test.

Comparison of the scratch track (Fig. 4.8) with the load profile (Fig. 4.9) shows that these gouges are due to the "stick-slip" phenomenon. As the indenter drives up into the PS film, stresses build up ahead of the indenter and the loads increase (Point A in Fig. 4.9). Due to these stresses, a crack initiates at the bottom of the tip and propagates into the polystyrene (Point B). Because of the stresses acting on the face of the indenter tip, the indenter finally rides up over the built-up material, and the load drops (Point C). The

polymer springs back beneath the tip and the process can be repeated again and again if the loading rate is low enough so that the indenter tip never reaches the interface.

However, if the rate at which the indenter is penetrating into the film is high enough, then the crack initiated by the tip, instead of propagating into the PS film, reaches the interface. At this point, the indenter is at the interface, but, instead of riding up over the material ahead of it, it keeps digging into the substrate and there is a sharp increase in both the tangential and the normal loads (Point D). At Point E, the indenter starts tearing into the film ahead of it and this causes the indenter to stop its motion into the substrate and the normal load becomes constant while the tangential load still increases. As the indenter moves ahead with its tip at the interface, the film behind it is being stretched and pulled and at Point F the stresses become high enough that the film delaminates. The strain energy released at this point is so high that it causes the indenter to jump away from the sample and both the normal and the tangential loads drop.

Scratch	Loading Rate (μm/sec)	Average G_i, LEFM (J/m^2)	Average G_i Viscoelastic (J/m^2)
1	62.5	0.0034	2.1e-3
2	100	0.0059	3.1e-3
3	125	0.0096	4.8e-3
4	150	0.0154	7.4e-3
5	175	0.0173	8.2e-3

Table 4.2. Effect of the loading rate on the interfacial properties of PS film on 28%EVA showing the viscoelastic nature of this system.

Since polymers are rate sensitive materials, the effect of different indenter penetration rates on the work of adhesion was studied. The work of adhesion was determined using the linear elastic estimate and is given in Table 4.2 for the different loading rates used. A plot of the work of adhesion versus the loading rate is shown in Fig. 4.10.
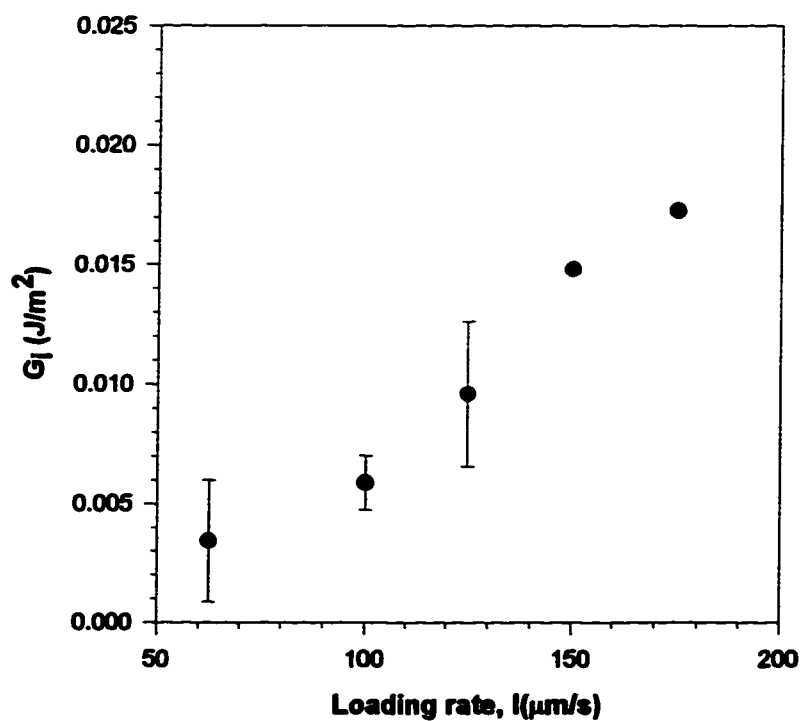
Fig. 4.10. The interfacial work of adhesion versus the loading rate.

This plot shows that the work of adhesion increases with the loading rate. The work of adhesion increases at higher loading rates due to an increase in the plastic, viscoelastic

deformation mechanisms. Similar trends in the fracture toughness of bimaterial blocks of different polyurethanes have been reported as a function of the speed of crack propagation (Bowen and Knauss, 1992 and Knauss, 1971). This led us to examine the viscoelastic nature of our system in more detail.

Instead of calculating the work of adhesion G_i by Eqn. 4.8, the left hand side of this equation was changed to a rate dependent work of adhesion. This rate dependent work of adhesion consists of two parts. One is the viscoelastic contribution to the interfacial strength which is incorporated as a function, ψ_i. This function depends on the rate of crack propagation or, in our case, the loading rate, L. The other component is the rate independent intrinsic work of adhesion G_i and the modified equation is,

$$G_i \times \psi_i(l) = \frac{\pi}{16}(C_{EVA} + C_{PS})(k_I^2 + k_{II}^2) \tag{4.9}$$

Thus, on calculating k_I and k_{II} by Eqn. 4.3 and Eqn. 4.4 and then using Eqn. 4.9 to get G_i the time dependent behavior of the sample has been accounted for. The function $\psi_i(l)$ is obtained from the work by Bowen and Knauss (1992), assuming linear viscoelastic behavior. This function is obtained experimentally using stress-intensity factor data. At the loading rates used, the value of $\psi_i(l)$ is fairly constant. The intrinsic work of adhesion at different loading rates after incorporating viscoelasticity is listed in Table 4.2. The intrinsic work of adhesion obtained is much lower than that obtained using the LEFM model. However, this is expected since, the viscoelastic dissipation is included within the function ψ_i and we get the true strength of the interface.
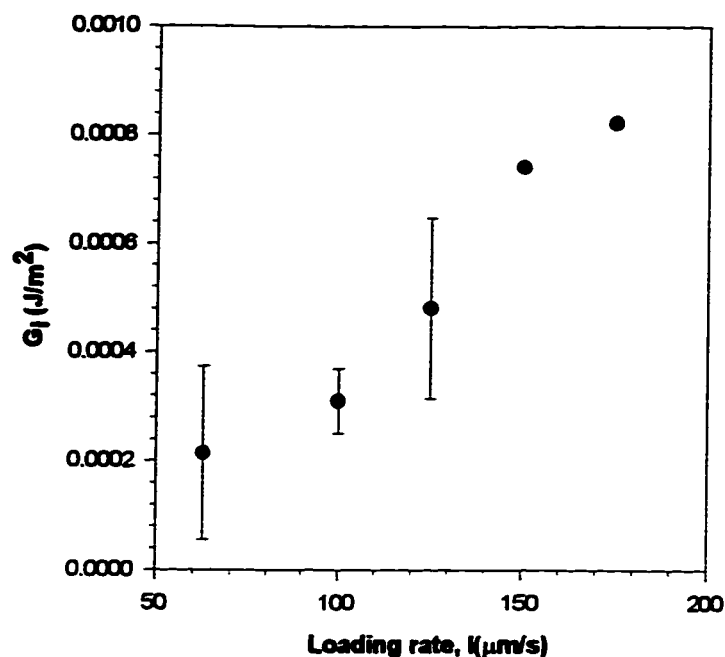
Fig. 4.11. The intrinsic work of adhesion as a function of the loading rate after taking into account the time dependent behavior of the system.

From Fig. 4.11, we see that the interfacial work of adhesion obtained after incorporating viscoelastic effects still increases. This is because in this analysis the viscoelastic contribution to the work of adhesion is not additive. These calculations have been done assuming that the results of Bowen and Knauss (1992) are applicable to other viscoelastic systems.

4.5. Conclusions

The microscratch test was used to determine the interfacial work of adhesion of a thin film/substrate polymeric system. In this test, a sharp drop in the normal and tangential

loads occurs when the film delaminates and this load drop is related to the adhesion strength of the system. The delamination of the film caused by the indenter is extensive and catastrophic. This was the first time a system of a thin film of a brittle polymer (PS) on a rubbery substrate (EVA) has been studied using this test. The adhesion between the PS film and the 28% EVA was the weakest compared to that between the PS and 9% and 15% EVA. This was confirmed using a Double Cantilever Beam (DCB) test, which showed that the work of adhesion between PS and EVA decreases with increasing vinylacetate content. The inverse dependence of the work of adhesion on the % vinylacetate was qualitatively explained using the diffusion theory of adhesion. The interfacial work of adhesion for the PS-28%EVA was calculated using a linear elastic fracture mechanics model for a crack at the interface between dissimilar materials. The values obtained for the work of adhesion using the linear elastic model are in the range of 0.001-0.02 J/m^2 and overestimate the work of adhesion due to elastic, plastic and viscoelastic dissipation in the sample. A preliminary investigation into the viscoelastic behavior of the system was attempted by measuring the work of adhesion at different rates of loading. It indicates that the work of adhesion is a function of the loading rate. An attempt was made to incorporate time dependence of the viscoelastic sample into the analysis. On doing this the work of adhesion decreases to 0.0002-0.0008 J/m^2.

4.6. References

Ahn, J., Mittal, K. L., and MacQueen, R. H., *Adhesion Measurements of Thin Films, Thick Films, and Bulk Coatings*, ed. K. L. Mittal, (ASTM Spec. Tech. Publ. 640, Philadelphia, 1978), p. 134.

Benjamin, P., and Weaver, C., *Proc. Roy. Soc. London* **A274**, 267(1963).

Bornside, D. E., Macosko, C. W., and Scriven, L. E., *J. Appl. Phys.* **66**, 5185(1989).

Bowen, J. M., and Knauss, W. G., *J. Adhesion* **39**, 43(1992).

Brown, H. R., *J. Mater. Sci.* **25**, 2791(1990).

Bull, S. J., Rickerby, D. S., Matthews, A., Leyland, A., Pace, A. R., and Valli, J., *Surf. Coatings Technol.* **36**, 503(1988).

Burnett, P. J., and Rickerby, D. S., *Thin Solid Films* **157**, 233(1988).

Cherry, B. W., *Polymer Surfaces*, Cambridge University Press, Cambridge, 1981.

Chu, Y. Z., and Durning, C. J., *J. Appl. Poly. Sci.* **45**, 1151(1992).

Coghill, M. D. E., and St. John, D. H., *Surf. Coatings Technol.* **41**, 135(1990).

Comninou, M., and Schmueser, D., *J. Appl. Mech.* **46**, 345(1979).

Comninou, M., *J. Appl. Mech.* **45**, 287(1978).

Creton, C., Kramer, E. J., Hui, C., and Brown, H. R., *Macromolecules* **25**, 3075(1992).

Croll, S. G., in *Adhesion Aspects of Polymeric Coatings*, ed. K. L. Mittal, (Plenum, New York, 1983), p.107.

Croll, S. G., *J. Appl. Poly. Sci.* **23**, 847(1979).

Engel, P. A., and Pedroza, G. C., in *Adhesion Aspects of Polymeric Coatings*, ed. K. L. Mittal (Plenum, New York, 1983), p.583.

England, A. H., *J. Appl. Mech.* **32**, 400(1965).

Erdogan, F., *J. Appl. Mech.* **32**, 403(1965).

Julia-Schmutz, C., and Hintermann, H. E., *Surface and Coatings Technology* **48**, 1(1991).

Kaelble, D. H., *Physical Chemistry of Adhesion*, Wiley-Interscience, New York, 1971.

Knauss, W. G., *J. Composite Materials* **5**, 176-192(1971).

Laugier, M. T., *J. Mater. Sci.* **21**, 2269(1986).

Malyshev, B. M., and Salganik, R. L., *Inter. J. Frac. Mech.* **1**, 114(1965).

Mittal, K. L., *Adhesion Measurements of Thin Films, Thick Films, and Bulk Coatings*, ed. K. L. Mittal, (ASTM Special Technical Publication, Philadelphia, 1976), p. 5.

Mittal, K. L., *Electrocomponent Science and Technology* **3**, 21(1976).

Rice, J. R., and Sih, G. C., *J. Appl. Mech.* **32**, 418(1965).

Rice, J. R., *Trans. ASME,* **55**, 98(1988).

Ritter, J. E., Lardner, T. J., Rosenfeld, L., and Lin, M. R., *J. Appl. Phys.* **66**, 3626(1989).

Sih, G. C., and Rice, J. R., *J. Appl. Mech.* **31**, 477(1964).

Van Krevelen, D. W., and Hoftyzer, P. J., *Properties of Polymers*, Elsevier Scientific Publishing Co., New York, 1976.

Venkataraman, S., Kohlstedt, D. L., and Gerberich, W. W., *J. Mater. Res.* **7**, 1126(1992).

Venkataraman, S., Kohlstedt, D. L., and Gerberich, W. W., *Thin Solid Films* **223**, 269(1993).

Venkataraman, S., M. Sc. Thesis, University of Minnesota (1992).

Venkataraman, S., Nelson, J. C., Hsieh, A. J., Kohlstedt, D. L., and Gerberich, W. W., *J. Adhesion Sci. Technol.* **7**, 1279(1993).

Weaver, C., *J. Vac. Sci. Technol.* **12**, 18(1975).

Williams, M. L., *Bull. Seismol. Soc. America* **49**, 199(1959).

Wu, S., *Polymer Interface and Adhesion*, Marcel Dekker, New York, 1982.

Wu, T. W., *J. Mater. Res.* **6**, 407(1991).

CHAPTER 5

Stability and Breakup of Thin Polymer Films

5.1. Introduction

As illustrated in Chapter 4 polymer films are being used in a variety of industrial and domestic applications. Along with the adhesion of these films to substrates, the stability of the film also plays an important role in determining the structural integrity of the application. Ideally, the film should be homogeneous, uniform in its thickness and should be stable at the operating conditions of the application. However, thin polymer films have been found to be thermally unstable and dewet by the formation of holes. It has also been reported that during the blending of two polymers, the dispersed phase polymer is stretched into thin sheets due to the shearing action. These sheets then breakup by the formation of holes and the final morphology is a fine dispersion of spherical droplets. In some applications these sheets may be the final morphology sought. Thus not only do we need to analyze the factors governing the breakup of polymer films in applications where they are directly used, but also in applications like polymer blends, where films are an intermediate stage in the overall morphological development. Coextruded polymer products consist of alternate layers of polymers. The mechanical strength of these products also depends on how stable these layers are. In this work, an attempt has been made to model the breakup of thin polymer films in a polymer matrix in the quiescent state.

The breakup or the dewetting of any liquid film is an energetic phenomenon and is preferred whenever the free energy decreases upon formation of a hole in the film. This is true for all films: (a) films surrounded by another medium, e.g. soap films, sheets of liquid produced by a nozzle, sheets of a polymer in a polymer blend or (b) films deposited on a substrate, where the film is bounded by the solid substrate on one side and a fluid on the other. The film ruptures only if the diameter of the hole is greater than the thickness of the film as this results in a loss in surface area decreasing the free energy of the system and causes the hole to grow further.

5.1.1. Breakup of Free Liquid Films

Free liquid films are films which are bounded on either side by the same material. This can be air in some cases like soap bubbles while in others it may be another liquid. The breakup of free Newtonian liquid sheets has been investigated extensively by several researchers. The systems that have been studied are the disintegration of sheets formed from nozzles and the breaking of soap bubbles. Dupré was the first to analyze the breakup of a film of a Newtonian liquid. He obtained an expression for the velocity at which the film breaks up by assuming that all the energy of the surface that has disappeared is converted into kinetic energy. The equation is given as:

$$v = \left(\frac{k\sigma}{\rho\ h} \right)^{1/2}$$

(5.1)

where, v is the hole velocity, σ the surface tension of the liquid forming the sheet, ρ its density, h is the thickness of the sheet and k is a numerical constant for which Dupré derived a value of 4.

Rayleigh (1891) was the first to photograph the breakup of a soap film using instantaneous photography. The soap film was broken by dropping metal balls through it. He noticed that for very thick films the metal ball went through the film without breaking it, but he was successful in breaking thinner films. No reason for this was given, but this phenomenon was confirmed and explained by Taylor and Michael (1973). Dombrowski et al. (1954) photographed the breakup of sheets produced by nozzles. They noticed that the holes in the sheets remain circular until they coalesce forming long threads. These threads become unstable due to Rayleigh-like instabilities and break down into drops. It was reported that the expansion of the holes occurs due to surface tension forces. For liquids having viscoelastic properties, the sheet disintegrates through the formation of waves. However, as the rate of shear is reduced, the viscosity increases rapidly as the stream moves away from the mouth of the nozzle and this prevents further breakup of the threads into drops and a web of fine threads results. De Vries (1958) also observed the disintegration of sheets formed from an aqueous Tee-pol solution. He reported that rupture occurs in the thinnest part of the sheet.

Eqn. 5.1 predicts a constant hole velocity, and this was experimentally confirmed by de Vries in 1958 and by Ranz in 1960. The strong dependence of hole velocity on film

thickness given in Eqn. 5.1 was also confirmed by many authors (de Vries, 1958; Taylor, 1959; Ranz, 1960; and Culick, 1960). Ranz (1960) further reported that all of the liquid from the expanding hole goes into the rim of the hole, while the rest of the film is unaffected by the hole. On the basis of a momentum balance, Taylor in 1959, and Culick in 1960, suggested a formula similar in all respects to Eqn. 5.1, except with k=2. The difference in the coefficient k, appears because of their assumption that all of the surface energy is not converted into kinetic energy, but rather that some is dissipated as heat due to frictional resistances. Fraser et al. (1962) analyzed the performance of a nozzle used in spraying and reported that aerodynamic waves cause the spray sheets to breakup into a network of unstable ligaments produced by the coalescence of expanding perforations. McEntee et al. (1969) reported similar results, where a soap film is punctured to form holes which grow at a constant velocity. They plotted the coefficient k in Dupre's equation versus the film thickness and found that the value of k=4 obtained by Dupre is never approached. This implied that some surface energy is always converted into heat due to frictional resistance. For films thicker than 100 nm they found that k=2, while for thinner films, k depends upon the thickness of the film. They have also reported the presence of disturbances (captured by high speed photography) ahead of the expanding rim of the perforations and these disturbances grow more rapidly than the holes.

Keller (1983) analyzed the breaking of a liquid film of uniform and non-uniform thickness. He obtained results similar to those of Culick for the uniform films. In 1966 Vrij analyzed the mechanism for the spontaneous rupture of thin, free liquid films. It was

reported that the stability of a film depends upon the processes of thinning and breaking. Thinning occurs by draining of the liquid due to gravitation and suction. When the thickness of the film is reduced to about 100 nm, other forces such as van der Waals attraction and double layer repulsion influence the draining process. Spontaneous rupturing of a film requires a high activation energy for films thicker than 10 nm. Thus, such films do not breakup spontaneously, but require external media such as vibrations, dust particles, etc. to cause rupture. It was proposed that films below a certain critical thickness were unstable and in these films surface corrugations due to thermal motion may grow causing rupture of the film. The kinetics of these fluctuations have been obtained assuming a laminar liquid flow inside the film. The life-time and critical thickness of an unstable film have also been calculated. The analytical results obtained have been compared with experimental data for the breakup of water and aniline films in air.

5.1.2. Breakup of Liquid Films on Surfaces

For a liquid film on a surface, the stability of the film depends on the physicochemical properties of the surface and the liquid. One of the most important criteria determining this stability is the wetting characteristic of the film on the surface as explained in § 1.2.

Taylor and Michael in 1969 performed experiments on the breaking of sheets of mercury and sheets of water standing on paraffin wax. The holes were formed in the sheets using cylindrical probes. They found that large holes opened whereas smaller ones closed up because in both cases the surface area decreases. It was noticed that the films

ruptured only when their thickness was below a certain critical value. If the liquid film is relatively thick, irrespective of the size of the hole produced in them by the probes, they always remained stable and did not rupture. This stability was the result of gravity damping out the destabilization due to the interfacial tension forces. The critical thickness above which the films were unconditionally stable was derived by Taylor and Michael and, is given by,

$$h = 2\left(\frac{\sigma}{\rho g}\right)^{1/2} \sin\frac{\theta}{2} \tag{5.2}$$

where σ is the surface tension of the liquid forming the film, ρ is its density, g is gravitational acceleration and, θ is the equilibrium contact angle. Once a hole forms in a film, either due to dust particles or external vibrations it may be stable or unstable depending on the interfacial energy and gravity.

Thermodynamically, film breakup becomes possible when the free energy of the film-solid system becomes equal to or greater than the free energy after the formation of a hole in the liquid film. The thickness of the film at this thermodynamic condition is called the critical thickness. Sharma and Ruckenstein (1989) explored the dependence of this critical thickness on the interfacial tension between the solid and the liquid and the equilibrium contact angle on the basis of the above thermodynamic argument. They found that the critical thickness is proportional to the hole radius and is nonlinearly dependent on the contact angle. In a subsequent investigation, Sharma and Ruckenstein (1990) calculated the profile of a hole formed in a film on the basis of the Young-Laplace

equation of capillarity. They calculated the free energy change produced by the formation of a hole. This free energy change was found to be a maximum at a thickness called the "transitional" thickness and decreases as the thickness is reduced until the critical thickness is reached. The film was assumed to be unstable between the transitional and the critical thickness.

Brochard Wyart and Daillant (1990) obtained analytical results for the breakup of films of wetting and nonwetting liquids on solid substrates. For a nonwetting liquid, they proposed that the film is metastable if it is thick and evolves via the nucleation and growth of a hole at constant velocity. If it is thin, the film is unstable and breaks up into microscopic droplets. On the other hand, for a wetting liquid, the film also breaks up via nucleation and growth of a hole. However, the hole growth rate is no longer constant and decreases with time as $t^{-1/2}$. In a subsequent paper, Redon et al. (1994) explained this nonlinearity in hole growth to be due to a slippage of polymer chains on the solid surfaces. Redon et al. (1991) performed experiments on films of silicone oils and alkanes deposited on grafted silicon wafers. They observed that these films dewet the solid surface by forming holes and the holes grow at a constant velocity. The holes are circular with a rim around them which grows with time. The film outside the rim remains undisturbed and the dynamics of hole growth is governed by hydrodynamics. The velocity of hole growth was inversely proportional to the fluid viscosity and was independent of the thickness of the film in a certain range of thicknesses.

Ksheshigi and Scriven (1991) used the Navier-Stokes equation for modeling the process leading to the rupture of a nonwetting liquid on a solid surface. They theorized that dewetting starts from either a pre-existing patch or initiates from some film thinning disturbance that grows until the film ruptures. Implications of this dewetting have been discussed for the coating industry. Zhao et al. (1993) observed the dewetting of polyethylene-propylene films of various molecular weights on Si surfaces when the film thickness was less than the polymer radius of gyration. The dewetting was studied using an atomic force microscope (AFM).

Reiter (1992, 1993 and 1994) was the first to document the entire process of the breakup of liquid films on solid surfaces. He studied polystyrene films (< 100 nm) spuncast on silicon wafers and observed that the smooth films became rough and broke up into holes via the amplification of thermal fluctuations. These films are stable at temperatures well below the glass transition temperature (T_g) but may become unstable above T_g. Above T_g, thermal fluctuations may increase in amplitude and lead to the rupture of the film. Reiter (1994) found that for very thin films, dewetting started even below T_g implying that the T_g is lower for thin films. The film broke up by forming holes of uniform size which grew simultaneously at a constant velocity and were randomly distributed. The holes formed ribbons at their edges which broke up into droplets. The final morphology was a random distribution of drops which made up the borders of almost equal sized polygons. An important observation made by Reiter, which experimentally confirmed earlier researchers, was the strong influence of film thickness on the breakup

characteristics. He found that the number of initial holes formed in the films, the number of polygons resulting finally, the size of these polygons all depended on the thickness of the film. The case of polymer/polymer dewetting has also been studied by Shull and Karis (1994) for a system of poly(ethylenepropylene) (PEP) films on polystyrene (PS) or polymethylmethacralate (PMMA) surfaces. The dewetting was initiated by immersing the system in alcohols which resulted in large equilibrium angles. The dewetting velocities obtained were constant. In some cases, crazing within the PS substrate led to inconsistent results. The crazing was thought to be caused by the solvents used for casting the PEP films.

Most of the research described above was for the dewetting of liquid films deposited on solid surfaces. However, Martin et al. (1994) were the first to analyze the problem of dewetting of a liquid film from a liquid substrate. They deposited a polydimethylsiloxane (PDMS) film on an immiscible fluorinated PDMS surface. This situation led to features different from those encountered for the case of a film on a solid surface such as (a) a deformable interface between the two liquids (b) presence of a flow field in the substrate due to hole opening and (c) dissipation in both the film and in the substrate. By varying the ratio of viscosities of the film and the substrate, they could study different situations ranging from the solid-like substrate to a liquid-like substrate. The viscosity ratio was varied from 1 to 10. The holes for these systems also opened at a constant velocity and were perfectly circular with a rim at their edges. The hole velocity was inversely proportional to the substrate viscosity. There was no significant effect of

film viscosity on the hole opening velocity. However, for a viscosity ratio higher than 10, they observed a regime where the holes grew at a nonlinear rate. The authors explained that this phenomenon was not completely understood and would be discussed later. The effect of film thickness was also studied and there was again a strong dependence of thickness on hole velocity.

Liu et al. (1994) also studied the dewetting of PS films deposited on polyvinylpyridine (PVP) - PS block copolymer films supported on a silicon wafer. They studied the role of molecular architecture of the copolymer surface on the dewetting process. The dynamics of dewetting were found to be a function of homopolymer (PS) thickness and the ratio of homopolymer to copolymer molecular weights. Brochard Wyart and de Gennes (1994) have presented a theoretical analysis for the case of a film of water dewetting between a solid and a rubber surface. The assumptions in this theory were that the rubber was deformable, the water film was metastable and the rejected water forms a rim around the hole when dewetting occurs. Based on these assumptions, they obtained an expression for the growth rate of holes in the water film which was not linear, but was $R(t) \sim t^{3/4}$, where R is the radius of the hole and t is time.

Faldi et al. (1995) have studied a system of a polycarbonate (PC) film deposited on another film of poly(styrene-co-acrylonitrile) (SAN), both films being 200 nm thick. These two films were supported on a rigid Si substrate. Upon annealing the samples to a temperature above the T_g of both the PC and the SAN ($\sim$ 190°C), the PC film dewetted

the SAN layer. The morphology and topography of the hole formed in the PC layer and the surrounding rim were studied using optical microscopy, SEM and AFM. The rim formed was asymmetric i.e. it was steep on the inside and decays gradually on the outside. The floor of the hole was a SAN layer, but the thickness of this layer was less than the original SAN layer. The reason for this was given to be a flow induced in the underlying melt by the hole opening.

It has been reported by Scott (1991), Sundararaj (1994) and Sundararaj et al. (1992, 1995) that thin sheets of the dispersed phase are an intermediate morphological feature while blending two immiscible polymers. Holes form in these sheets and the holes coalesce with each other producing drops microns in size. This was the first time the formation of holes in a thin polymer sheet within a polymer matrix was reported. To study the breakup mechanism in detail, a quiescent experiment was designed where a thin polymer film was embedded within the matrix of another immiscible polymer. The specific system was that of a PS film within a PMMA matrix. The system was then annealed at a temperature above the T_g of both polymers. The sheets broke up into holes which grew at a constant velocity. The breakup mechanism was modeled (Sundararaj, 1994) using an energy balance approach and the following expression for the hole velocity was obtained

$$v = \frac{2\sigma\delta}{\eta_d(\delta + h)} \tag{5.3}$$

where σ is the interfacial tension for the PS/PMMA system, δ is a length scale where the fluid is accelerated, η_d is the zero shear rate viscosity of the film at the experimental

129

temperature and h is the thickness of the film. Comparison between experimental and predicted velocities was reasonable (Sundararaj, 1994).

In this work, the stability of a thin film of one polymer when inserted into a melt of another polymer and when confined on both sides by the melt of the other polymer has been studied. All the systems studied were immiscible. The effect of various parameters on the breakup mechanism have been studied. At this point a distinction should be made between the process leading to the initiation of breakup and that occurring after breakup has been initiated. The latter process has been studied in detail. From this point on, the process occurring after breakup will be referred to as the breakup or dewetting process. An attempt has also been made to model the dewetting process using hydrodynamic arguments.

5.2. Experimental

5.2.1. Materials

Two types of polystyrene (PS) were used in this work. These were supplied by the Dow Chemical Company under the tradename STYRON 666D and STYRON 618. The weight average molecular weights of the PS666D and the PS618 were 200,000 and 175,000 respectively and their glass transition temperature (T_g) was 100°C. The polymethylmethacralate (PMMA) was supplied by Rohm & Haas. It had a weight average molecular weight of 110,000 and a T_g of 105°C. Some rheological properties of these materials are given in Table 5.1. These properties were obtained along with other

dynamic rheological data using a Rheometrics RMS 800 rheometer with 25 mm parallel plate fixtures at 10% strain.

	Zero Shear Viscosity (kPa.s)		Characteristic Relaxation Time λ (s)	
Temperature	180°C	220°C	180°C	220°C
PS666D	28.65	2.35	6.73	2.14
PS618	14.0	0.85	4.67	1.00
PMMA	221.4	42.0	10.3	3.25

Table 5.1. Rheological properties of polymers at two temperatures.

5.2.2. Sample Preparation

The sample consisted of a film of one of the polymers sandwiched between two discs of the other immiscible polymer. The polymer discs were compression molded in a Carver Model C laboratory press under pressure at 200°C. Thick stainless steel plates (125 mm × 125 mm × 10 mm) covered with aluminum foil were placed on either side of the mold. The mold was filled with polymer pellets. After heating for 10 min, the polymer was subjected to a pressure of 1 ton for around 10 minutes. The mold was water cooled and discs with a diameter of 10 mm and thickness of 1.3 mm were obtained.

The thin films were produced by spincasting the polymer from a solution. To prepare the solution, the polymer pellets were dissolved in a suitable solvent. The choice of solvent depended on several factors such as time required to dissolve the polymer,

toxicity and the boiling point of the solvent. The boiling point should be lower than the glass transition temperature of the polymer, so that residual solvent can be evaporated after spincasting. The solvent chosen for both the PS and PMMA was toluene.
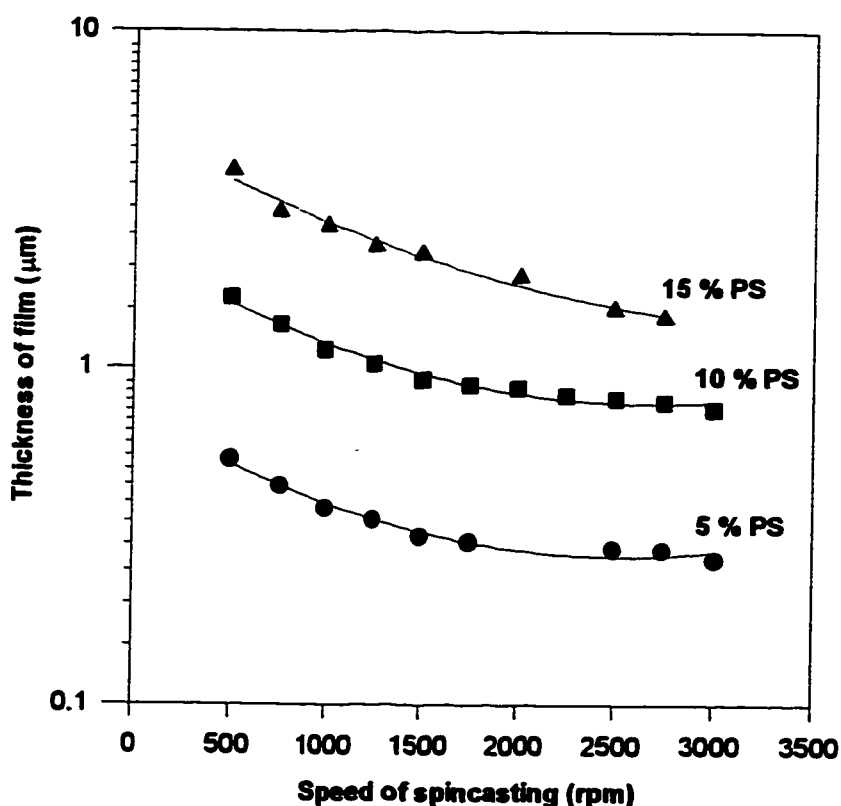
Fig. 5.1. Calibration curve of the Laurell spincaster for PS in toluene

The spincaster used was a Laurell vacuum spin caster (Model WS-200-4T2) with a Teflon body. It had capability for varying the time of rotation from 0-180 seconds and the rotation speed from 200-4000 rpm. Different film thicknesses could be obtained by changing the rotation speed and the concentration of polymer solution used. The

spincaster was calibrated using polymer films cast from different concentration solutions and at different speeds and one such calibration curve was shown in Fig. 4.2 for a 5% PS solution in toluene. The thickness of each film was obtained using an Alphastep Surface Profilometer. A comprehensive calibration curve for three different concentrations of PS in toluene is shown in Fig. 5.1. A glass slide was stuck on the chuck of the spincaster using double sticking tape. The slide was covered completely with the polymer solution and was then spun at a certain speed for a desired amount of time. Most of the solvent was removed during the spincasting process. However, to remove any residual solvent which might affect the experiment, the slide was placed in a closed circulation laboratory oven at 80°C for more than 24 hours.
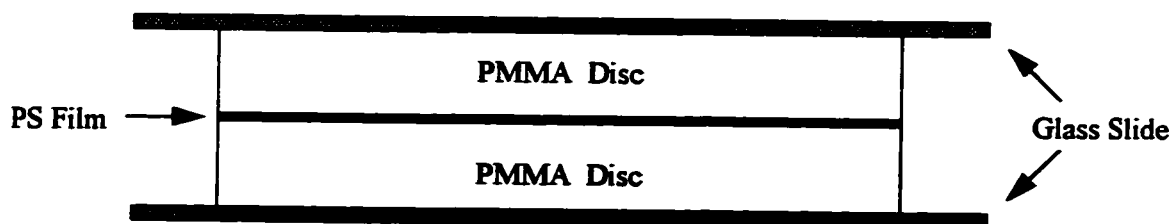
Fig. 5.2. Sample used to study the breakup of a polymer film within a polymer matrix

To introduce the film onto the disc of the other polymer, it was floated off onto the surface of water. This floating off procedure was shown in Fig. 4.3 and discussed in §4.2.2. The disc with the film on it was placed on a glass slide and again put into the closed circulation laboratory oven for about an hour to evaporate any water. At the same time another disc was placed on a glass slide and also put into the oven. After an hour,

this disc was put on top of the film, obtaining the configuration shown in Fig. 5.2. This configuration was again annealed for an hour at 135°C. The sample was now ready.

5.2.3. Annealing Sample

The sample was taken from the oven at 135°C and immediately placed into a Mettler FP-82HT hot stage which was maintained at 100°C. The temperature was ramped at 20°C/min to 200°C. The hot stage was controlled by a Mettler FP90 Central Processing Unit which allowed for precise temperature control within the stage. The stage consisted of two windows, one below and the other above the sample, through which the dewetting process could be viewed. The glass slides at the top and bottom of the polymer discs (Fig. 5.2) prevented the polymer from sticking to the surface of the viewing windows.
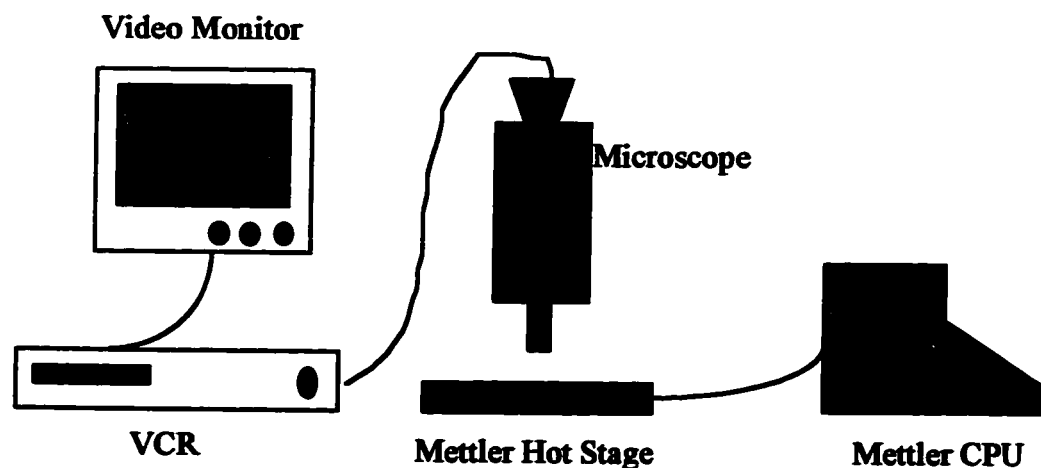
Fig. 5.3. Schematic of the apparatus used to observe the dewetting process

The stage was placed below the objective of an Olympus Metallurgical microscope (Universal Model BHSM - 313U) which had a PULNiX camera (Model TM-745E)

134

attached to it. The camera was connected to a high resolution Olympus endoscopic video monitor (Model OEV141) through a VCR (JVC SR-S360U). The hot stage was programmed to increase the temperature to the desired value. A schematic of the experimental setup is shown in Fig. 5.3. The entire dewetting process was continuously monitored and was recorded using the VCR.

5.3. Results and Discussion

5.3.1. The Dewetting Process

On heating the sample to a temperature above its glass transition temperature, both the polymer film and the substrates were in the melt state. This sample was completely different from those studied by Reiter (1993, 1994) and Martin et al. (1994) where a film was deposited on a substrate or by Ranz (1960) for soap films. In this case, the system was of a liquid polymer film embedded within a liquid matrix. As the temperature of the hot stage increased to the set temperature a melt front was seen to pass across the surface of the sample. This was found to occur about 20°C above the T_g of the matrix polymer. The melt front signified that the sample was no longer in the solid state, but had become liquid-like. The sample flowed and its dimensions changed somewhat before becoming stable. An attempt was made to minimize this flow to prevent the film from experiencing a shearing force which might accelerate the initiation of the breakup process. In addition once the sample was placed inside the hot stage, care was taken to ensure that the hot stage was not disturbed as this too may initiate breakup.

135

The dewetting process progresses through a number of stages which are illustrated in Fig. 5.4. After a certain amount of time, the first holes become visible in the film and dewetting begins. Observing the initial phase of breakup is controlled by the optics since the highest magnification that could be achieved was approximately 800X. Therefore the first observable hole was around 2 µm in diameter. The density of holes formed was found to depend on the thickness of the film being used and this will be discussed later in this chapter. The time required for breakup to occur depended on the annealing temperature. The higher the temperature, the quicker was the initiation of breakup and this agrees with results reported by Reiter (1993). However, according to Reiter, once dewetting was initiated, the dynamics of this process did not depend on the temperature.

For a very thin liquid film (<100 nm) deposited on a solid or a liquid surface, thermal fluctuations cause modulations of the film as shown in Fig. 5.5 and the film is reported to break up via a spinodal decomposition mechanism (Brochard Wyart and Daillant, 1990). These modulations may increase in magnitude (Fig. 5.5b) and when two such modulations meet (Fig. 5.5c), it results in the formation of a hole in the film. This was experimentally confirmed by Reiter (1993). In this work however, the situation was different. The thickness of films used in this study was in the range of 0.2 - 4 µm and also the holes appeared randomly throughout the film.
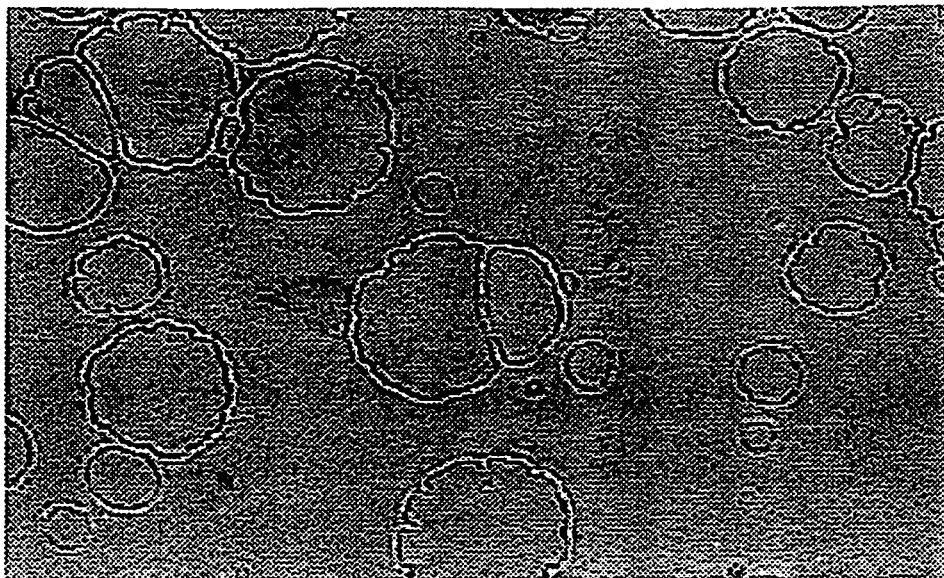
(a)
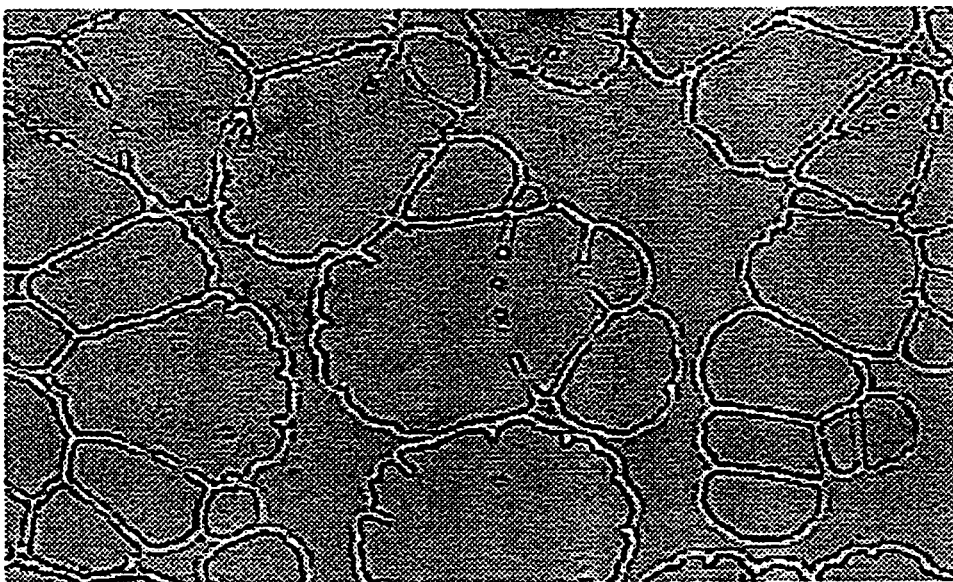
(b)

Fig. 5.4. The dynamics of the dewetting process for a polymer film embedded within a polymer matrix, (a) holes form in the film, (b) holes coalesce with neighboring holes, (continued on next page.....)
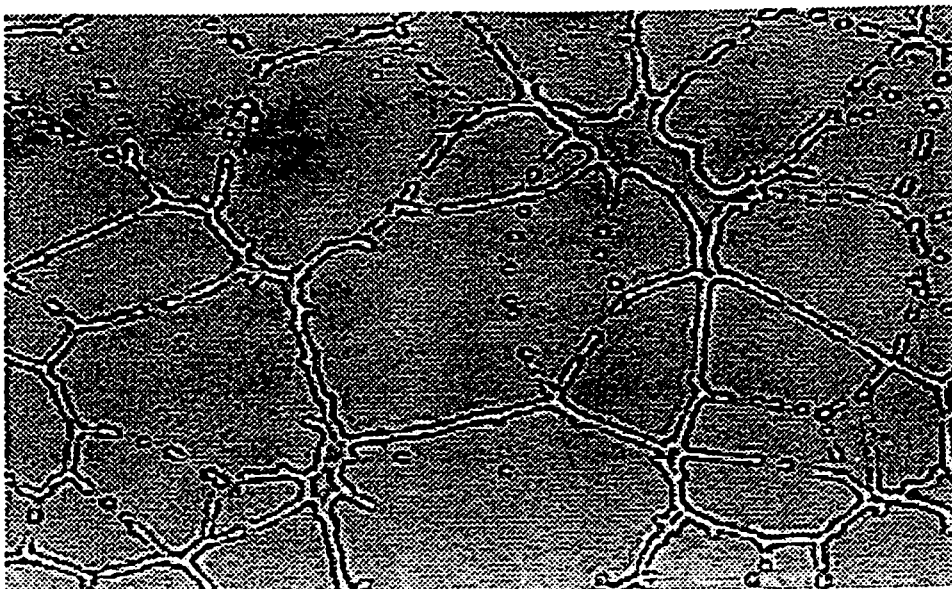
(c)
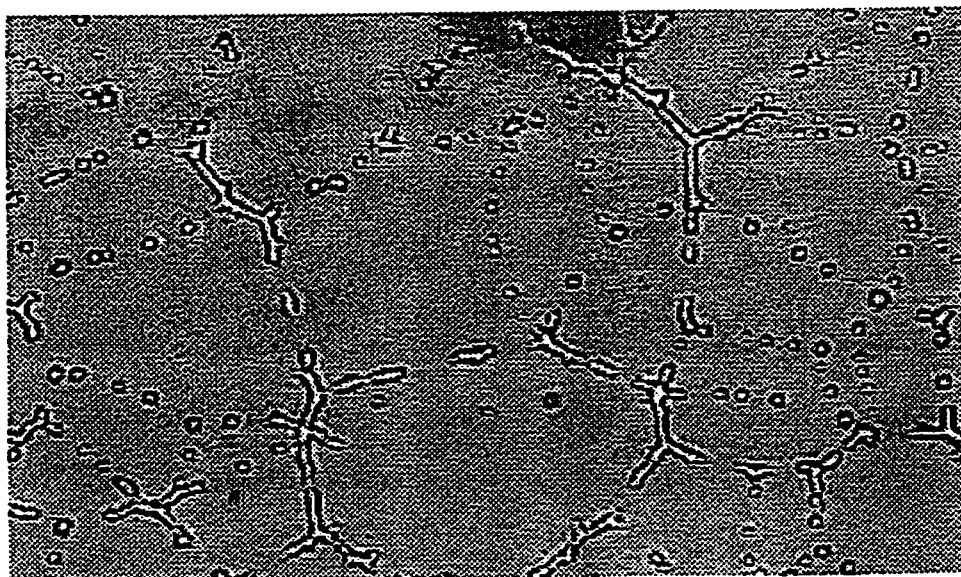
(d)

Fig. 5.4. (..continued) The dynamics of the dewetting process for a polymer film embedded within a polymer matrix, (c) coalescing holes form polygon shaped structures, (d) only drops remain.
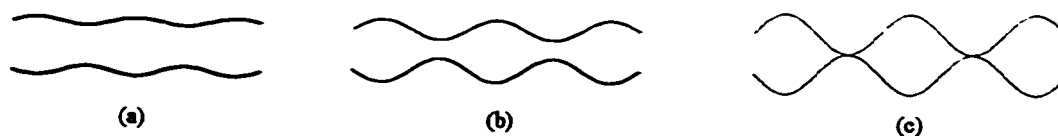
Fig. 5.5. Thermal fluctuations on the surface of the film leading to eventual breakup

It was concluded that the breakup was not due to a spinodal decomposition mechanism in our experiments. According to Vrij (1966), films thicker than around 10 nm do not rupture via a spinodal decomposition mechanism, but require external media such as vibrations, dust particles, etc. to cause rupture. One of these could be the cause for the initiation of dewetting in this case.

The newly formed holes formed grew and began coalescing with neighboring holes (Fig. 5.4b). The material between two coalescing holes was drained out from the sides and as the distance between these holes decreased, a ribbon was formed separating the holes. The drainage of material into these ribbons resulted in polygon shaped structures with the ribbons as their sides (Fig. 5.4c). The entire film broke up into this network of polygons. These ribbons then decayed via Raleigh instabilities into droplets (Fig. 5.4d). Spheres are thermodynamically the most stable geometric configuration since they have minimum free energy. The formation of these droplets is the final stage in the dewetting process and no further morphological change occurs after this stage is reached. As in Fig. 5.4d, the final stage still retains the polygon patterns. As pointed out by Reiter (1993),

such polygonal structures frequently occur in nature and can be found in soap froths, plants, etc.

5.3.2. Rate of Dewetting
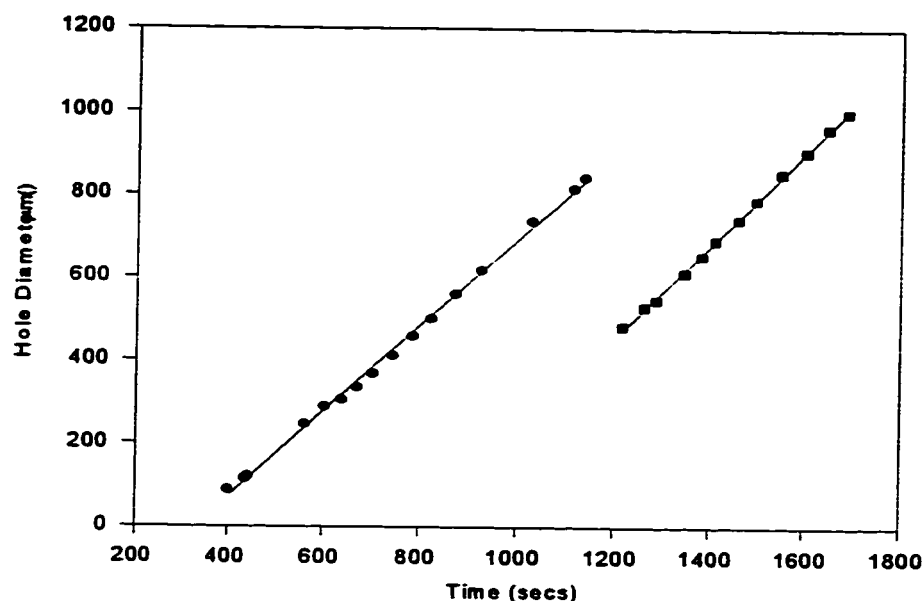
Fig. 5.6. Hole diameter versus time for two different holes formed in a PS film embedded within a PMMA matrix.

The entire dewetting process was recorded using the camera and VCR as explained in §5.2.3. The velocity at which the holes grew was measured. The area of the film visible during the experiment was limited by the size of the viewing window of the hot stage. Approximately 1.7 mm^2 of the sample surface was visible when using the lowest magnification objective of the microscope. At the highest magnification, approximately 0.1 mm^2 of sample area was visible. Since the camera remained focused on one area of

the sample, it was assumed that this area was representative of the entire sample. The video recording was played back and the diameter of a number of holes in this area was measured. The holes measured were at a sufficient distance from any neighboring holes so that their growth was not affected by neighboring holes. At least 10 measurements of its diameter were made at different times. Fig. 5.6 shows the plot of the diameter of two holes as a function of time. All the holes grew at a constant velocity in all the samples until they began to coalesce with other holes. This observation agrees with those reported by de Vries (1958) and Ranz (1960) for the growth of holes in free liquid films, and by Brochard-Wyart and Daillant (1990) and Reiter (1993) for the dewetting of liquid films deposited on substrates.

5.3.3. Factors Affecting Dewetting

All the literature on the breakup of liquid films indicates that the velocity at which the holes grew was dependent on the thickness of the film. As shown originally by Dupré for the breakup of a Newtonian liquid film, the velocity was inversely proportional to the square root of the thickness. This was experimentally confirmed by several authors. For liquid films supported on solid or liquid substrates, Reiter (1993, 1994) confirmed the strong dependence of breakup characteristics on film thickness. However, in this work, Fig. 5.7 shows that the velocity at which the holes grow in the film does not depend on the film thickness within the range of film thicknesses studied (0.2 - 1.5 μm). Therefore it can be said that a liquid polymer film within a liquid polymer matrix behaves differently from the film/substrate arrangements previously studied.
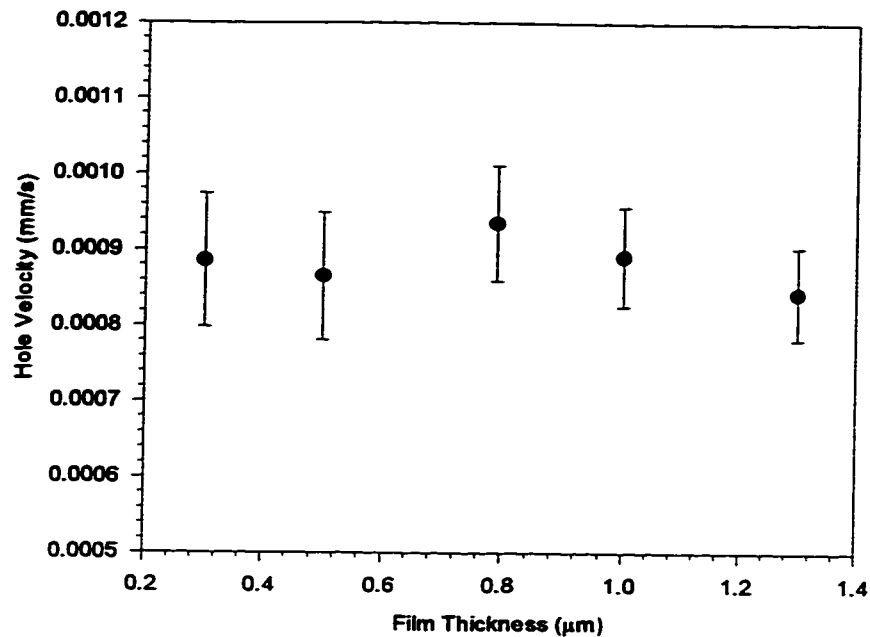
Fig. 5.7. Velocity of hole growth as a function of the thickness of the film for a PS film in a PMMA matrix annealed at 230°C

5.3.3.1. Factorial Design

An attempt has been made to analyze the factors affecting the breakup process. Conventionally, the method used to study the effect of a number of factors on a system is the "one factor at a time" approach. In this method each factor is varied while keeping all the others constant and the response of the system to this change is studied. However, this would imply that the factors act on the response additively. In addition, to study the effect of, for example, three variables on a system response replicating each experiment 4 times, the number of experiments required would be 16. The "one factor at a time" method not only requires a large number of experiments but cannot account for nonadditivity of variables.

A factorial design which can give more information with less experiments is used (Box, 1978 and Montgomery, 1984). In a factorial design, we select two levels for each variable and then run the experiments with all possible combinations. These levels are called "high" and "low" or designated by "+" and "-" respectively. The number of experiments required to study the effect of three factors is then $2^3 = 8$. Several levels can be chosen, but the number of experiments required increases. Thus on using a two level factorial design the number of experiments reduces by a factor of two as compared to the "one factor at a time" approach. In general, for a 2^k factorial design, where k is the number of variables, the "one factor at a time" method requires (k+1)/2 times as many runs and yields less useful information. In addition to reducing the number of runs, a factorial design detects and estimates interactions between variables that measure the nonadditivity of responses. It should be noted that the effect of each variable on the measured response is assumed to be unimodal. Therefore, some preliminary information should be available before performing factorial designs.

Variable	Value	
	High (+)	Low (-)
Film Thickness, F	2 μm	0.5 μm
Test Temperature, T	230°C	180°C
Annealing Time, A	1 hour	4 hours

Table 5.2. Summary of high and low values of the variables studied in the factorial design.

This technique was first tested by carrying out a factorial design in which there are three quantitative variables - film thickness, test temperature (in the hot stage) and the time for which the sample is annealed in the oven prior to it being placed in the hot stage. The measured response was the hole velocity. From Fig. 5.7, it was clear that the film thickness had no effect on the breakup velocity and the factorial design was used to confirm this. The factorial design was applied to a system of a PS film embedded in a PMMA matrix and the values of the variables used are given in Table 5.2. The runs were carried out with the combinations of the variables as shown in Table 5.3 along with the hole velocity obtained for each run.

Run	Order of Run	Combination	Test Temperature (°C)	Annealing Time (hr)	Film Thickness (μm)	Hole Velocity (nm/s)
1	3	+ + +	230	4	2	1880
2	8	+ + -	230	4	0.5	1490
3	5	+ - +	230	1	2	1070
4	1	+ - -	230	1	0.5	1230
5	4	- + +	180	4	2	13.4
6	2	- + -	180	4	0.5	15.4
7	7	- - +	180	1	2	12.6
8	6	- - -	180	1	0.5	19.9

Table 5.3. Table indicating combination of runs carried out and the response

The order of runs was randomized as shown in Table 5.3. For example, the combination "+++" was the third run carried out. To calculate the main effects i.e. the effect of the variables T, A and F on the hole velocity and the interaction effects, T×A, T×F, A×F and T×A×F the scheme used was as shown in Table 5.4. To present the data in a clearer manner, instead of using the hole velocity, log(hole velocity) was used.

T	A	F	T×A	T×F	A×F	T×A×F	log(hole velocity)
+	+	+	+	+	+	+	3.2747
+	+	-	+	-	-	-	3.1732
+	-	+	-	+	-	-	3.0294
+	-	-	-	-	+	+	3.0899
-	+	+	-	-	+	-	1.1271
-	+	-	-	+	-	+	1.1875
-	-	+	+	-	-	+	1.1004
-	-	-	+	+	+	-	1.2989

Table 5.4. Signs for calculating effects for a 2^3 factorial design.

In the above table the signs for the two factor and three factor interactions were obtained by multiplying the signs of their respective variables. Thus the sign for A×F was obtained by multiplying together the sign of A and F. Now, to calculate each effect, the sign for that effect on its corresponding hole velocity was used and then the array was added up. For example, for the T×F effect, the array gave (3.2747-3.1732+3.0294-3.0899-

1.1271+1.1875-1.1004+1.2989) = 0.2908. This was divided by 4 to obtain the value of the effect. The values for the effects obtained are shown in Table 5.5. From the values of the estimated effects it was observed that the T main effect dominated. This was further demonstrated by plotting the data on normal probability paper as shown in Fig. 5.8.

Effects	Estimated effect
T	1.9640
A	0.0626
F	0.0559
T×A	0.1051
T×F	0.0727
A×F	0.0739
T×A×F	-0.0057

Table 5.5. Estimated effects from a 2^3 factorial design.
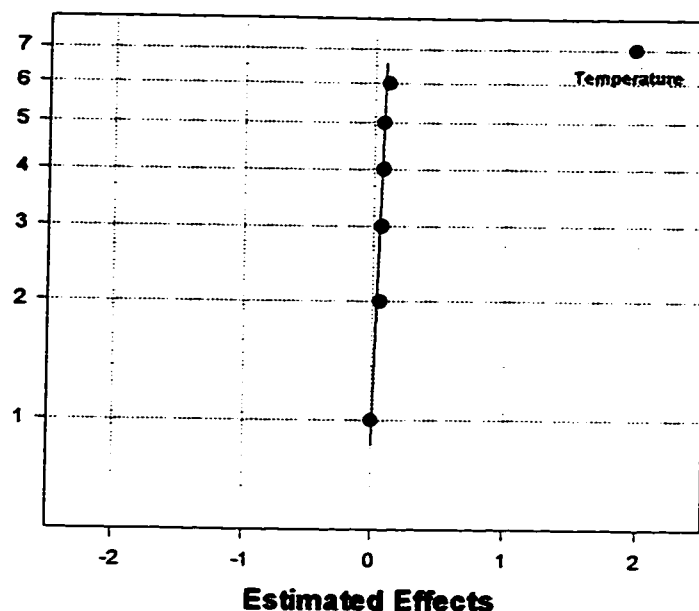
Fig. 5.8. Normal plot of effects for a 2^3 factorial design with the test temperature (T), annealing time (A) and the film thickness (F) as the variables.

In this figure it was observed that the temperature effect did not fall on the line drawn through all the other effects. Thus, Fig. 5.8 confirmed the fact that amongst the three effects, only temperature affected the hole velocity significantly. Since the factorial design predicted that the hole velocity was independent of the thickness of the film, confidence in its ability to predict the significance of variables on the hole velocity was strengthened.

Other variables were identified which might affect the rate of the dewetting. These were the viscosity of the film and the method of introducing the film onto the substrate. One of the methods for introducing the film was floating off the film onto the substrate as explained in §5.2.2. The other method was directly spincasting the film onto the substrate instead of using a glass slide. It was believed that in direct spincasting, the solvent used

147

might modify the substrate surface thereby affecting the dewetting process. Instead of carrying out a 2^2 factorial design, the test temperature was chosen again as the third variable for a 2^3 factorial design. This was done to determine the significance of the interaction of viscosity and temperature on hole velocity. The viscosity was varied by using two different polystyrenes - PS666D and PS618. The factorial design was carried out similar to the previous design and for the same system of a PS film in a PMMA matrix and the values of the variables used are given in Table 5.6.

Variable	Value	
	High (+)	Low (-)
Test Temperature	230°C	180°C
Viscosity	PS666D $\eta_o = 30$ kPa.s	PS618 $\eta_o = 15$ kPa.s
Method of film introduction	Direct Spincasting	Floating Off

Table 5.6. Summary of high and low values of the variables studied in the second factorial design.

The sequence of high's and low's was the same as for the first factorial design and is given in Table 5.7 along with the measured response variable i.e. hole velocity. The calculation of the main effects and the interaction effects was as given in Table 5.4 and the results are shown in Table 5.8. A normal plot for this design is shown in Fig. 5.9.

Run	Order of Run	Combination	Viscosity	Test Temperature (°C)	Method of film introduction	Hole Velocity (nm/s)
1	4	+ + +	PS666D	230	Direct	1080
2	6	+ + -	PS666D	230	Float	1146
3	1	+ - +	PS666D	180	Direct	13.33
4	7	+ - -	PS666D	180	Float	13.64
5	3	- + +	PS618	230	Direct	1280
6	2	- + -	PS618	230	Float	1394
7	5	- - +	PS618	180	Direct	15.15
8	8	- - -	PS618	180	Float	13.08

Table 5.7. Table indicating combination of runs carried out and the response for second design.

Effects	Estimated effect
V	-0.0490
T	1.9469
S	-0.0022
V×T	2.3793
V×S	-0.0158
T×S	-0.0293
V×T×S	0.0212

Table 5.8. Estimated effects from a 2^3 factorial design.
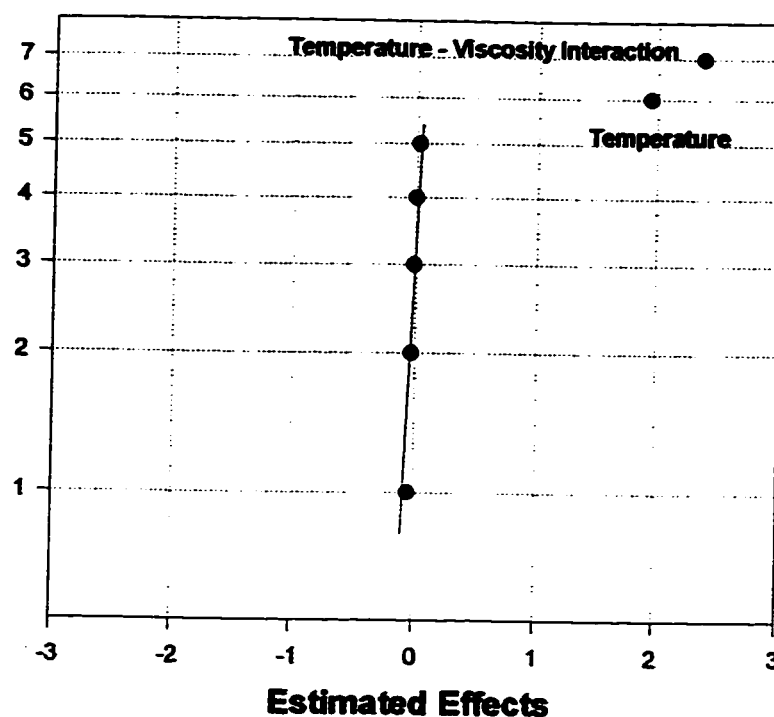
Fig. 5.9. Normal plot of effects for a 2^3 factorial design with the test temperature (T), film viscosity(V) and the method of introduction of film (S) as the variables.

The resulting estimated effects were again plotted on normal probability paper and are shown in Fig. 5.9. This shows that except for the T main effect and the T×V interaction effect all the other effects lie on the straight line. Thus not only is the test temperature an important variable in the breakup of a polymer film within a substrate but so is its interaction with the viscosity of the film. Fig, 5.9 also shows that the interaction effect was stronger than the main effect. The method of introduction of the film on the substrate has no effect on the hole velocity. This helped simplify all further sample preparation. It was not necessary to follow the tedious procedure of floating off the film but the film could be directly spincast onto the substrate.

Thus, the factorial design method was useful in determining the effect of system variables on the system response. It yielded useful information about the effect of each variable on the response without a large number of experimental runs. Another advantage was that it identified interactions between variables which would have remained hidden in a "one factor at a time" methodology. From the experimental runs, it was concluded that the most important factor affecting the breakup process was the test temperature. All further experimentation focused on the effect of temperature and viscosity on the hole velocity.

5.3.3.2. Effect of Temperature and Viscosity
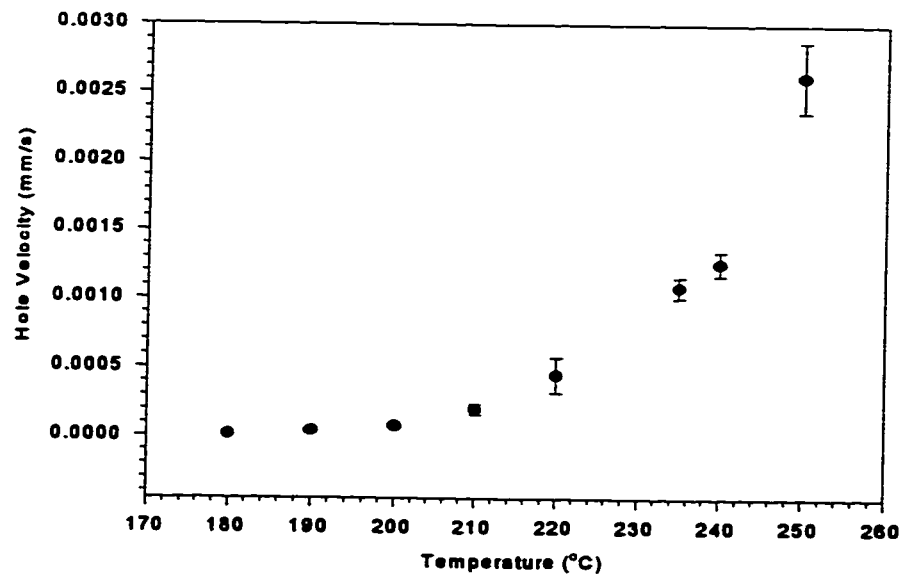
Fig. 5.10. Hole velocity versus the test temperature for the dewetting of a 1 μm film of PS666D inside a PMMA matrix.

Samples were prepared as described in § 5.2.2, however, the PS film was directly spuncast on the surface of the PMMA substrate. The thickness of the films used in this study was 1 μm. The samples were tested at different temperatures in the hot stage. The temperature ranged from a minimum of 180°C to a maximum of 230°C. A temperature above 250°C was not attempted, since it would lead to sample degradation. Two different polystyrenes were used - PS666D and PS618. The results for the dewetting of a film of PS666D embedded inside a PMMA matrix is shown in Fig. 5.10. The plot shows that at higher temperatures there was a dramatic increase in the dewetting velocity. This was due to the large decrease in viscosity as the temperature is increased.
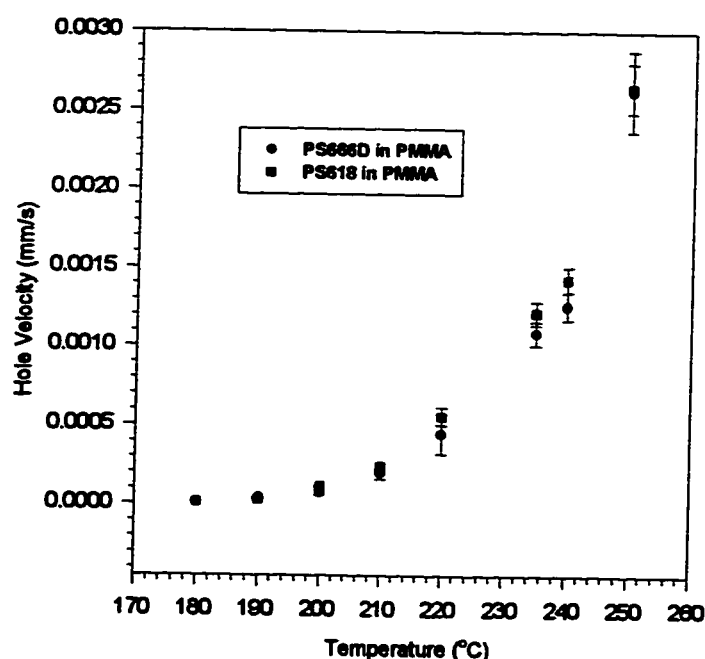
Fig. 5.11. Comparison of the hole velocity for two different viscosity PS - PS666D and PS618, both films being 1 μm thick.

On comparing this with the dewetting dynamics for a PS 618 film inside PMMA (Fig. 5.11), the same trend as for the PS666D is observed, but there is no appreciable change in the hole velocity. From Table 5.1 it was found that although the viscosity of PS666D is twice that of PS618 at 180°C and almost three times at 220°C, there was no significant change in the hole velocity. This seemed to indicate that the film viscosity may not play a very significant role in the dewetting process.
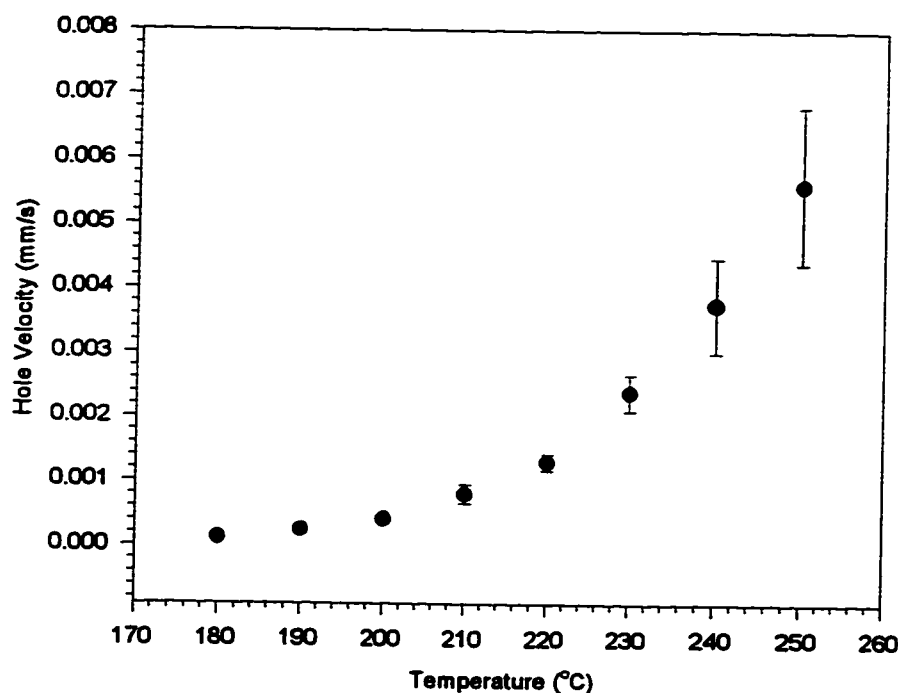
Fig. 5.12. Hole velocity versus the test temperature for the dewetting of a 1 μm thick PMMA film inside PS666D.

Since the PMMA had a viscosity much higher than the two polystyrenes, an attempt was made to reverse the system so that a PMMA film was embedded into a PS matrix. This would give some indication about the relative importance of the film and

153

matrix viscosities on the hole velocity. The results for this inverted system are as shown in Fig. 5.12. The variation of velocity with temperature was similar to the PS film in PMMA system. Fig. 5.13 compares this result with that for the PS666D film inside PMMA. It was found the hole velocity for the PMMA film in PS666D was always higher than that for the other system.
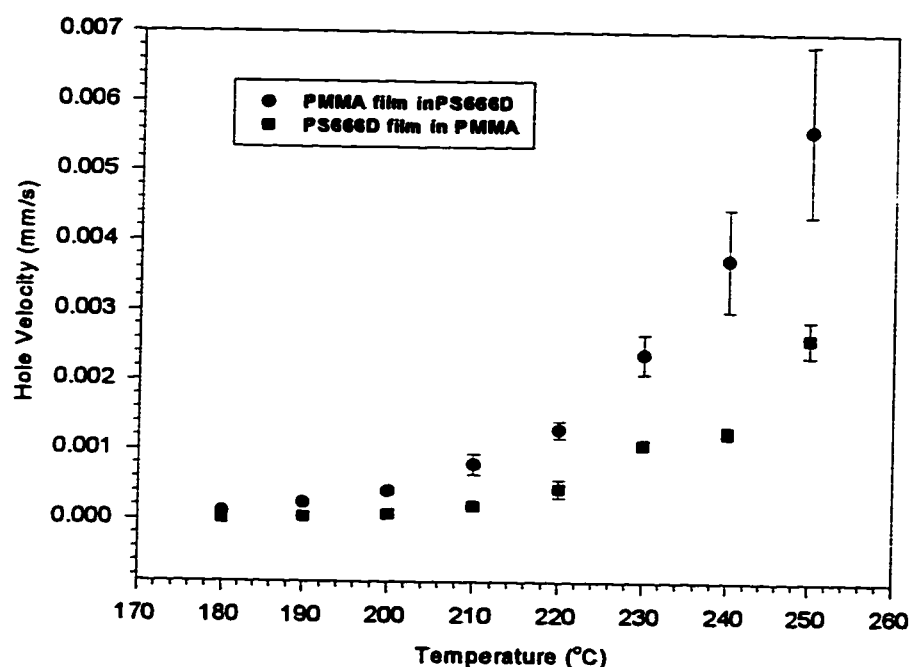
Fig. 5.13. Comparison of the dewetting velocity for a system of a PS666D film in PMMA with a PMMA film in PS666D system. All films used were 1 μm thick.

This difference was greatest at the highest temperature. If the film viscosity was controlling breakup, then the breakup velocity would increase as the film viscosity decreased. However, in this case, for a higher viscosity film (PMMA), the velocity was higher than that for a lower viscosity one (PS666D). This suggested that the matrix and not the film viscosity was the controlling factor in the dewetting of a melt film embedded

154

inside another melt. To confirm this, a PMMA film was embedded within a PS618 substrate and the results for this system are shown in Fig. 5.14. Fig. 5.14 shows that the velocity at which breakup occurs was higher for the lower viscosity PS618 matrix when compared to the higher viscosity PS666D matrix. Thus, the matrix viscosity is a governing factor in the breakup of a polymer film embedded within a polymer matrix.
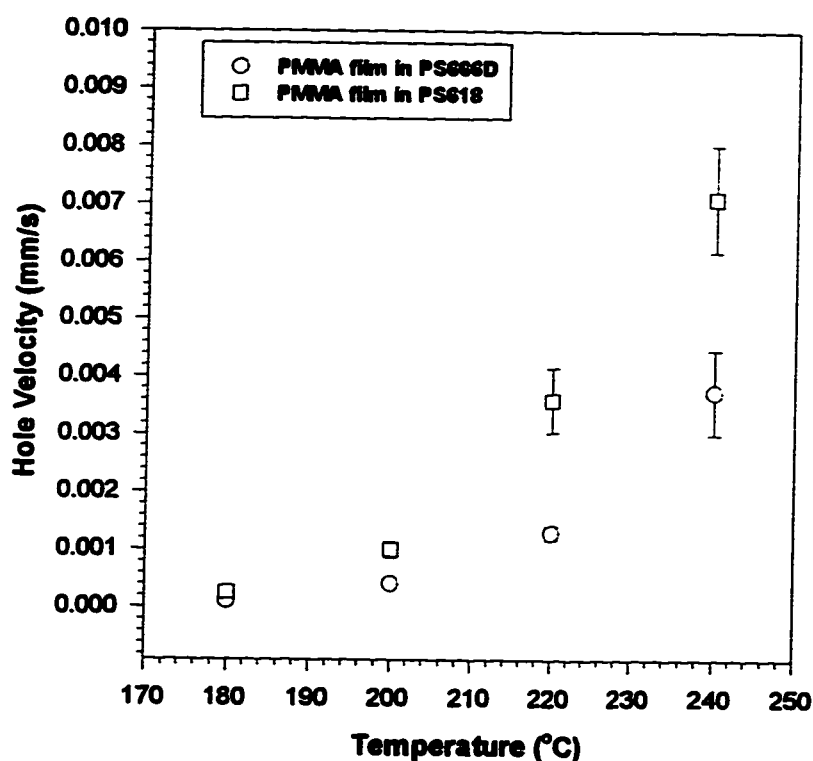
Fig. 5.14. Comparison of the hole velocity for a PMMA film embedded within two different viscosity matrices - PS666D and PS618.

Since the viscosities of the polymers used played a crucial role in determining the dynamics of the dewetting process, it was decided to compare the breakup velocities as a function of the viscosities directly. The viscosities of the polymers as a function of

temperature were required. However, the form of the temperature dependence is rather complex (Macosko, 1994). The most commonly used equation which correlates the viscosity of a polymer melt with temperature is the Williams-Landel-Ferry (WLF) equation (Van Krevelen, 1976). This equation resulted from the dependence of viscosity on the free volume for glassy polymers. This equation has validity in the region of T_g to $T_g + 100$ for melts of glassy polymers and is given as,

$$\log \eta(T) = \log \eta(T_S) - \frac{C_1(T - T_S)}{C_2 + (T - T_S)} \tag{5.3}$$

If T_S was chosen to be the T_g of the polymers i.e. 100°C, the values of C_1 and C_2 are 17.44 and 51.6K respectively. Macosko (1994) lists values of T_S, C_1 and C_2 for many polymers. Van Krevelen (1976) reported a better fit with $T_S = T_g + 43K$ and $C_1 = 8.86$ and $C_2 = 101.6K$. An attempt was made to fit the viscosity data for the PS666D, PS618 and PMMA given in Table 5.1 using both sets of values. However, the WLF did not fit the data very well especially at higher temperatures. Both the PS and the PMMA have T_g's around 100°C. Therefore, for these polymers, the temperatures beyond 200°C are outside the range of the WLF equation ($T_g < T < T_g + 100$).

Another equation which has been used to fit viscosity - temperature data is the Andrade - Eyring equation (Macosko, 1994 and Van Krevelen, 1976). This equation is applied at temperatures well above any transition temperatures of the polymers and was developed on the basis of a hole-theory of liquids. It is given as,

$$\eta = \eta_\infty \exp\left[\frac{E_\eta}{RT}\right] \tag{5.4}$$

In the above equation E_η is an activation energy for viscous flow. The transition to the exponential Andrade - Eyring equation from the WLF equation was found to occur at around $T_g/T = 0.85$, where the temperature is in Kelvin (Macosko, 1994). For the polymers used in this work ($T_g \sim 100°C$), this transition occurred at around 170°C. Since the lowest temperature used was 180°C the Andrade - Eyring equation was used to fit the data. This is shown in Fig. 5.15 for the PS666D and the PMMA data and the Andrade - Eyring equation fits the data reasonably well.

Using these correlations between viscosity and temperature, the viscosities at any temperature could be predicted. Fig. 5.10 and Fig. 5.12 were replotted with the viscosities calculated using the Andrade - Eyring equation and Fig. 5. 16(a) and Fig. 5.16(b) were obtained for the dewetting dynamics of a film of PS666D embedded within a PMMA matrix and the reverse system, respectively. Fig. 5.16 (a) and (b) showed that the hole velocity decreases as the viscosity in increased, which was expected. Martin et al. (1994) observed an inverse dependence of substrate viscosity on the hole growth rate for PDMS films deposited on immiscible fluorinated PDMS surfaces. They reported that the film viscosity had no significant effect on the dewetting process. Sundararaj (1994) obtained an expression for the dewetting velocity (Eqn. 5.3) where the velocity was inversely proportional to the substrate viscosity.
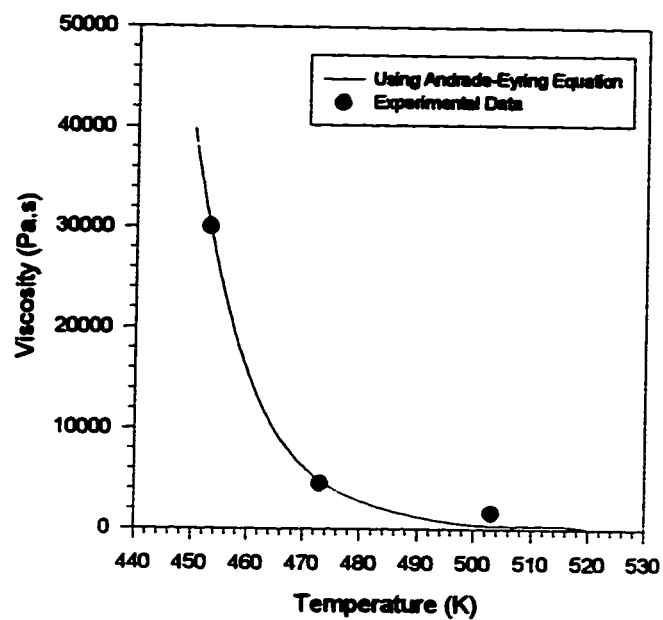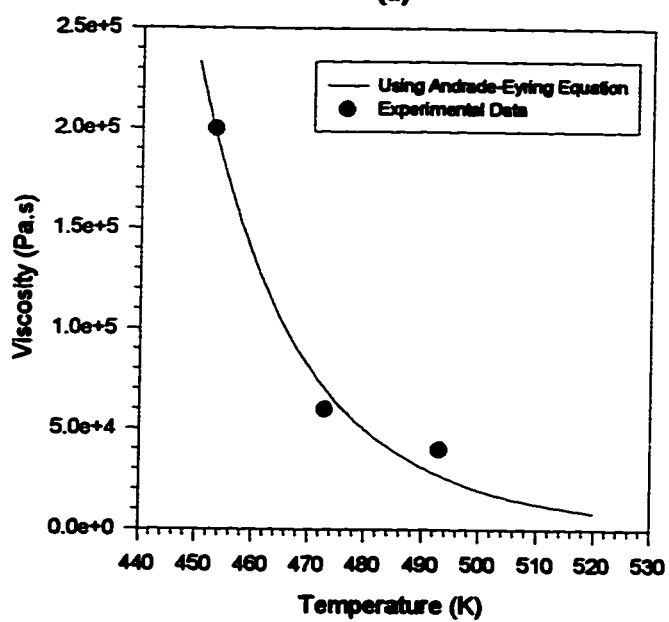
Fig. 5.15. Using the Andrade - Eyring equation to fit the viscosity - temperature data for, (a) PS666D and (b) PMMA.
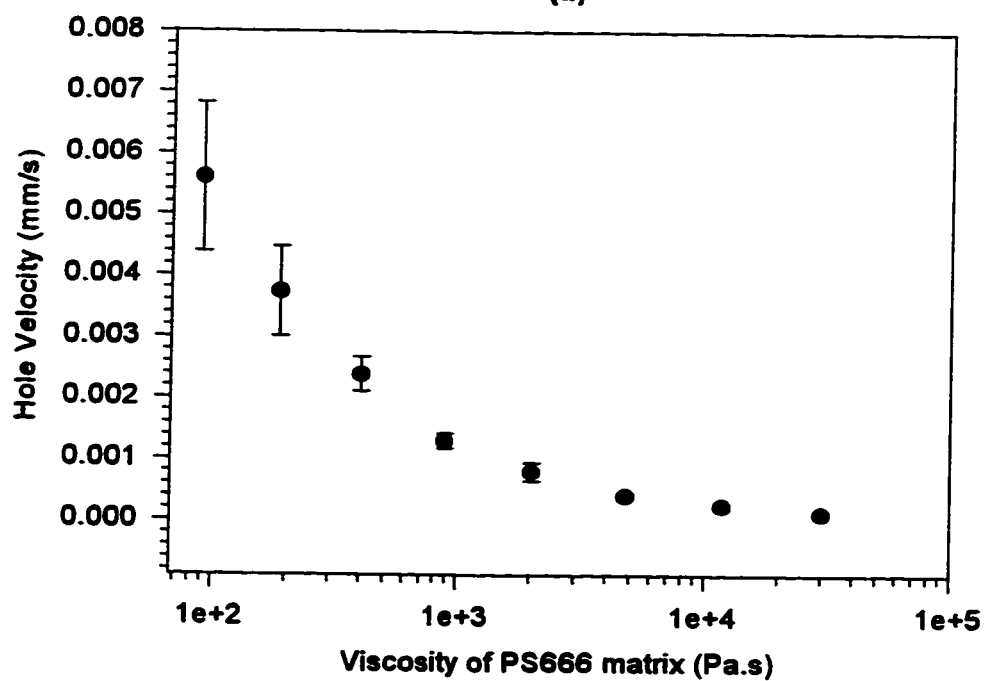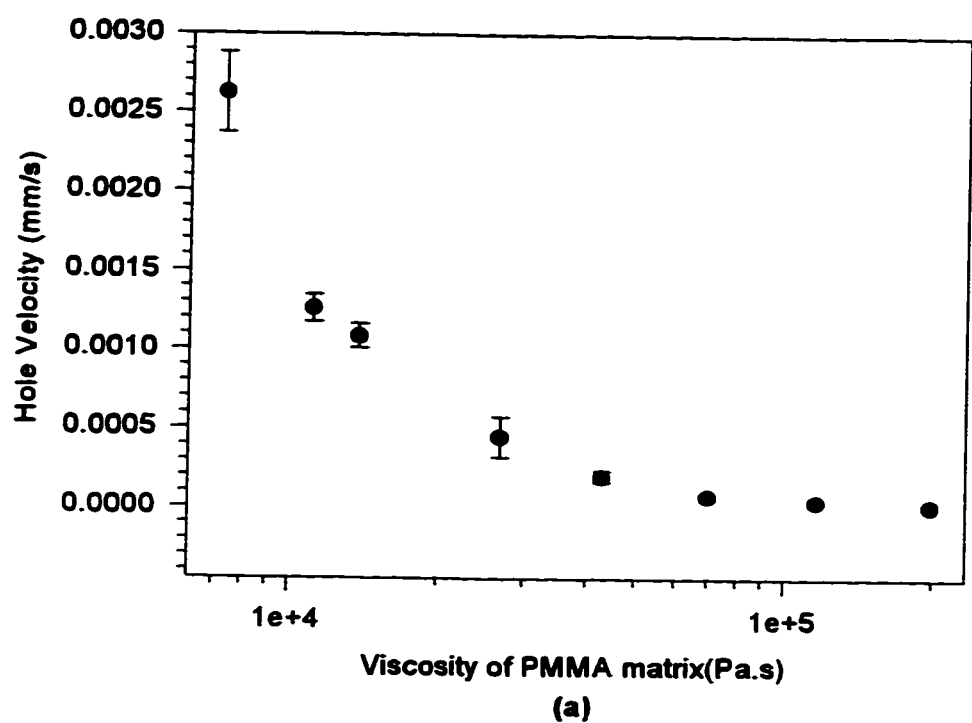
Fig. 5.16. Hole velocities plotted as a function of the matrix viscosity for, (a) PS666D film in a PMMA matrix and (b) PMMA film in a PS666D matrix.

159

There have been no reports in literature about a dependence of hole velocity on matrix viscosity as shown in Fig. 5.16. This dependence on matrix viscosity also implied that the dewetting process was controlled by the hydrodynamics of the system.

5.4. Model of the Dewetting Process

To explain the dependence of the hole velocity on matrix viscosity, an attempt was made to build a model of the dewetting process using concepts from fluid hydrodynamics instead of using surface physics like many authors have previously used to explain the dewetting of film deposited on surfaces. A model which could predict the constant hole growth rate without any dependence on film thickness and with inverse dependence on matrix viscosity as shown in Fig. 5.16 was needed.

As stated in §5.1.1 Dupré developed an expression for the growth rate of holes formed in soap films by equating the decrease in energy due to a loss in interfacial area to the kinetic energy of the moving rim of the hole.. This expression was modified by Culick (1960) to take into account the viscous dissipation occurring within the film due to frictional resistances. Some of the concepts originally proposed by Dupré and Culick (1960) to analyze the dewetting process for our system were used.

The hole growth process is as represented in Fig. 5.17. The film of thickness h is surrounded by the matrix polymer. The hole is nucleated at the origin O and grows

outwards with a radius R(t) and a velocity v(t). The hole is surrounded by a rim which is assumed to have a circular cross-section of radius r(t).
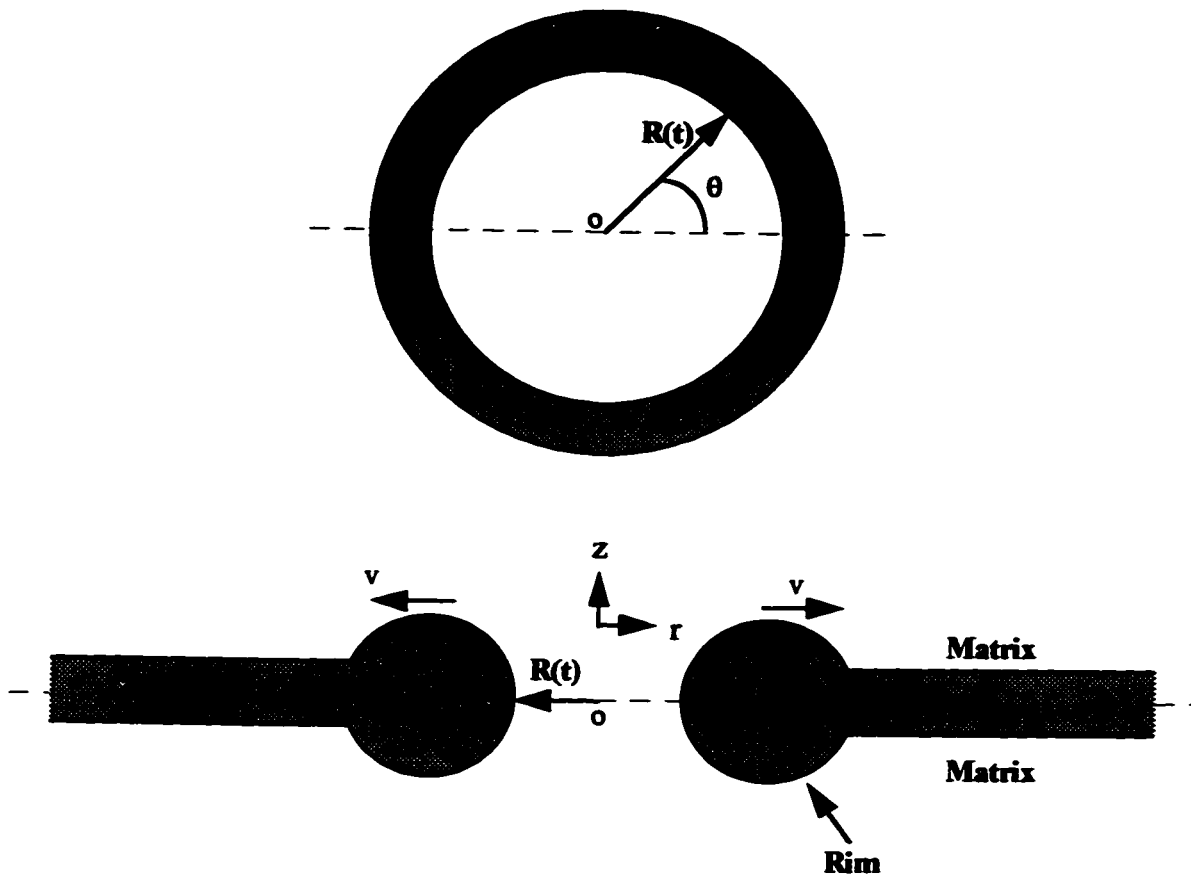
Fig. 5.17. Schematic of the dewetting process showing a toroidal hole growing with radius R(t) and the rim of radius r(t) (adapted from Sundararaj, 1994).

It was further assumed that all the material lost in forming the hole accumulates in the rim. This would imply that there was no material flowing out into the bulk of the film. Using mass conservation the size of the rim could be estimated as,

Volume of the hole = Volume of the rim

$$\pi \{R(t)\}^2 h = [2 \pi R(t)] [\pi \{r(t)\}^2]$$

161

$$r(t) = \sqrt{\frac{R(t)h}{2\pi}} \qquad\qquad (5.5)$$

Since the Reynolds number for this type of flow is very small inertial effects could be neglected. For a rim opening out in an extremely viscous polymer melt, the viscous forces resisting this motion become important. Sundararaj (1994) had analyzed the opening out of a hole in a polymer film within a polymer matrix. In his analysis, a balance was established between the rate at which surface energy is lost due to a decrease in interfacial area, the rate of viscous dissipation within the film and the rate of energy loss due to deformation of the matrix as the rim grows. The deformation of the matrix implies that a velocity gradient exists within the matrix, with a maximum velocity, v at the surface of the rim and this velocity decays to zero at a certain distance from the rim. However, in this work it is assumed that the film is rigid and that there is no viscous dissipation within the film. This is a reasonable assumption as the film is extremely thin ($\sim$ 1 μm) as compared to the thickness of the matrix phase ($\sim$ 2500 μm). On equating the rate of energy loss to the viscous losses in the matrix, the following balance is obtained,

$$\frac{d}{dt}(R^2(t)\sigma\ \theta) = \frac{d}{dt}(\int\limits_{0}^{h}\ \int\limits_{0}^{\theta}\ \eta_m\dot{\gamma}\,R(t)\ d\theta\ dz)\ R(t) \qquad\qquad (5.6)$$

where θ is a small included angle in a sector of the hole in the plane of the film, $\dot{\gamma}$ is the shear rate in the matrix near the interface, σ is the interfacial tension for the matrix/film

system and η_m is the viscosity of the matrix. Rearranging the above equation using $\dot{\gamma} = \partial u/\partial z = v/h$ where, u is the velocity in the matrix phase,

$$2R(t)\frac{dR(t)}{dt}\sigma \ \theta = \eta_m \frac{v}{h}(2R(t)\frac{dR(t)}{dt})\theta \ h \qquad (5.7)$$

On simplifying the above equation,

$$v = \frac{\sigma}{\eta_m} \qquad (5.8)$$

Thus, an expression for the hole growth velocity which predicts that the velocity is independent of the radius of the hole (R(t)), the film thickness and strongly dependent on the matrix viscosity is obtained.
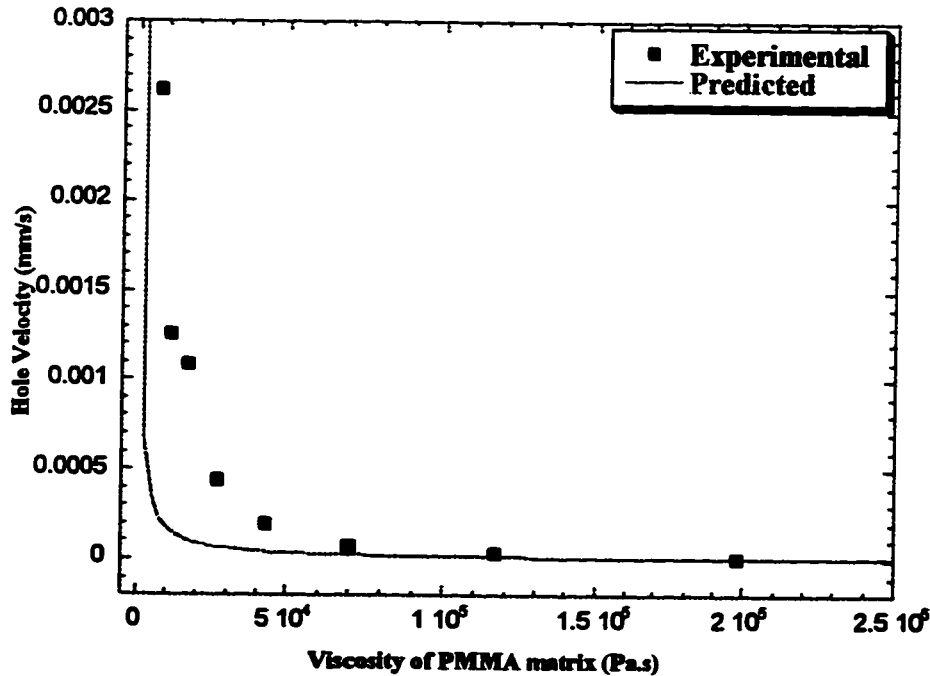
Fig. 5.18. Comparison of predicted velocity with experimental velocity as a function of the matrix viscosity for a PS666D film embedded within a PMMA matrix.
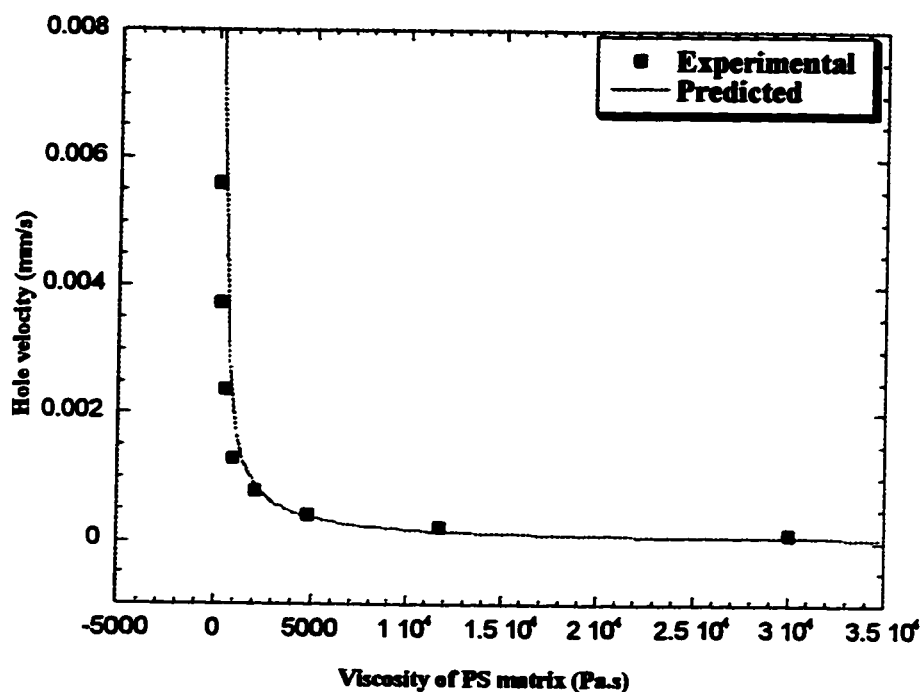
Fig. 5.19. Comparison of predicted velocity with experimental velocity as a function of matrix viscosity for a PMMA film embedded within a PS666D matrix.

The velocity predicted using this equation is compared with the experimental velocity as shown in Fig. 5.18 and Fig. 5.19. The above figures indicate that Eqn. 5.8 reasonably predicts the velocity of dewetting. The prediction is better for the case of the PMMA film within the PS666D matrix as compared to the PS666D film in the PMMA matrix system. The predicted hole velocity increases more sharply than the experimental data for the PS film embedded in the PMMA matrix.

5.5. Conclusions

Polymer films embedded within a polymer substrate were found to be unstable and dewet through the formation of holes. The polymer films studied ranged from a thickness of 0.2 μm to 3 μm. The holes grew to coalesce into polygonal shaped structures with ribbons of the film material forming their sides. The ribbons ultimately broke up and the final morphology in the dewetting process was a dispersion of droplets throughout the matrix. The mechanism leading to the initiation of dewetting was not a spinodal decomposition mechanism. The initiation of dewetting depended on the temperature at which the system was tested. Higher temperatures led to quicker initiation of dewetting.

The holes grew at a constant velocity and this velocity was independent of the thickness of the film. Therefore a film within a melt matrix dewets with a different mechanism than films in air or a film deposited on a substrate. To determine the factors controlling the breakup process, a factorial design was performed. It was found that the test temperature and its interaction with viscosity were the most important factors controlling the dewetting process. Factors which were not important were the time for which the polymer disc/film/polymer disc system was annealed in the oven, the thickness of the film and the method by which the film is introduced onto the substrate disc. Thus, a factorial design succeeded in providing useful information related to the breakup process with only a few experiments.

The velocity at which the holes grow in the film increases as the temperature is increased and a correlation was observed between the two. The film viscosity did not have an appreciable effect on the hole velocity. However, the matrix viscosity plays an important role in controlling this velocity. A higher matrix viscosity leads to slower dewetting velocity. This suggests that once dewetting is initiated, the subsequent process depends on the hydrodynamics of the system. The hydrodynamics were modeled using an energy balance approach and an expression for the dewetting velocity was obtained. This equation predicts no dependence of velocity on film thickness and its prediction of hole velocity as a function of viscosity is quite reasonable.

5.6. References

Box, G. E. P., Hunter, W. G., and Hunter J. S., *Statistics for Experimenters*, John Wiley & Sons, New York, 1978.

Brochard Wyart, F., and Daillant, J., *Can. J. Phys.* **68**, 1084(1990).

Brochard Wyart, F., and de Gennes, P. G., *J. Phys.:Conden. Matter* **6**, A9(1994).

Culick, F. E. C., *J. Appl. Phys.* **31**, 1128(1960).

De Vries, A. J., *Rec. Trav Chim.* **77**, 383(1958).

Dombrowski, N., and Fraser, R. P., *Phil. Trans. Roy. Soc.* **247**, 13(1954).

Faldi, A., Composto, R. J., and Winey, K. I., *Langmuir* **11**, 4855(1995).

Faldi, A., Winey, K. I., and Composto, R. J., *Mat. Res. Soc. Symp. Proc.* **366**, 71(1995).

Frankel, S., and Mysels, K. J., *J. Phys. Chem.* **73**, 3028(1969).

Fraser, R. P., Eisenklam, P., Dombrowski, N., and Hasson, D., *AIChE. J.* **8**, 672(1962).

Keller, J. B., *Phys. Fluids* **26**, 3451(1983).

Ksheshigi, H. S., and Scriven, L. E., *Chem. Engg. Sci.* **46**, 519(1991).

Liu, Y., Rafailovich, M. H., Sokolov, J., Schwarz, S. A., Zong, X., Eisenberg, E., Kramer, J., Sauer, B. B., and Satija, S., *Phys. Rev. Lett.* **73**, 440(1994).

Macosko, C. W., *Rheology-Principles, Measurements, and Applications*, VCH Publishers Inc., New York, 1994.

Martin, P., Buguin, A., and Brochard Wyart, F., *Europhys. Lett.* **28**, 421(1994).

McEntee, W. R., and Mysels, K. J., J. Phys. Chem. **73**, 3018(1969).

Montgomery, D. C., *Design and Analysis of Experiments*, John Wiley & Sons, New York, 1984.

Ranz, W. E., *J. Appl. Phys.* **30**, 1950(1960).

Rayleigh (Lord), *Scientific Papers*, ed. J. W. Strutt, Dover Publication Inc., 1964, New York, v. 3, p. 441.

Redon, C., Brochard Wyart, F., and Rondelez, F., *Phys. Rev. Lett.* **66**, 715(1991).

Redon, C., Brozska, J. B., Brochard Wyart, F., *Macromolecules* **27**, 468(1994).

Reiter, G., *Phys. Rev. Lett.* **68**, 75(1992).

Reiter, G., *Langmuir* **9**, 1344(1993).

Reiter, G., *Macromolecules* **27**, 3046(1994).

Scott, C. E., *Polym. Bull.* **26**, 341(1991).

Sharma, A., and Ruckenstein, E., *J. Coll. Int. Sci.* **133**, 358(1989).

Sharma, A., and Ruckenstein, E., *J. Coll. Int. Sci.* **137**, 433(1990).

Shull, K., and Karis, T. E., *Langmuir* **10**, 334(1994).

Sundararaj, U., Macosko, C. W., Rolando, R. J., and Chan, H. T., *Polym. Eng. Sci.* **32**, 1814(1992).

Sundararaj, U., Ph. D. Thesis, University of Minnesota, USA (1994).

Sundararaj, U., Dori, Y., and Macosko, C. W., *Polymer* **36**, 1957(1995).

Taylor, G. I., *Proc. Roy. Soc. A*, **vol CCLIII**, 313(1959).

Taylor, G. I., and Michael, D. H., *J. Fluid Mech.* **58**, 625(1973).

Van Krevelen, D. W., *Properties of Polymers*, Elsevier Scientific Publishing Co., New York, 1976.

Vrij, A., *Discuss. Faraday Soc.* **42**, 23(1966).

Zhao, W., Rafailovich, M. H., Sokolov, J., Fetters, L. J., Plano, R., Sanyal, M. K., Sinha, S. K., and Sauer, B. B., *Phys. Rev. Lett.* **70**, 145(1993).

CHAPTER 6

Future Work and Recommendations

6.1. Effect of Vinylacetate Content on Adhesion

We have studied the adhesion of ethylene-vinylacetate (EVA) copolymers to different substrates. One property studied in detail was the effect of VA content on the adhesion. In the peel test, it was found that the adhesion of the EVAs to PC and PET increased with VA content (§2.5.6) and this was explained on the basis of a matching of polarities between the adhering phases. Using the DCB (§3.3.1) and the Microscratch test (§4.4), the adhesion of EVA to PS decreased with VA content. It was believed that polarity was not important for this system, but there was enhanced diffusion for low viscosity EVAs.

The polarity can be related to the solubility parameter (δ) of the polymers. The solubility parameters of polymers cannot be estimated from the physical constants of the polymers because of their nonvolatility (Brandrup and Immergut, 1975). It is therefore defined as the same as that of a solvent in which the polymer will mix (a) in all proportions, (b) without heat change, (c) without volume change, and (4) without reaction or any special association. On the other hand direct evidence of the diffusion mechanism can be found by studying the interface between the polymers using techniques like transmission electron microscopy (Van Oene and Plummer, 1977), radiothermoluminiscence, paramagnetic probe, UV luminiscence and optical microscopy (Wu, 1984). The best method would be to measure the diffusion coefficient of the polymers. This has been done for several polymers acting as the diffusant through

different mediums and the values are reported by Wu (1982). The effect of VA content, annealing temperature, pressure, molecular weight, molecular weight distribution, polymer chain conformation, chain branching, etc. on adhesion can then be investigated by studying the effect of these parameters on the diffusion coefficient.

6.2. Role of Primed PET film in the Peel Test

The PET films used in the Peel test were coated with a thin layer of a proprietary primer. This primer plays a very important role in determining the strength of the adhesive bond between the PET and the EVAs. On analyzing the surfaces of the EVA samples after peeling (Fig. 2.12), it was noticed that samples annealed for 15 seconds showed a smooth surface while those annealed for 20 seconds had cracks on the surface. Also the adhesion increases from being undetectable at 15 seconds to around 400 J/m^2 at 20 seconds (Fig. 2.13). This increase in adhesion in a short interval of 5 seconds suggests that the primer is heat activated and requires a certain initiation period to become active. This could mean that a chemical bond is formed between the primer and the EVA which leads to the strong adhesion. It has been reported (Garbassi et al., 1994) that polyolefins and their copolymers like EVAs have relatively non-polar surfaces and their adhesion characteristics are poor. Thus, to improve the adhesion of the EVAs to the PET, the primer introduces reactive functional groups which form a chemical bond with species present on the EVA surface. Confirmation of this would require studying the composition of the primer and the nature of the interaction between it and the EVA.

The PET/EVA sample which was tested using the peel test had a tri-layer configuration shown in Fig. 6.1. It was concluded that the cracks observed on the surface of the EVA strips indicated cohesive failure within the EVA. However, this conclusion was reached based on the assumption that the PET/primer interface was not important and failure could occur only at the primer/EVA interface. This can be confirmed by analyzing the surface of the peeled samples using a analytical technique like Secondary Ion Mass Spectroscopy (SIMS) (Garbassi et al., 1994).

Primer

Fig. 6.1. Peel sample configuration for the system PET/EVA.

This techniques would give us information about the polymer functional groups present on the surface. Thus, the presence of ethylene or vinylacetate groups on the surface would indicate cohesive failure within the EVA. However, if ester groups were detected, this would mean that the failure was within the PET and not the EVA and then the PET/primer interface would need to be considered.

6.3. Adhesion in Polymer Blends and Composites

With the large costs involved in developing a new polymer, an alternative is combining different polymers to obtain enhanced properties. These may take the form of polymer blends, polymer composites or coextruded materials. Examples of polymer blends are

rubber-toughened plastics. In these, the rubber particle size and the rubber/matrix adhesion are two important factors determining their impact properties. For polymer composite materials, desirable properties can be obtained only if stresses can be transferred from the polymer matrix to the high strength reinforcing fibre across the polymer/fibre interface. This transfer is governed by the strength of the polymer/fibre interface i.e. the adhesion at the interface (Shah, 1995). '

However, most workers (Kojima et al., 1995; Shah, 1995; Liu and Baker, 1994 and D'Orazio et al., 1986) have focused on the morphology of blends and composites and related this to the improvement in mechanical properties. Visual inspection of the interface between dispersed phase droplets and the matrix phase in blends and between fibre and polymer in FRPs have led to inferences about the adhesion at this interface. Some workers have measured mechanical priorities like the tensile modulus and the impact strength of polymer blends and composites and used these along with morphological micrographs to speculate about the adhesion at the interface.

The missing link between morphology and mechanical properties is quantification of the adhesion at the interface. This can be accomplished by using either the DCB test for polymer blends and composites or the peel test for coextruded materials. These adhesion measurement tests can also be used to study the improvement in properties brought about by the compatibilization of polymer blends. This would require the introduction of a known concentration of compatibilizer at the interface between the two

homopolymers and then measuring the adhesive strength of this interface. In glass fibre-reinforced nylon composites materials, surface treatment techniques like etching, plasma treatment, etc. modify the surface of the fibres leading to improved adhesion and consequently better mechanical properties (Shah, 1995). A glass plate can be subjected to the above treatments and adhered onto a nylon plate. The DCB test can be used to quantify the adhesion at the nylon/glass interface for each treatment. The adhesion values obtained could then be compared with the effect of the treatments on the mechanical properties of the composite.

6.4. Morphological Development in Polymer Blends

As discussed in Chapter 5, a polymer film was embedded in a polymer matrix and the breakup of this film was studied in detail in the quiescent state. It was also mentioned that sheet formation is an intermediate morphological feature in the blending of polymers. To understand this phenomenon, the effect of shear rate on the breakup process should be investigated. It is expected that the hole velocity would be higher due to the shear and the holes formed would be deformed into oblong structures. Such an experiment would be more representative of the situation in the blending of polymers in a batch mixer or an extruder and would yield useful information about the initial morphology development in these equipment. However, the current experimental setup cannot be used to study this. A suggestion would be to insert the present sample configuration between two counter-rotating glass discs surrounded by a heating medium and then study the breakup of the film. Sundararaj (1994) and Levitt et al. (1996) used such an apparatus to study sheet

formation under simple shear conditions. Another experiment would be study the breakup of a multilayer configuration of polymer sheets and investigate the effect of interaction between adjoining layers on the breakup dynamics.

6.5. Barrier Properties

A barrier is related to permeability, which in turn is a combination of diffusion and solubility in the polymer (Garbassi et al., 1995). Lowering one or both of them results in an improved barrier. Improving the barrier properties of polymers is very important in packaging applications (food, pharmaceuticals, cosmetics, fine chemicals, etc.). Tubes and hoses for gasoline require solutions to improve barrier properties. Barriers can be provided by multilayer systems (obtained by coextrusion, lamination, etc.), blends with lamellar morphology and surface treatments. The latter can be coating substrates with barrier polymers or treatments like fluorination, sulphonation, metallization, etc.

Coating operations involve the application of heat and this frequently leads to the breakup of the coated film resulting in pits forming on the substrate surface (Ksheshigi and Scriven, 1991). The inside of containers are frequently coated with barrier polymers which are exposed to different liquids (milk, juices, etc.). As has been demonstrated in Chapter 5, the stability of such a film against breakup depends on the temperature it is subjected to, its thickness and the viscosity of the surrounding medium. So, to prevent pitting during the coating process and also to maintain the structural integrity of the coated film while in use, the above factors must be considered.

In some applications a certain rate of diffusion of a permeant (e.g. oxygen, water, aromas, etc.) through the film is required. The ability of the embedded film to breakup at different rates can be used to tailor the barrier properties in such applications. This would require an outer matrix polymer which is permeable to the diffusing substance and an embedded film which acts as a barrier to the permeant. The barrier film can be destabilized by the application of heat, which would result in holes forming. By freezing the process, a barrier film with holes would be obtained. The permeant would diffuse through the holes formed and the rate of diffusion would depend on the average diameter of holes and the average number of holes per unit area of film. These two factors could be controlled by changing the matrix viscosity and the film thickness.

6.6. Statistical Design of Peel and DCB Tests

In Chapter 5, the efficacy of statistical design techniques in providing useful information with minimum experimental effort was demonstrated. These techniques should also be used to analyze the DCB and peel tests and understand the significance of various factors governing these tests. In the peel test, a factorial design on the peel angle, the peel rate and the thickness of the EVA strip would yield information about the factors most affecting the experimental setup and the test could be made more accurate by keeping these factors constant. In Chapter 2, it was speculated that the affect of melt index (MI) on adhesion was more pronounced than that of the VA content. To confirm this observation a factorial design using the VA content of the copolymer, the MI and the

175

annealing time and temperature, would provide an insight about the factors affecting adhesion the most. Similarly, in the DCB test, the rate of blade insertion, the thickness of the polymer plates and the thickness of the blade could affect the experimental setup and make the results more noisy. A design on these factors could make the automated test more sensitive and improve its performance as a product development test.

6.7. Internal Stresses in Polymer Films

In the Microscratch Test, a delamination of the film occurs which is measured as a drop in the tangential and normal loads. This delamination is due to a release in interfacial energy. During sample preparation, the polystyrene film was produced by a spincasting technique (§4.2). It has been reported (Croll, 1979 and 1983) that the spincasting process generates internal stresses within the film and at the interface between the film and the substrate. Thus some of the energy being released when the film delaminates could be due to the release of these stresses and might not be related to the adhesion at the interface. A procedure for approximately calculating these internal stresses developed during spincasting has been reported by Croll (1979, 1983). This is recommended for any future studies on the adhesion of spincast films to substrates.

6.8. Experimental Improvements

6.8.1. The Peel Test

The sample preparation procedure produced EVA sheets of varying thickness due to non-uniform pressure applied in the plate press. As seen in § 2.5.4, the thickness of the EVA

strip influences the peel strength. Thus, a sheet preparation technique which ensures a uniform sheet thickness should be used. The extruded 10% EVA sheets exhibited striations on their surface after peeling (§ 2.5.5). These striations were thought to be an artifact of the extrusion process. They could be a result of a non-uniform temperature profile across the die through which the polymer is extruded. This could lead to a periodic difference in crystallinity across the length of the sheet and hence a difference in adhesion. To prevent these striations on the surface and the large fluctuations in adhesion along the sample length, a uniform temperature should be maintained across the die.

Two different peel configurations were attempted on the Instron machine, the 180° peel and the T peel. In the 180° peel test, it was noticed that towards the end of the test, the EVA which was being peeled off started bending backwards making the peel angle greater than 180°. Similarly in the T peel test (Fig. 2.4), as the sample was peeled apart, the unpeeled part of the sample dangled loosely which could affect the peel angle. Since, the peel test is strongly dependent on the peel angle, the above situations could lead to erroneous results. Auxiliary devices can be attached to the Instron machine which can keep this angle constant and also vary the angle. It is recommended that these devices be used to keep the angle constant and also study the effect of varying the peel angle on the peel strength.

6.8.2. The Double Cantilever Beam Test

As illustrated in §3.2.3, in this test the crack at the interface is observed visually and recorded onto a VCR. The crack had to be clearly visible for its length to be measured. This makes the optics in this test extremely important. For some systems the crack was very faint and measuring it was difficult. An improvement over the currently used method would be to inject a die into the interface after the crack has formed. This would make the crack clearer and would mean that the use of the DCB test would not be limited by atleast one material being optically clear, i.e. amorphous. For some systems the adhesion was too strong and the crack formed was too small to be measurable. For these tough systems, it is recommended that a thicker blade be used. Referring to Eqn. 3.6, we see that a thicker blade (larger Δ) would result in a longer crack length (larger a). However, care should be taken in ensuring that the end of this blade does not dig into any of the polymer phases and remains positioned at the interface. Also, a better procedure is required for introducing the blade into the interface and then clamping it into the razor blade holder (§3.2.4). The current procedure requires frequent eyeballing and adjustment to get the blade in at the interface and this consumes a lot of time.

6.8.3. The Microscratch Test

In this test, a delamination of the film occurs which was related to the adhesion of the film to the substrate. Comparing the scratch morphology (Fig. 4.8) with the tangential and normal forces measured (Fig. 4.9), the sequence of events occurring during the scratch

process was speculated upon. However, to exactly determine the nature of this scratch process, a suggestion would be to attach a high resolution, high magnification camera inside the microscratch apparatus which would record the scratch process as it progresses. While calculating the stress-intensity factors and the work of adhesion we used material constants (shear modulus and Poisson ratio) for the bulk polymers. These constants have been found to be different for thin films and vary with the thickness of the film. Thus, the constants should be estimated for the thickness of the film used in our systems (1 μm).

6.7.4. Stability and Breakup of Thin Polymer Films

While observing the dewetting process, the sample area visible was limited by the size of the observation window. The largest area that could be viewed was around 1.7 mm^2, while the total area of the sample was around 300 mm^2. All measurements were for this small area under the assumption that it was representative of the entire sample surface. Thus, a larger viewing window is recommended. Another suggestion would be to use a higher magnification lens with a longer working distance. With the highest magnification (800X) used, the smallest size of the holes observable was around 2 μm. A higher magnification would result in the capture of the onset of breakup at an earlier stage and this would help in understanding the cause of breakup. The Andrade-Eyring equation was used to fit the viscosity versus temperature data (3 data points) and this fit was used to predict the viscosities at other temperatures. As seen from Fig. 5.14, the equation fits the data reasonably. However, a better equation should be developed by fitting the Andrade-Eyring equation through a larger number of data points. The best method would be to

obtain the experimental viscosities for the polymers being studied at all the temperatures using the Rheometrics RMS 800 rheometer.

6.9. References

Brandrup, J., and Immergut, E. H., *Polymer Handbook*, Wiley Interscience, New York (1975).

Croll, S. G., in *Adhesion Aspects of Polymeric Coatings*, ed. K. L. Mittal, (Plenum, New York, 1983), p.107.

Croll, S. G., *J. Appl. Poly. Sci.* **23**, 847(1979).

D'Orazio, L., Mancarella, C., Martuscelli, E., Casale, A., Filippi, A., and Speroni, F., *J. Mat. Sci.* **21**, 989(1986).

Garbassi, F., Morra, M., and Occhiello, E., *Polymer Surfaces: From Physics to Technology*, John Wiley & Sons, New York (1994).

Kojima, T., Ohnaga, T., and Inoue, T., *Polymer* **36**, 2197(1995).

Ksheshigi, H. S., and Scriven, L. E., *Chem. Engg. Sci.* **46**, 519(1991).

Levitt, L., Macosko, C. W., and Pearson, S. D., *Polym. Eng. Sci.* **36**, 1647(1996).

Liu, N. C., and Baker, W. E., *Polymer* **35**, 988(1994).

Shah, D., M. Sc. Thesis, University of Alberta, Canada (1995).

Sundararaj, U., Ph. D. Thesis, University of Minnesota, USA (1994).

Van Oene, H., and Plummer, H. K., *ACS Org. Coatings Plast. Prep.* **37**, 498(1977).

Wu, S., *Polymer Interface and Adhesion*, Marcel Dekker, New York (1982).

APPENDIX A

Peel Data for PC/EVA and PET/EVA Systems

The peel test was carried out on an INSTRON Model # 1130 tensile tester equipped with a 500 N tension loadcell. All tests were carried out with a crosshead speed of 50 mm/min and at room temperature. The data was recorded on a chart recorder and a typical curve obtained is as shown in Fig. A-1.1.
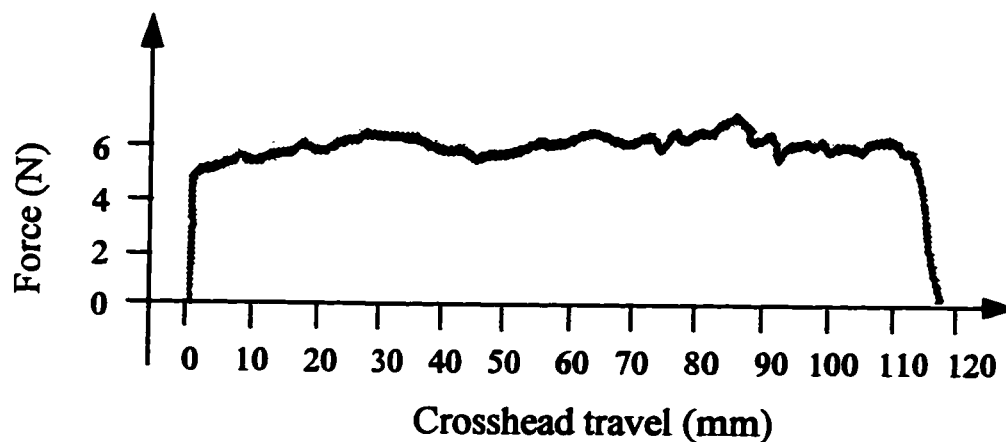
Fig. A-1.1. Force versus displacement of crosshead on the Instron Model # 1130 for a PC/16%EVA system annealed at 150°C for 15 minutes.

The curve obtained on the chart paper of the recorder was transferred to a PowerMac 6100 using a HP ScanJet 3p scanner. The image was then analyzed using NIH Image Analysis software Version 1.57 and the area under the curve was obtained. For the above curve,

Area = A = 2100.5 mm^2

This area was converted using the following calibrations,

1 mm on X-axis = 1 mm of extension

1 mm on the Y-axis = 0.333 N

Therefore, area under the curve = $2100.5 \times 0.333 \times 0.001 = 0.6995$ N.m

To calculate the average force for the above curve,

$$\text{Average force} = \frac{\text{Area under curve}}{\text{Distance moved by crosshead}} = \frac{0.6995}{0.121} = 5.7807 \text{ N}$$

Thus, the work of adhesion for the PC/16%EVA system for the 180° peel test is

$$\text{Peel strength, } G = \frac{\text{Average Force}}{\text{Width of sample, b}} = \frac{5.7807}{0.025} = 231.23 \text{ J/m}^2$$

Similarly the peel strengths for all other samples were estimated and listed in Table A-1 and Table A-2.

TABLE A-1

System	Anneal Temp (°C)	Anneal Time	Area (mm²)	Area (N.m)	Length (mm)	Avg Force (N)	Width, b (mm)	G (J/m²)	Avg G (J/m²)	Std Dev
PC/16%EVA	100	5 min	1246.2	0.4150	89	4.6628	29	160.8	139.2	18.75
			976.44	0.3252	86	3.7809	29	130.4		
			913.33	0.3041	89	3.4173	27	126.8		
		10 min	1137.8	0.3789	87	4.3549	29	150.2	157.9	15.92
			1332.7	0.4438	98	4.5283	28	161.7		
			1238.3	0.4123	89	4.6331	26	178.2		
			1190.8	0.3965	90.5	4.3817	31	141.3		
		20 min	3365.3	1.1206	104.5	10.7240	30	357.5	319.2	42.07
			2348.1	0.7819	101	7.7416	28	276.5		
			2725.7	0.9077	108	8.4041	29	289.8		
			3064.4	1.0205	107	9.5370	27	353.2		
		1 min	907.82	0.3023	98	3.0847	30	102.8	108.2	18.56
			685.13	0.2282	91	2.5071	27	92.9		
			980.57	0.3265	97.5	3.3490	26	128.8		
	150	20 min	3286.1	1.0943	124	8.8248	28	315.17	290.94	24.17
			2489.1	0.8289	114	7.2709	25	290.84		
			1808.9	0.6024	107.5	5.6033	21	266.82		
		2 min	1143.4	0.3808	105	3.6263	27	134.31	128.78	14.07
			1117.9	0.3723	102	3.6497	25	145.99		
			889.79	0.2963	107	2.7692	24	115.38		
			466.28	0.1553	100	1.5527	13	119.44		
		10 min	1436.3	0.4783	101.5	4.7121	28	168.29	179.71	13.89
			1487.6	0.4954	105.5	4.6955	24	195.65		
			1293	0.4306	95	4.5322	27	167.86		
			1563.7	0.5207	116	4.4889	24	187.04		
		15 min	1769.4	0.5892	114.5	5.1459	25	205.84	229.61	28.66
			2346.3	0.7813	118	6.7355	25	289.42		
			2100.5	0.6995	121	5.7807	25	231.23		
			1903.3	0.6338	130	4.8753	23	211.97		

TABLE A-1 (continued p.2)

Peel Data

System	Anneal Temp (°C)	Anneal Time	Area (mm²)	Area (N.m)	Length (mm)	Avg Force (N)	Width, b (mm)	G (J/m²)	Avg G (J/m²)	Std Dev
PC/29%EVA	100	5 min	281.71	0.0930	83	1.1201	20	56.003	62.614	5.666
			558.79	0.1844	110	1.6784	24	69.849		
			475.36	0.1569	101	1.5532	25	82.126		
			487.72	0.1610	112	1.437	23	62.48		
		10 min	291.5	0.0962	94	1.0234	24	42.64	99.079	76.221
			468.67	0.1547	98	1.6111	28	61.964		
			666.43	0.2199	109	2.0176	25	80.705		
			1911.2	0.6307	122	5.1697	24.5	211.01		
		15 min	676.73	0.2233	113	1.9763	23.5	84.097	121.4	69.779
			1789.2	0.5904	111	5.3192	25	212.77		
			1058.4	0.3493	103	3.3909	25	135.63		
			358.97	0.1185	97	1.2212	23	53.097		
	150	10 min	2126.6	0.7081	118.5	5.9759	24	249	220.71	27.32
			1739.7	0.5793	121	4.7879	24	199.49		
			1685.5	0.5613	115	4.8806	25	195.22		
			1947.5	0.6485	113	5.7392	24	239.13		
		20 min	5267.4	1.7540	155	11.316	23	492.02	409.97	81.32
			4593.7	1.5297	125	12.238	27	453.24		
			3699.9	1.2321	122	10.099	26	388.42		
			2427.5	0.8084	120	6.7364	22	306.2		
		1.5 min	236.27	0.0787	84	0.93664	25	37.486	31.72	5.949
			171.92	0.0572	89.5	0.63966	25	25.586		
			166.25	0.0554	75	0.73815	23	32.093		

TABLE A-1 (continued p.3)

Peel Data

System	Anneal Temp (°C)	Anneal Time	Area (mm²)	Area (N.m)	Length (mm)	Avg Force (N)	Width, b (mm)	G (J/m²)	Avg G (J/m²)	Std Dev
PET/10%EVA	100	50 min	636.04	0.2099	100	2.0989	23	91.258	78.214	18.033
			352.1	0.1162	84	1.3832	24	57.635		
		55 min	518.85	0.1712	81.5	2.1009	24.5	85.75		
			960.26	0.3169	73.5	4.3114	23.5	183.46	144.72	35.522
			730.52	0.2411	76.5	3.1513	23	137.01		
			859.79	0.2177	81.5	2.6715	23.5	113.68		
		57 min	2108	0.6957	74	9.4006	24	391.69	367.14	26.125
			1426.7	0.4708	63	7.4731	22	339.69		
			968.84	0.3197	36	8.881	24	370.04		
	150	15 min	747.41	0.2467	57	4.3271	21.5	201.26	203.05	25.75
			931.68	0.3075	71	4.3303	23	188.28		
			1221.3	0.4030	80	5.0377	21	239.89		
			841.87	0.2778	76	3.6555	20	182.77		
		25 min	1921.7	0.6342	83	7.6404	22	347.29	363.57	23.02
			2197.3	0.7251	83	8.7363	23	379.84		
			1144.9	0.3778	78.5	4.8128	24	200.53		
			841.87	0.2778	86.5	3.2118	25	128.47		
		10 min	747.39	0.2466	65	3.7944	19	199.71	152.84	43.14
			866.11	0.2858	86.5	4.298	24	179.08		
			472.55	0.1559	85	2.3991	20	119.96		
			569.3	0.1879	69.5	2.7032	24	112.63		
		20 min	2017.8	0.6659	78	8.5369	21	406.52	211.11	73.31
			1481.7	0.4890	81	6.0365	20.5	294.46		
			1077.4	0.3555	76.5	4.6475	25.5	182.26		
			992.31	0.3275	82	3.9934	25.5	158.61		

TABLE A-1 (continued p.4)

Peel Data

System	Anneal Temp (°C)	Anneal Time	Area (mm²)	Area (N.m)	Length (mm)	Avg Force (N)	Width, b (mm)	G (J/m²)	Avg G (J/m²)	Std Dev
PET/16%EVA	100	40 secs	3781.7	1.2479	104.5	11.942	24.5	487.43	659.4	150.98
			2896.3	0.9558	50	19.115	27.5	695.1		
			5123.1	1.6906	103.5	16.335	21	777.84		
		45 secs	10252	3.3833	105	32.221	21	1534.4	1376.9	147.99
			9388.7	3.0983	95	32.613	23.5	1387.8		
			10010	3.3034	102	32.386	23	1408.1		
			7221.1	2.3830	88	27.079	23	1177.4		
		30 secs	2692	0.8884	61	14.563	25	582.53	483.76	88.397
			2056.7	0.6787	52	13.052	23	567.49		
			1215.3	0.4011	47	8.5331	22	387.87		
			1248.6	0.4120	40	10.301	22	468.21		
			907.91	0.2996	33	9.0791	22	412.69		
		20 secs	3310.8	1.0928	96	11.381	21.5	529.35	359.34	110.6
			2592.2	0.8554	94	9.1002	22	413.65		
			1730.5	0.5711	87	6.5641	22	298.37		
			1688.2	0.5571	81	6.8779	24.5	280.73		
			1629.3	0.5377	89	6.0414	22	274.61		

186

TABLE A-1 (continued p.5)

Peel Data

System	Anneal Temp (°C)	Anneal Time	Area (mm²)	Area (N.m)	Length (mm)	Avg Force (N)	Width, b (mm)	G (J/m²)	Avg G (J/m²)	Std Dev
PET/29%EVA	100	75 secs	4131.9	1.3635	85	16.041	24.5	654.75	521.59	115.54
			2730.9	0.9012	83	10.858	23.5	462.03		
			2872.5	0.9479	92	10.304	23	447.98		
		60 secs	2518.2	0.8310	96	8.6563	21.5	402.62	318.06	83.999
			1278.6	0.4219	89	4.7409	22	215.49		
			1735.6	0.5727	92	6.2254	21.75	286.22		
			2073.6	0.6843	93	7.3579	20	367.9		
		45 secs	1780.7	0.5876	107	5.4919	22.5	244.08	276.72	55.283
			2149.9	0.7095	100	7.0948	22	322.49		
			1725.5	0.5694	78.5	7.2538	22	329.72		
			1690.5	0.5579	84	8.6411	23	288.74		
			967.45	0.3193	67	4.7651	24	198.54		
		90 secs	5679.9	1.8744	87	21.544	23.5	916.78	979.08	90.138
			5049.2	1.6662	89	18.722	21	891.51		
			7544.5	2.4897	107	23.288	21.5	1082.2		
			5607.7	1.8505	88	21.029	20.5	1025.8		
	150	10 secs	7545.4	2.4900	88	28.295	24	1179	1183.2	34.37
			4770.1	1.5741	62.5	25.186	20.5	1228.6		
			6557.8	2.1641	84	25.763	22.5	1145		
		5 secs	4935.9	1.6289	57.5	28.328	24	1180.3		
			5611.1	1.8516	82	22.581	24	940.88	1145.1	178.22
			8859.9	2.9238	96	30.456	24	1269		
			7189.9	2.3727	88	26.962	22	1225.5		
		2 secs	1847	0.6095	63	9.6749	24	403.12	570.33	133.43
			2369.9	0.7821	74	10.569	22	480.39		
			3082.2	1.0171	85	11.966	21	589.82		
			3896.4	1.2858	80	16.073	22	730.58		
			3628	1.1972	81.5	14.69	22	667.73		

TABLE A-2

Peel Data for Different Thickness of EVA's

Annealing Temperature : 100°C

Sample	Thickness (mm)	Area (mm²)	Area (N.m)	Length (mm)	Avg Force (N)	Width (mm)	G (J/m²)	Avg G (J/m²)	Std Dev
PET/16%EVA	0.5020	4510.7	1.4885	70.5	21.1140	23	918.0	858.94	74.50
		3833.9	1.2652	68.0	18.6060	24	775.3		
		4241.2	1.3996	66.0	21.2060	24	883.6		
	0.5610	1922.3	0.6344	76.0	8.3467	23	362.9	540.91	45.52
		2757.8	0.9101	75.0	12.1340	23	527.6		
		2719.1	0.8973	81.0	11.0780	22	503.5		
		2842.5	0.8720	67.0	13.0150	22	591.6		
	0.4500	995.1	0.3284	89.5	3.6692	24	152.9	130.03	26.14
		1007.4	0.3324	98.0	3.3922	25	135.7		
		322.8	0.1065	75.0	1.4202	23.5	60.4		
		753.2	0.2485	102.0	2.4367	24	101.5		
	0.6230	1287.0	0.4247	77.0	5.5158	24	229.8	245.08	13.24
		905.5	0.2988	75.0	3.9843	24	166.0		
		1291.8	0.4263	70.0	6.0901	24	253.8		
		1326.3	0.4377	71.0	6.1644	24.5	251.6		
	0.2310	212.6	0.0701	88.0	0.7972	23.5	33.9	33.92	
	0.2500	1110.8	0.3666	97.0	3.7790	25	151.2	42.46	.08
		246.4	0.0813	76.5	1.0630	25	42.5		
		289.7	0.0956	98.0	0.9753	23	42.4		

TABLE A-2 (continued p.2)

Sample	Thickness (mm)	Area (mm²)	Area (N.m)	Length (mm)	Avg Force (N)	Width (mm)	G (J/m²)	Avg G (J/m²)	Std Dev
PET/29%EVA	0.1957	2029.1	0.6696	82.0	8.1658	25.0	326.6	359.91	36.21
		2523.7	0.8328	95.0	8.7665	22.0	398.5		
		2269.6	0.7490	96.0	7.8019	22.0	354.6		
	0.2121	2546.8	0.8405	98.0	8.5760	22.0	389.8	455.36	52.44
		1286.0	0.4244	41.0	10.3510	21.0	492.9		
		1991.0	0.6570	70.0	9.3863	21.5	436.6		
		1272.1	0.4198	38.0	11.0470	22.0	502.2		
	0.7838	2770.9	0.9144	74.0	12.3570	22.0	561.7	645.89	119.11
		5068.1	1.6725	93.5	17.8880	24.5	730.1		
	0.6876	3788.5	1.2502	79.0	15.8250	23.0	688.1	758.71	64.50
		4412.8	1.4562	74.5	19.5470	24.0	814.4		
		4483.5	1.4796	75.0	19.7280	25.5	773.6		
	0.6138	4974.1	1.6415	73.0	22.4860	25.0	899.4	879.55	28.12
		4558.8	1.5044	70.0	21.4920	25.0	859.7		
	0.4430	3132.1	1.0336	68.0	15.2000	26.5	573.6	659.21	78.89
		3650.7	1.2047	83.0	14.6150	21.5	675.1		
		4075.5	1.3449	90.0	14.9430	20.5	728.9		

APPENDIX B

Microscratch Test Data

The data for the microscratch test is obtained from the normal and tensile loads which are being measured continuously throughout the test and the SEM micrograph of the scratch track. The theoretical development used to estimate the stress-intensity factors and the work of adhesion from this data was given in §4.3. As stated in this section a linear elastic mechanics model was used for our analysis and the stress-intensity factors were calculated as,

$$k_I = \frac{1}{\pi}\left(\frac{2}{a}\right)^{1/2}\left[P \cos(\varepsilon \ \log a) + Q \ \sin(\varepsilon \ \log a)\right] \qquad (B.1)$$

$$k_{II} = \frac{1}{\pi}\left(\frac{2}{a}\right)^{1/2}\left[Q \cos(\varepsilon \ \log a) - P \ \sin(\varepsilon \ \log a)\right] \qquad (B.2)$$

In the above equations, P and Q are the normal and tangential forces acting on a crack situated at the interface (Fig. 4.5). From Fig. 4.9, these forces are assumed to be those at point F where, both the normal and tangential loads drop sharply. In Eqn. B.1 and B.2, a is the length of the crack formed when the normal load becomes constant. Referring to Fig. 4.9, we find that this is at point E. Thus, in our system we calculate the crack length as shown in Fig. B.1, i.e. $a = x - y$.

Fig. B.1. The scratch track for a 0.55 μm PS film on 28% EVA.

The material constants used in estimating k_I and k_{II} are as follows:

Poisson ratios: $\gamma_{PS} = 0.38$, $\gamma_{EVA} = 0.49$

Shear modulii: $\mu_{PS} = 1.2$ GPa, $\mu_{EVA} = 0.015$ GPa

Thus, for plane strain, $\eta_{PS} = 3 - 4\gamma_{PS} = 1.48$ and $\eta_{EVA} = 3 - 4\gamma_{EVA} = 1.04$

$C_{PS} = 2.07$ (GPa)$^{-1}$ and $C_{EVA} = 136$ (GPa)$^{-1}$

So, $\varepsilon = \dfrac{1}{2\pi} \log\left[\dfrac{C_{EVA}}{C_{PS}}\right] = 0.289$

The values for the stress-intensity factors and the work of adhesion at different loading rates are given in Table B-1.

APPENDIX B

Data from the Microscratch Test

Loading Rate (μm/s)	Normal Load P(N)	Tangential Load Q(N)	x (μm)	y (μm)	Crack Length a=x-y (m)	K_I (MPa.m$^{1/2}$)	K_{II} (MPa.m$^{1/2}$)	Work of Adhesion G(J/m²)	Average G(J/m²)	Std Dev
75	0.0105	0.0160	40.0	25.0	15,0E-8	-295.2	279.2	0,0045	0,0042	0,0004
	0.0100	0.0145	35.0	20.0	15,0E-8	-265.7	263.1	0,0038		
	0.0110	0.0155	30.0	15.0	15,0E-8	-282.9	287.8	0,0044		
62.5	0.0095	0.0135	45.0	25.0	20,0E-8	-178.2	193.3	0,0019	0,0034	0,0028
	0.0090	0.0135	45.0	35.0	10,0E-8	-390.6	338.3	0,0072		
	0.0088	0.0132	47.0	28.0	19,0E-8	-186.5	188.9	0,0019		
	0.0113	0.0165	45.0	25.0	20,0E-8	-219.0	230.6	0,0027		
100	0.0110	0.0130	25.0	13.0	12,0E-8	-298.0	339.8	0,0055	0,0059	0,0011
	0.0110	0.0125	23.0	11.0	12,0E-8	-284.8	337.9	0,0053		
	0.0105	0.0103	25.0	15.0	10,0E-8	-283.5	372.9	0,0059		
	0.0105	0.0110	28.0	16.0	12,0E-8	-247.4	318.8	0,0044		
	0.0110	0.0130	25.0	15.0	10,0E-8	-366.8	399.5	0,0079		
	0.0105	0.0115	27.0	17.0	10,0E-8	-321.4	377.7	0,0066		
	0.0105	0.0115	30.0	19.0	11,0E-8	-288.0	346.8	0,0055		
125	0.0105	0.0105	21.0	12.0	9,0E-8	-327.5	410.9	0,0075	0,0096	0,0030
	0.0100	0.0105	20.0	13.0	7,0E-8	-439.3	492.1	0,0118		
150	0.0106	0.0100	20.0	14.0	6,0E-6	-495.1	594.3	0,0162	0,0154	0,0007
	0.0104	0.0093	17.0	11.0	6,0E-6	-458.7	581.4	0,0148		
175	0.0108	0.0105	15.0	9.0	6,0E-6	-520.9	606.5	0,0173	0,0173	0,0001
	0.0110	0.0104	18.0	12.0	6,0E-6	-515.0	616.8	0,0174		